Università degli Studi di Padova

Sede Amministrativa: Università degli Studi di Padova

Sede Consorziata: Università degli Studi di Bologna

Dipartimento di Tecnica e Gestione dei Sistemi Industriali, DTG Vicenza

Dipartimento di Ingegneria Industriale, DIN Bologna

DOTTORATO DI RICERCA IN INGEGNERIA MECCATRONICA E DELL'INNOVAZIONE MECCANICA DEL PRODOTTO

CURRICOLO: MECCATRONICA

CICLO XXIX

Effect of friction, surface treatment and adhesive-reinforcement on the behavior of threaded connections

Effetto dell'attrito, dei trattamenti superficiali e dell'incollaggio sul comportamento dei collegamenti filettati

Coordinatore: Chiar.mo Prof. Roberto Caracciolo

Supervisore: Chiar.mo Prof. Dario Croccolo

Dottorando: Ing. Stefano Fini

SOMMARIO

Lo studio in oggetto ha come obbiettivo l'analisi dei fenomeni che caratterizzano sistemi di giunzione per attrito; come i collegamenti filettati. Questo tipo di giunzione noto ormai da millenni (una delle prime applicazioni è riconducibile ad Archimede) permette di trasformare una coppia torcente in una forza assiale, tipicamente utilizzata per bloccare due o più componenti grazie alle forze di attrito che nascono tra i corpi collegati. Uno dei principali punti di forza di questo tipo di accoppiamento è la possibilità di montare e smontare i particolari collegati oltre ad essere applicabile quasi a qualsiasi tipo di materiale. Per contro il sistema di giunzione è caratterizzato da un basso rendimento: solo una modesta quantità della coppia esercitata al serraggio viene effettivamente convertita in forza assiale. Inoltre la forza assiale ottenuta presenta tipicamente valori variabili all'interno di un ampio intervallo. Questo comportamento è dovuto all'effetto combinato di due distinti momenti d'attrito che nascono in un caso tra il sottotesta della vite o del dado e la superficie di uno degli elementi da bloccare, nell'altro tra i filetti di vite e madrevite. La relazione tra coppia di serraggio ed effettiva forza assiale ottenibile è molto sensibile all'effetto dei vari coefficienti d'attrito: questi coefficienti a loro volta presentano una significativa variabilità dovuta sia ai processi produttivi utilizzati per realizzare i vari componenti che ai diversi parametri di serraggio, come ad esempio la presenza di lubrificazione o la velocità di serraggio. I collegamenti filettati trovano ampia applicazione sia nel campo delle costruzioni civili che nel campo della meccanica, dove a causa di una sempre maggiore spinta verso una riduzione dei pesi ed una maggiore automatizzazione delle procedure di montaggio (si pensi al settore automotive), è necessario avere un accurato controllo sulle prestazioni del collegamento al fine di garantire la sicurezza della giunzione con tempi di assemblaggio e costi ridotti. Al fine di controllare un collegamento filettato occorre focalizzare l'attenzione sui tre principali fenomeni che lo governano: andamento dei coefficienti d'attrito in fase di serraggio, self-relaxation (diminuzione del tiro assiale offerto dalla vite nei primi secondi successivi al serraggio, dovuto ad un assestamento elastoplastico del materiale), self-loosening (perdita di tiro assiale nel tempo tipicamente sotto l'azione di carichi taglianti esterni). Di seguito verrà presentata una panoramica generale sull'argomento tratta dalla letteratura esistente, un'indagine sperimentale sull'effetto della lubrificazione con lubrificante solido sui coefficienti

d’attrito per serraggi ripetuti e diversi trattamenti superficiali e l’effetto del numero di filetti in presa sulle prestazioni di un frenafiletti anaerobico. Queste analisi sono partite dallo studio di un caso reale di self-loosening su un collegamento filettato in un albero pignone di una trasmissione per macchine movimento terra, dove si evidenziano i vari fenomeni che caratterizzano questo tipo di collegamenti. L’attività di ricerca si pone l’obbiettivo di aumentare le conoscenze sull’effetto della lubrificazione sui diversi fenomeni che concorrono a determinare le prestazioni di un collegamento bullonato.

ABSTRACT

This study aims at analyzing the phenomena which characterize threaded connections. This type of joint has been known for thousands years (one of the first applications is attributable to Archimedes) allows transforming a torque into an axial force, typically used to lock two or more components thanks to the friction forces that arise between the connected bodies. One of the main strengths of this type of coupling is the possibility to assemble and disassemble the assembled parts; in addition, it can be applicable to almost any type of material. However, the joint system is characterized by a low efficiency: only a modest amount of the tightening torque is actually converted into axial force. In addition, the obtained axial force is typically affected by a large scatter. This behavior is due to the combined effect of two different friction effects that arise between the under-head of the screw (or nut) and the surface of the elements to be locked in the first case, and between the screw threads and female screw in the second one. The relationship between tightening torque and preload axial force is very sensitive to the effect of the various friction coefficients that rule the tribological behavior of the joint:, these coefficients have a significant variability due to the processes used to manufacture the components, and to the different tightening parameters, such as the presence of lubrication or the tightening speed. Threaded connections do have a wide array of applications, both in the field of civil engineering and in mechanics. For instance, in the automotive compartment, due to a steadily growing strive towards weight reduction and increased automation of assembly procedures, an accurate knowledge of the performance of threaded connections has recently become critical in order to

achieve the safety of the junction at an adequate production cost. In order to control a threaded connection, it is necessary to focus on the three main factors that characterize its behavior: the coefficients of friction at tightening, the self-relaxation phenomenon (decrease of axial preload in the first few seconds after tightening, due to sinking of the load bearing area in the clamped parts), self-loosening (loss of axial preload, typically due to the action of external shearing forces). In the following, literature review will be presented first, then it will be shown an experimental investigation on the effect of solid lubrication on the friction coefficients, carried out for repeated tightenings and different surface treatments. Moreover, the effect of the number of engaged threads on the performance of an anaerobic threadlocking adhesive will be examined. The need for these analyses arose from the study of an in-field failure occurred in a pinion shaft of a transmission for earth moving machines, which, as it will be shown in the following, probably failed due to a combination of the aforementioned typical issues of threaded components. The research has the aim of increasing the knowledge about the effect of lubrication on the different phenomena that contribute to determining the performance of a bolted connection.

TABLE OF CONTENTS

1. GENERAL CONSIDERATIONS ABOUT THREADED CONNECTIONS

1.1 Introduction

Despite of their large diffusion and the great amount of studies conducted on the screw connections there are some different aspects which are not so clarified or the information is not available in the literature. In this first part, a review on the literature is carried out in order to analyze the different aspects which affect the relation between the tightening torque and the axial preload with some insights on the contact between the different parts involved.

1.2 Definition of the characteristic dimensions of a thread

Considering a metric standard profile (ISO M) Fig. 1.1, the thread section is triangular and the thread angle β on the longitudinal section of the screw is equal to 60°.

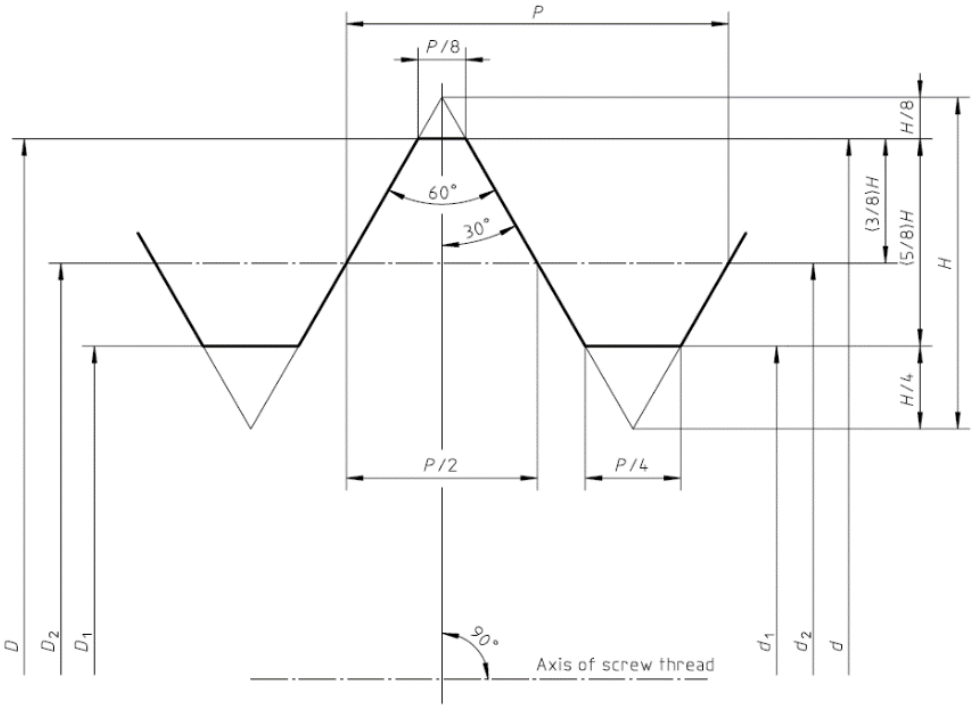

Figure 1.1 The basic metric profile (from ISO 68-1)

Where:

D	is the basic major diameter of internal thread (nominal diameter)
d	is the basic major diameter of external thread (nominal diameter)
D_2	is the basic pitch diameter of internal thread
d_2	is the basic pitch diameter of external thread
D_1	is the basic minor diameter of internal thread
d_1	is the basic minor diameter of external thread
H	is the height of the fundamental triangle: $H = \frac{\sqrt{3}}{2} P$
P	is the pitch

1.3 Relationship Between Tightening Torque and Preloading Force

According to the scheme of Fig. 1.2 and Fig.1.3, it is possible to relate the axial preloading force F_V to the peripheral force F_U by means of the normal force F_N and of the friction force [1].

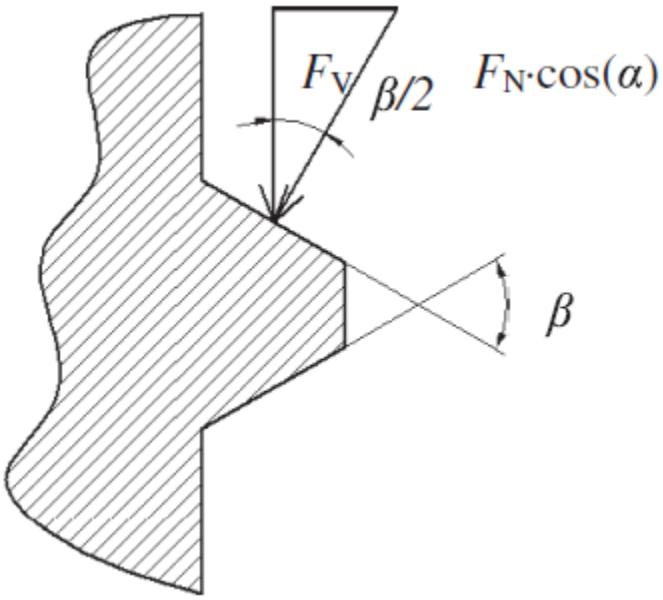

Figure 1.2 Triangular thread in the longitudinal section of the screw

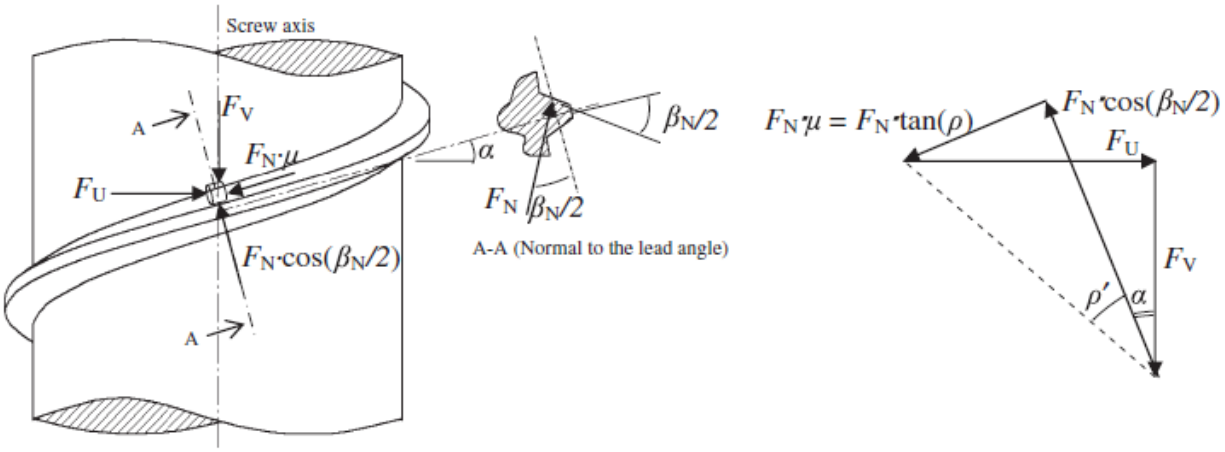

Figure 1.3 An example of a triangular thread and its equilibrium forces

Define the geometrical mean diameter of the thread d_{thm} (mm), according to Equation (1.1); assume μ' as the friction coefficient of the triangular thread and p (mm) as the thread pitch. The force balance yields Equation (1.2) in which angle α is the lead angle of the thread (Equation (1.3)) and angle ρ' is the friction angle of the triangular thread, as reported in Equation (1.4).. Utilizing d_{thm} instead of the effective thread friction diameter d_{th} which depends on thread contact pressure, introduces a comparatively small error [2]

$$d_{thm} = \frac{d + d_1}{2} \tag{1.1}$$

$$F_u = F_v . \tan(\alpha + \rho') \tag{1.2}$$

$$\alpha = \arctan\left(\frac{p}{\pi \cdot d_{thm}}\right) \tag{1.3}$$

$$\mu' = \tan(\rho') \tag{1.4}$$

The friction coefficient of the triangular thread μ', differs from the friction coefficient of the square thread μ, since the thread angle β is measured on the longitudinal section of the screw, as shown in Fig. 1.2. The thread angle β_N (Fig. 1.3) is measured on a section normal to the lead angle α: the angles on the two different planes are linked by a trigonometric relationship,

reported in Equation (1.5). A rigorous calculation of the μ' coefficient is therefore given by Equation (1.6):

$$\tan\beta_N = \tan\beta \cdot \cos\alpha \tag{1.5}$$

$$\mu' = \mu\sqrt{1+\cos^2(\alpha)\cdot\tan^2\left(\frac{\beta}{2}\right)} \tag{1.6}$$

According to [3, 4] and to the force scheme in Figure 1.3, and as a consequence of the small value of angle α, Equation(1.6) transforms into Equation (1.7)

$$\mu' = \frac{\mu}{\cos\left(\frac{\beta}{2}\right)} \tag{1.7}$$

In the case of a metric standard (ISO M) profile the friction force is 15% higher than the equivalent one of the square thread because the friction coefficient of the triangular thread is μ'≈1.155μ: the triangular thread provides, with the same axial preloading force F_V, a friction force greater than that produced by the square thread (15,5% more). The torque T_{th} related to the peripheral force F_U on the screw after tightening, is given by Equation (1.8).

$$T_{th} = F_U \cdot \frac{d_{thm}}{2} = F_V \cdot \tan(\alpha+\rho')\cdot\frac{d_{thm}}{2} \tag{1.8}$$

The total torque T expression must take into account both the thread and the nut friction forces. Thus, Equation (8) must be rewritten as Equation (9) in which μ_A is the friction coefficient and d_b is the effective underhead bearing radius.

$$T = T_{th} + T_b = F_V \cdot \left(\tan(\alpha+\rho')\cdot\frac{d_{thm}}{2} + \mu_A \cdot \frac{d_b}{2}\right) \tag{1.9}$$

If the diameter d_b is assumed equal to the mean of the internal d_{bi} and external d_{be} diameters, an error depending on the pressure distribution in the underhead is introduced [5]. Due to the properties of the tangent function, Equation (1.9) can be rewritten as Equation (1.10):

$$T = T_{th} + T_b = F_V \cdot \left(\frac{\tan(\alpha) + \tan(\rho')}{1 - \tan(\alpha) \cdot \tan(\rho')} \cdot \frac{d_{thm}}{2} + \mu_A \cdot \frac{d_b}{2} \right) \tag{1.10}$$

Substituting Equations (1.3, 1.4, 1.7) into Equation (1.10) it is possible to obtain Equation (1.11), in the form reported by Shigley and Mischke [6], and Juvinall and Marshek [7]:

$$T = F_V \cdot \left(\frac{\frac{p}{\pi \cdot d_{thm}} + \frac{\mu}{\cos\left(\frac{\beta}{2}\right)}}{1 - \frac{p}{\pi \cdot d_{thm}} \cdot \frac{\mu}{\cos\left(\frac{\beta}{2}\right)}} \cdot \frac{d_{thm}}{2} + \mu_A \cdot \frac{d_b}{2} \right) \tag{1.11}$$

Since $p/(\pi d_2) \cdot (\mu/\cos(\alpha/2))$ is negligible with respect to 1, Equation (1.11) becomes Equation (1.12), originally proposed by Motosh [8]:

$$T = F_V \cdot \left(\frac{p}{2 \cdot \pi} + \frac{\mu}{\cos\left(\frac{\beta}{2}\right)} \cdot \frac{d_{tm}}{2} + \mu_A \cdot \frac{d_{hm}}{2} \right) \tag{1.12}$$

For the metric standard (ISO M) profile, Equation (1.12) can be rewritten as Equation (1.13):

$$T = F_V \cdot \left(0.159 \cdot p + 0.577 \cdot \mu \cdot d_{thm} + \mu_A \cdot \frac{d_b}{2} \right) \tag{1.13}$$

By applying Equation (1.11), the preloading force F_V can be related to the total torque T once the friction coefficients μ and μ_A are known and it is well known that these coefficients are strongly influenced by the surface status or treatment (roughness or presence of lubricant and material deposition). In this formulation, it was neglected the three-dimensional effect which affects the torque T: such approximation introduces a very small error, in the order of 0.5% for a uniform contact pressure in the threads and a low dependence from the friction coefficient and the pitch. On the opposite, equation (1.13) introduces an error of 2% for the same contact pressure condition and a noticeable dependence from the pitch and the thread friction coefficient. [9]

1.4 Considerations about the actual underhead and thread diameter in the case of a uniform contact pressure

In the previous section, it was illustrated how the bearing and thread diameters influence the relationship between tightening torque and preload in bolted joints(Equations (1.11,1.13)). Some hypotheses were introduced during the calculation of these diameters, in order to simplify the analytical solution. These assumptions are based on research carried out by Nassar et al. [2] [5]. The first of these is to consider the mean geometrical underhead and thread diameter, instead of the actual one. The second assumption is that the friction coefficient is constant over the thread or in the underhead surfaces. Generally, the friction coefficient varies over the bolt surfaces due to the variation in the sliding speed, as the radial location from the fastener axis changes. A method to describe the variation is given by Rabinowicz [11] as:

$$\mu_r = \mu_i \cdot \left(\frac{r_i}{r} \right)^{0.1} \tag{1.14}$$

Where μ_i is the value of the coefficient of friction in the contact point nearest to the minor radius $r_{\min}$ and r is the generic radius. For the purpose of calculating the magnitude of the error introduced with the mean geometrical diameters and the constant friction coefficient, a weighted average of the thread friction coefficient may be calculated:

$$\mu_{average} = \frac{\int_{r_i}^{r_e} \mu_r dA}{\int_{r_i}^{r_e} dA} \tag{1.15}$$

For the thread, dA becomes:

$$dA = 2\pi \cdot r \frac{dr}{\cos\beta} \tag{1.16}$$

$$\mu_{average} = \mu_i \left(\frac{1.052\left(\gamma_t^{1.9} - 1\right)}{\gamma_t^{2} - 1} \right) \tag{1.17}$$

Where:

$$\gamma_t = \frac{r_{the}}{r_{thi}} \tag{1.18}$$

r_{the} and r_{thi} are respectively the external and the internal contact radius of the thread. At the end of fastener tightening, the amount of torque for the generic thread T_i, consumed to overcome thread friction is:

$$T_i = \int_A \mu_r \cdot P \cdot r dA \tag{1.19}$$

Considering the mean friction coefficient and the effective thread contact radius, the torque needed to overcome thread friction can be written as:

$$T_i = \mu_{average} \cdot \frac{F_i}{\cos\beta} \cdot r_t = \mu_{average} \cdot r_t \cdot 2\pi \cdot \int_{r_{thi}}^{\gamma r_{thi}} P \cdot r dr \tag{1.20}$$

Substituting Equation. (1.14) into Equation(1.19), and Equation(1.17) into Equation (1.20) and comparing the resulting expressions for T_i, the effective thread friction radius r_{th} results as follows:

$$r_{th} = \frac{\left(\gamma^2 - 1\right) \cdot r_{thi}^{\,0.1}}{1{,}052 \cdot \left(\gamma^{1.9} - 1\right)} \cdot \frac{\int_{r_{thi}}^{\gamma r_{thi}} r^{1.9} \cdot P dr}{\int_{r_{thi}}^{\gamma r_{thi}} r \cdot P dr} \tag{1.21}$$

Assuming P(r)=constant, Equation (1.21) becomes:

$$r_{th} = \frac{\left(\gamma_t^{\,2} - 1\right) \cdot r_{thi}^{\,0.1}}{1.052 \cdot \left(\gamma_t^{\,1.9} - 1\right)} \cdot \frac{\frac{1}{2.9} \cdot \left(\gamma_t^{\,2.9} - 1\right)}{\frac{1}{2} \cdot \left(\gamma_t^{\,2} - 1\right)} \cdot r_{thi}^{\,0.9} = \frac{0.656 \cdot \left(\gamma_t^{\,2.9} - 1\right)}{\left(\gamma_t^{\,1.9} - 1\right)} \cdot r_{thi} \tag{1.22}$$

Repeating the same procedure for the bearing radius, *dA* and $\mu_{baverage}$ in the underhead become:

$$dA = 2\pi \cdot r \cdot dr \tag{1.23}$$

$$\mu_{average} = \mu_i \left(\frac{1.052\left(\gamma_b{}^{1.9} - 1\right)}{\gamma_b{}^{2} - 1} \right) \tag{1.24}$$

Where:

$$\gamma_b = \frac{r_{be}}{r_{bi}} \tag{1.25}$$

r_{be} and r_{bi} are respectively the external and the internal contact radius of the head. At the end of fastener tightening, the amount of torque in the underhead T_b consumed to overcome the friction torque is:

$$T_b = \int_A \mu_r \cdot P \cdot r dA \tag{1.26}$$

Considering the mean friction coefficient and the effective underhead contact radius, the torque dissipated to overcome friction in the underhead can be written as:

$$T_b = \mu_{average} \cdot F_v \cdot r_b = \mu_{average} \cdot r_b \cdot 2\pi \cdot \int_{r_{bi}}^{\gamma_b r_{bi}} P \cdot r dr \tag{1.27}$$

Substituting of Equation. (1.14) into Equation (1.26), Equation.(1.23) into Equation (1.27) and comparing the resulting expressions for T_b, the effective bearing friction radius r_b can be written as reported in Equation (1.28):

$$r_b = \frac{\left(\gamma_b{}^{2} - 1\right) \cdot r_{bi}{}^{0.1}}{1.052 \cdot \left(\gamma_b{}^{1.9} - 1\right)} \cdot \frac{\frac{1}{2.9} \cdot \left(\gamma_b{}^{2.9} - 1\right)}{\frac{1}{2} \cdot \left(\gamma_b{}^{2} - 1\right)} \cdot r_{bi}{}^{0.9} = \frac{0.656 \cdot \left(\gamma_b{}^{2.9} - 1\right)}{\left(\gamma_b{}^{1.9} - 1\right)} \cdot r_{bi} \tag{1.28}$$

For metric screws with hexagonal head designed according to ISO 4017, and for the most common dimensions from M6 to M48, the value of Υ_{th} and Υ_b vary within a small range. (see

Fig.1.4). Introducing the Υ_{th} and Υ_b values in Equations (1.22) and (1.28) one can calculate the errors introduced by considering the average diameters in place of the effective diameters, under the assumption of a constant contact pressure distribution.

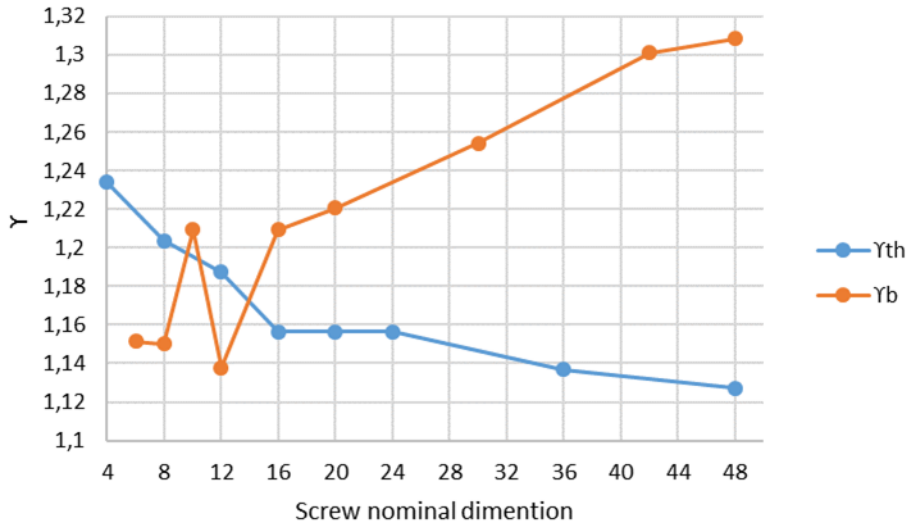

Figure 1.4 ϒth and ϒb trend for the different screw nominal diameter

Considering the mean underhead radius r_{bm} instead of the effective radius r_b, for a constant pressure distribution, the error introduced on the bearing radius equation (1.29) has the trend reported in Fig.1.5 as a function of Υ_b. For the hexagonal head screw this error is low but for a flanged screw it can grow up to more than 2%.

$$error\% = \frac{r_b - r_{bm}}{r_b} \tag{1.29}$$

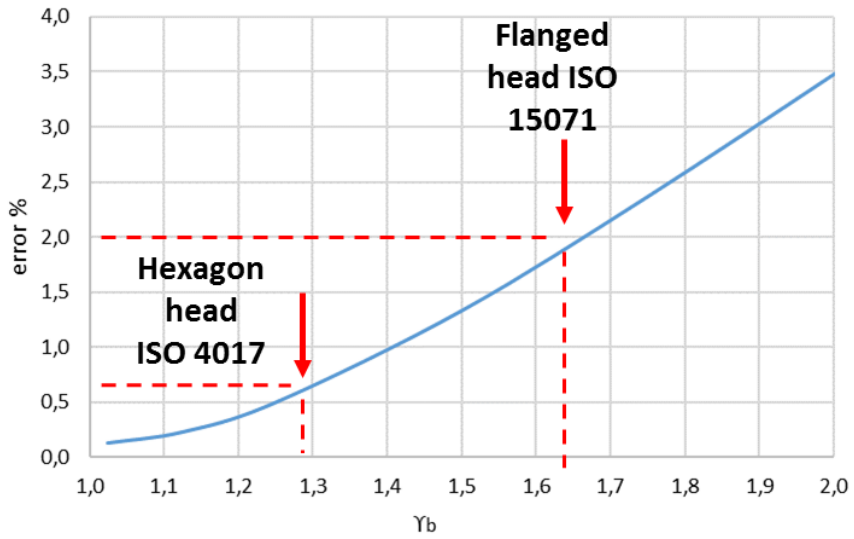

Fig 1.5 error on the underhead radius considering the mean radius instead of the effective radius, reported for the different values of Υ_b

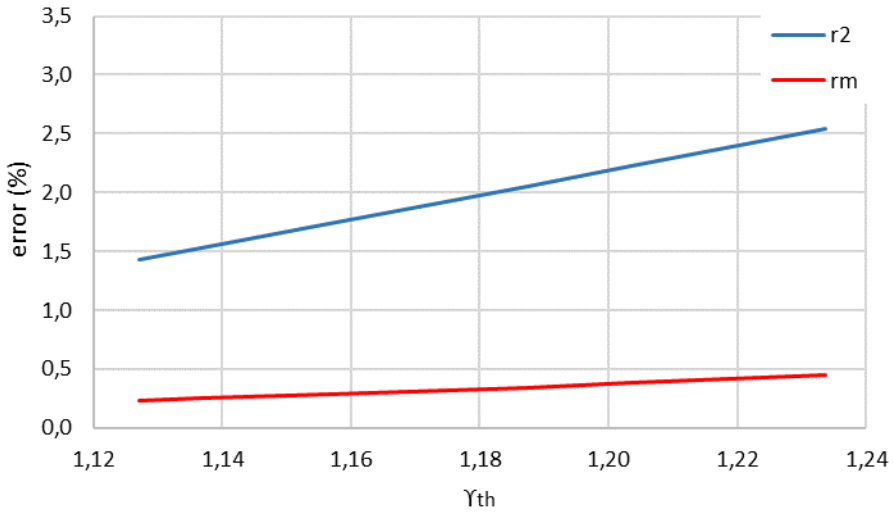

Fig 1.6 error on the thread radius considering the mean or the pitch radius instead of the effective radius, reported for the different values of Υ_{th}

For the thread radius, the value of Υ_{th}, decreases with the increase of the nominal diameter of the screw and with the decrease of the pitch (Fig.1.4). The error introduced when the mean diameter is adopted instead of the effective thread diameter equation (1.30) is negligible (less than 0,5%)), but when the pitch radius r_2 is adopted instead of the mean radius, such error grows up to values between 1.5% and 2.5%, depending on the screw size.

$$error\% = \frac{r_m - r_{th}}{r_{th}} \tag{1.30}$$

1.5 Considerations about the actual underhead and thread diameters, in the case of real contact pressure distribution

In the previous section, it was shown how the effective contact diameter can be calculated for the thread and the underhead, under the assumption of constant pressure distributions on such surfaces. In general, the real pressure distribution could be very different from a uniform one, as some authors have already reported [2,5,9,12,13,14,15]. In order to evaluate the error introduced considering a constant pressure distribution instead of the actual one, the real thread contact radius and bearing contact radius were calculated for the real pressure distribution. In order to understand the effective pressure distribution in the thread and in the underhead, finite elements analyses (FEA) were performed, considering the commonly used fasteners with standard hexagonal head.

In the case of the underhead, FEA has been performed on a screw-sleeve assembly. The primary purpose of such analysis was correlating the shape of the screw head to a pressure distribution in the case of a standard hexagonal head metric screw, size M8 and class 8.8, coupled with asleeve made of steel. The screw geometry was modeled according to the international standard ISO 4017. The secondary aim of this FEA analysis was to assess how the pressure distribution in the underhead is affected by a change in sleeve materials., The specimen was modeled in two dimensions, enforcing the axial symmetry of the model around y-axis (Figure 1.7).

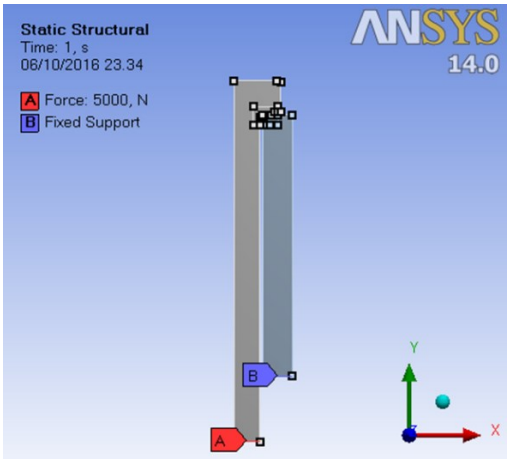

Figure 1.7 boundary conditions for the axisymmetric model

The geometry was meshed with three-node triangular elements (PLANE 182 in the Ansys nomenclature). The resulting mesh is shown in Figure 1.3: a refinement window can be seen in the central area of the head. The general element size is set to d=0.5mm, whereas in the

refinement window it drops down to d'=0.025mm. In order to found the correct mesh sizing in the contact region, a convergence analysis was carried out. In order to achieve a progressive contact line counting at least ten elements [16,17,18] the contact region between the screw head and the sleeve underwent a further refinement of the mesh, resulting in an element size of d''=0.001mm The overall number of nodes is n=144719.

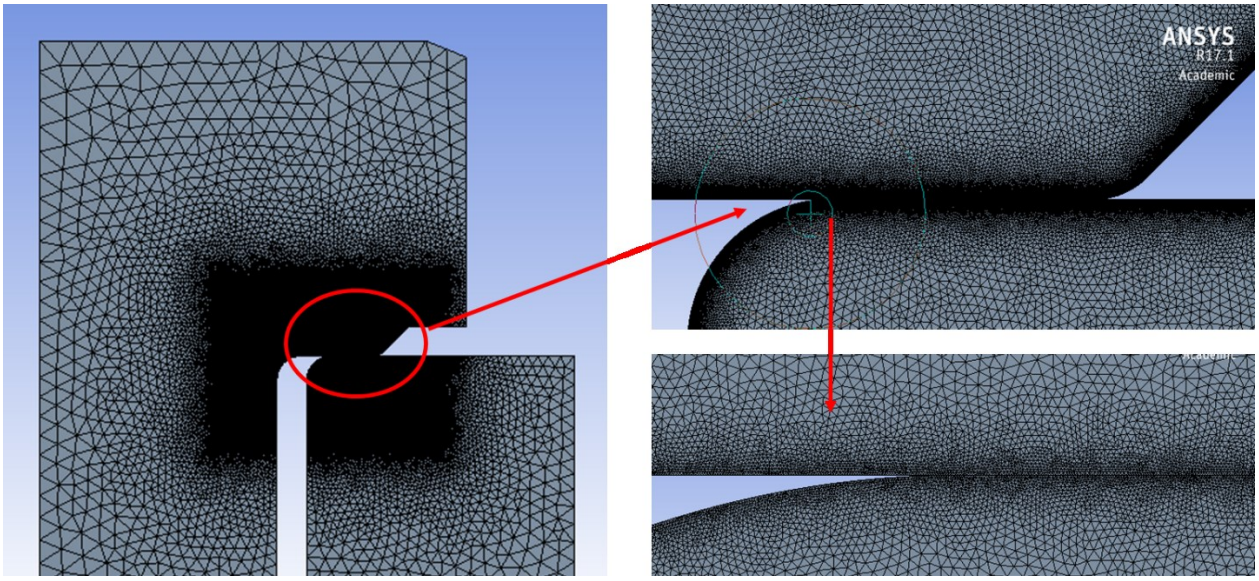

Figure 1.8 Not deformed mesh of the FEA model (under head region)

The contact between the head and the sleeve is set as frictionless after a comparison between the results obtained with this condition and a friction coefficient set a 0.15 (Fig.1.9). The differences were found to be negligible and the frictionless condition has been chosen, in the light of its lower computational demand. The screw preload is simulated by a force applied at the lower end of the shank Fv=20,000N approximately equal to the preload recommended for an 8.8 screw by the International standard ISO 898-1. The free face of the sleeve was fixed. The analysis was carried out considering the elastic-plastic properties of the materials: a bilinear isotropic hardening behavior was assumed. The material properties are reported in Tab. 1.1.

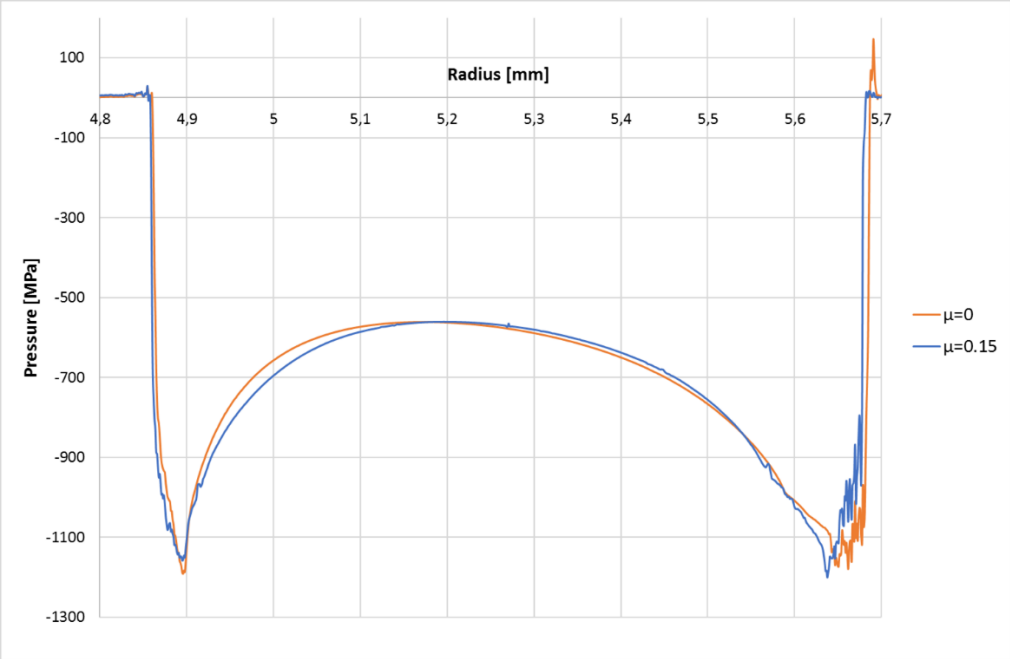

Figure 1.9 comparison between frictionless and frictional analysis

Table 1.1. materials properties

MATERIAL	UTS [Mpa]	Sy [Mpa]	A%	Elastic Modulus [Mpa]	Poisson ratio v	Ref.
EN AW 7075	540	485	7	72000	0,33	EN 755-2
Ti6Al4V	860	780	10	113800	0.342	ISO 5832-3
EN-GJS-500-7C	500	320	7	169000	0,275	EN 1563
42CrMo4	800	640	12	210000	0,30	ISO 898-1

Focusing on the underhead contact area, the resulting normal stress distribution along y-axis is shown in Fig. 1.10. It can be seen that the normal stress show peaks at the inner and at the external radius of the thread, as expected for the case of a rounded indenter pushed against an elastic half-plane. This result is also consistent with the surface texture of the underhead area observed after tightenint: wear appears to be concentrated at the outer and inner boundaries of the contact region (Fig 1.11, from [19]).

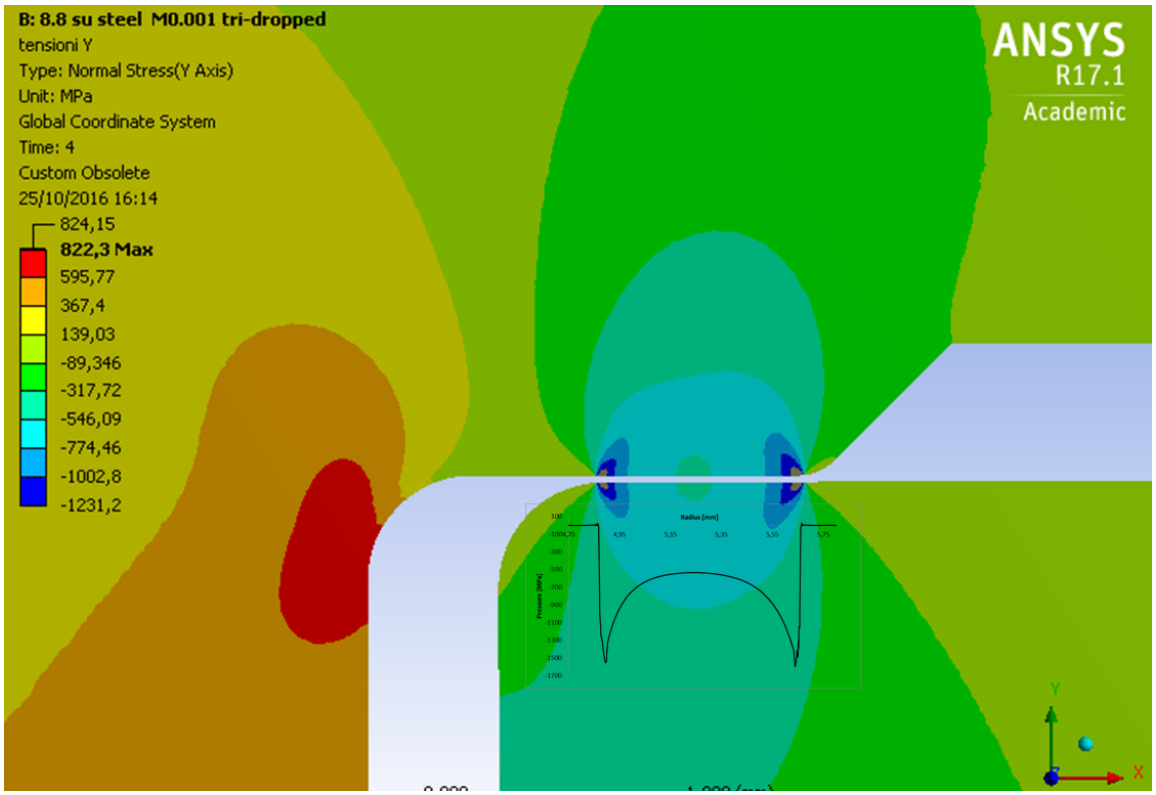

Figure 1.10 Normal pressure distribution (underhead region)

Figure 1.11 Surface texture after the tightening of an hexagonal

metric screw over an aluminum sleeve

For different sleeve materials, the normal stress distribution in the underhead keeps the same trend shown for steel in Figures 1.9 and 1.10, but with some difference in the peak values due to the different elastic modulus and elastic plastic behaviors (see Fig.1.12)

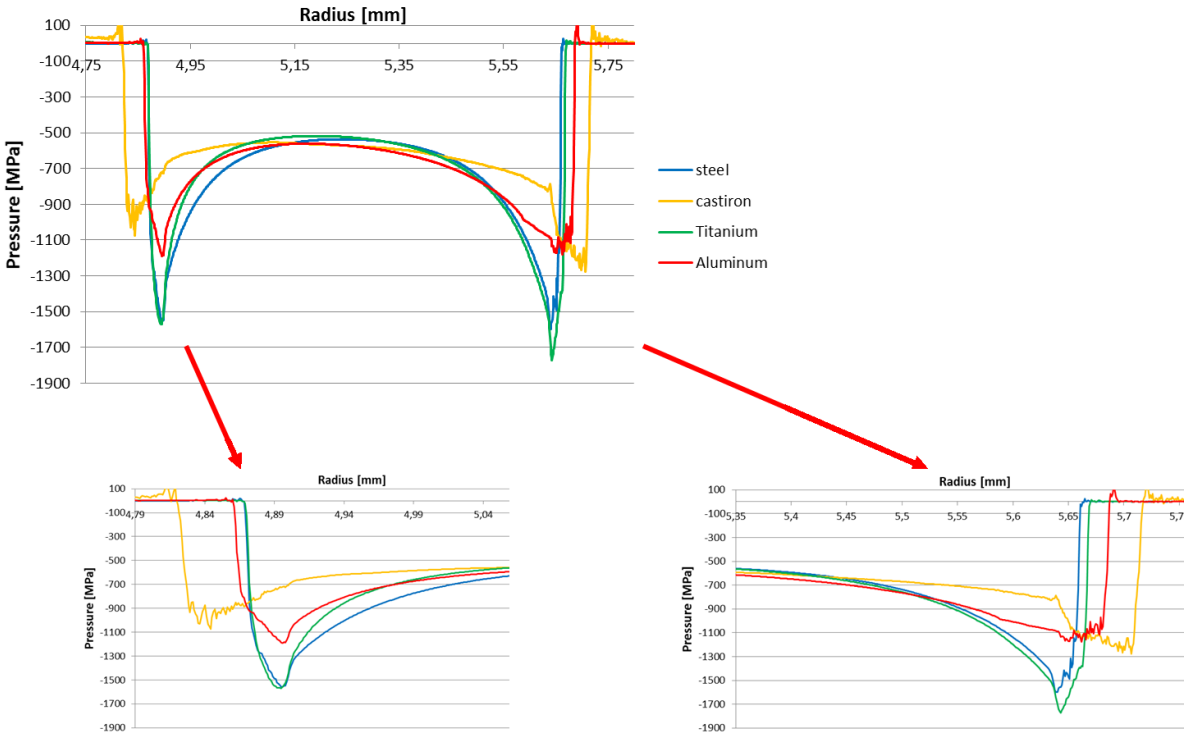

Figure 1.12 Contact pressure distribution in the underhead region

Considering the normal stress distribution on the contact surface, it is possible to calculate by a numerical integration the effective contact radius for the different sleeve materials. The results obtained by the numerical integration are reported in Tab. 1.2 with the percentage difference obtained comparing this radius with the radius obtained by Equation (1.28) and with the mean geometrical radius.

Table 1.2. Error in the bearing radius

material	Effective bearing radius r_e [mm]	mean geometric radius r_m [mm]	teorical bearing radius r_b [mm]	error % r_e vs r_m	error % r_e vs r_b
42CrMo4	5,283	5,265	5,279	0,34%	0,07%
EN-GJS-500-7C	5,306			0,77%	0,50%
Ti6Al4V	5,305			0,76%	0,49%
EN AW 7075	5,303			0,73%	0,46%

Considering the results reported in Tab 1.2 the percentage error introduced by using r_m instead of r_b, in the calculation of the bearing friction torque component, for standard hexagonal head screw, is very low.

For the thread contact, a FEA has been performed on a screw-sleeve assembly with a threaded sleeve. The primary purpose of such analysis was to understand the real behavior of the normal pressure on the thread surface: in the literature [2,5,9,12], some different pressure distributions on the thread are reported an the different effect on the effective thread radius are analyzed, but it is not identified a specific trend as the most likely occurring for the standard ISO thread. The screw and the thread of the sleeve were modeled according to the international standard ISO 4017 and following the tolerance recommended by ISO 965-1 for a thread connection combination 6H/6g. To model the components, tolerances corresponding to the maximum clearance condition have been used. The screw adopted for the analysis was a M8 class 8.8. In order to proceed with a FEA simulation, the specimen has been modeled in two dimensions, enforcing the axial symmetry of the model around y-axis (Fig.1.13).

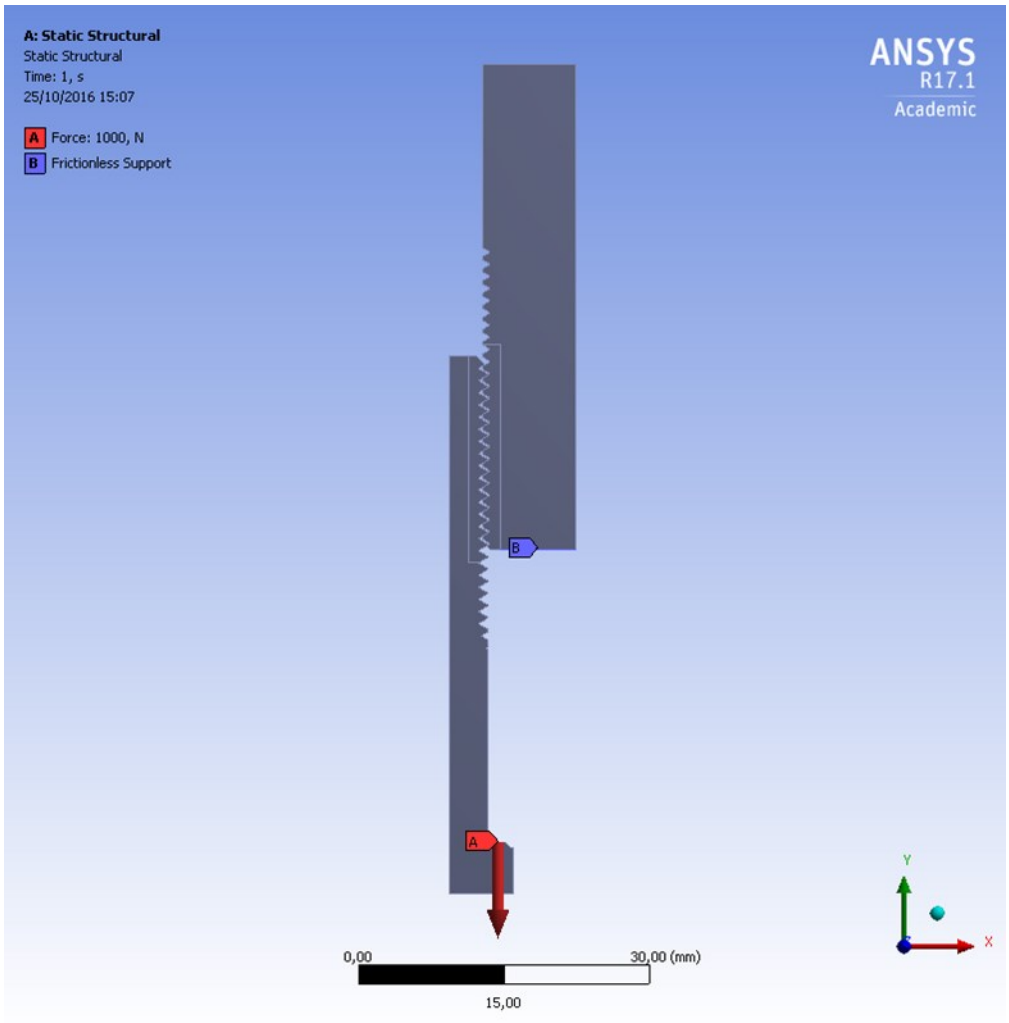

Figure 1.13boundary conditions for the axisymmetric model

The geometry has been meshed with three-node triangular elements (PLANE 182 in the Ansys nomenclature) The mesh is shown in Fig. 1.14: a refinement window can be seen in the central area. The general element size is d=0.5mm, whereas in the refinement window it drops down to d'=0.03mm. In order to find the correct mesh sizing in the contact region a convergence analysis was carried out. In the contact region between the screw head and the sleeve, a further refinement of the mesh was carried out, following the lines described above, with an elements size d''=0.0015mm The overall number of nodes is n=535849

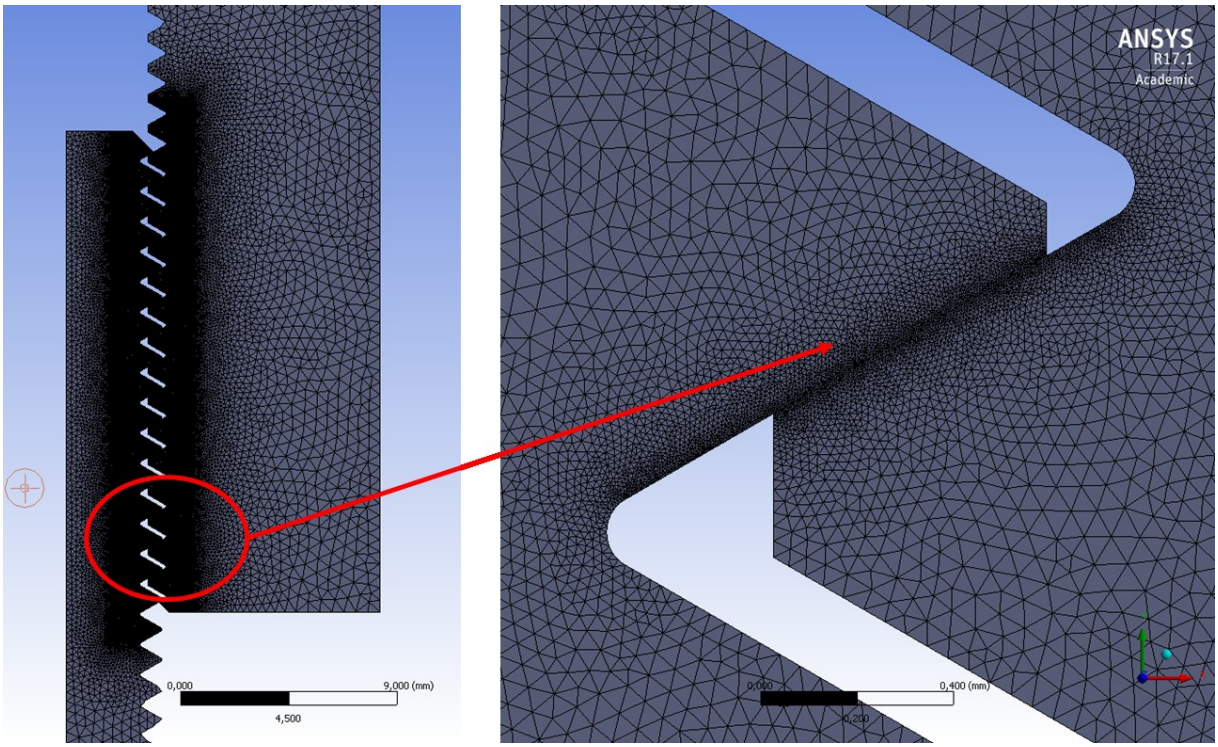

Figure 1.14 Not deformed mesh of the FEA model (threaded region)

The contact between the threads is set as frictionless. The screw preload is simulated by a force applied at the underhead surface, equal to F_V=20000 N (incremented in four load steps from 5000N to 20000N) corresponding to the preload recommended for an 8.8 screw by ISO 898-1;the face of the sleeve was constrained by means of a frictionless support. The analysis was carried out considering the elastic-plastic properties of the materials with a bilinear isotropic hardening behavior. The materials properties are reported in Tab. 1.1. The analysis was carried out considering steel 42CrMo4 (commonly adopted for manufacturing 8.8 screws) and the same steel for the sleeve in the first case, whereas in the second case aluminum EN AW 7075 was selected for the sleeve.

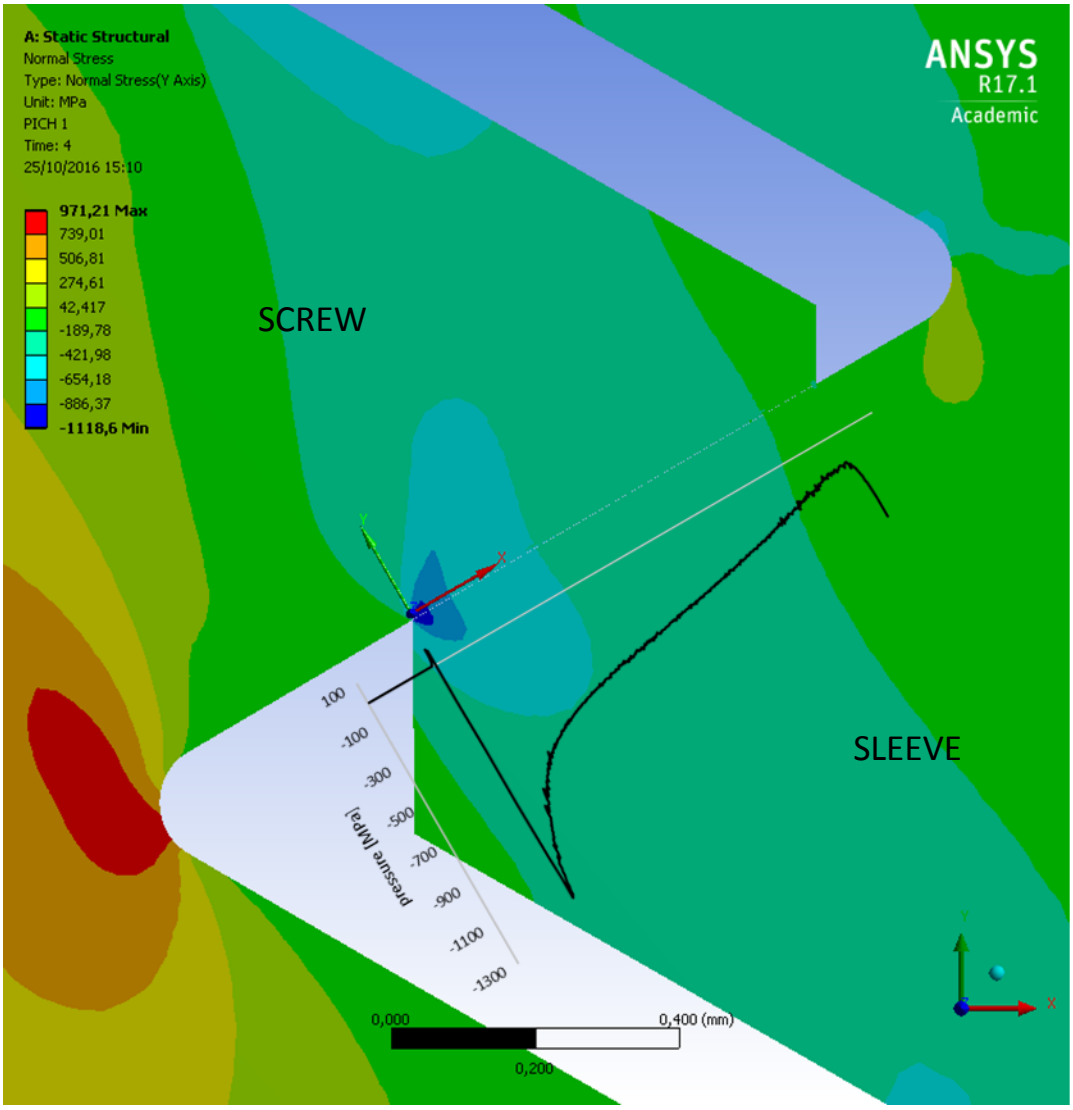

Figure 1.14 Contact pressure distribution (threaded region screw and sleeve in steel)

The resulting normal stress distribution along the y-axis (local coordinates system with Y-axis normal to the thread flank, X-axis parallel to the flank) is shown in Fig.1.15. It can be seen that; the normal stress is concentrated at the inner contact radius of the thread in the steel case. This behavior it is due to the greater stiffness of the sleeve thread. The tolerances adopted: 6g for the screw and 6H for the sleeve thread, is the most common in the practice. The thread dimensions resulting from this choice reduce the stiffness of the screw thread with respect to the sleeve thread. In fact, for the aluminum bushing, the pressure peak drops on the inner radius and the outer radius increases rather. (Fig. 1.15). The effective pressure distribution resulting in two peaks comparable to the extremes of the supporting surface. Considering the normal stress distribution on the contact surface, it is possible to calculate by a numerical integration the effective contact radius. The results obtained by the numerical integration are reported in tab. 1.3 with the percentage difference obtained comparing this radius with: the pitch radius r_2

suggested in the international standard VDI 2230 and adopted by several authors [14,15,19], the radius r_{th} obtained by the equation (1.22) and the mean geometrical radius r_{thm}.

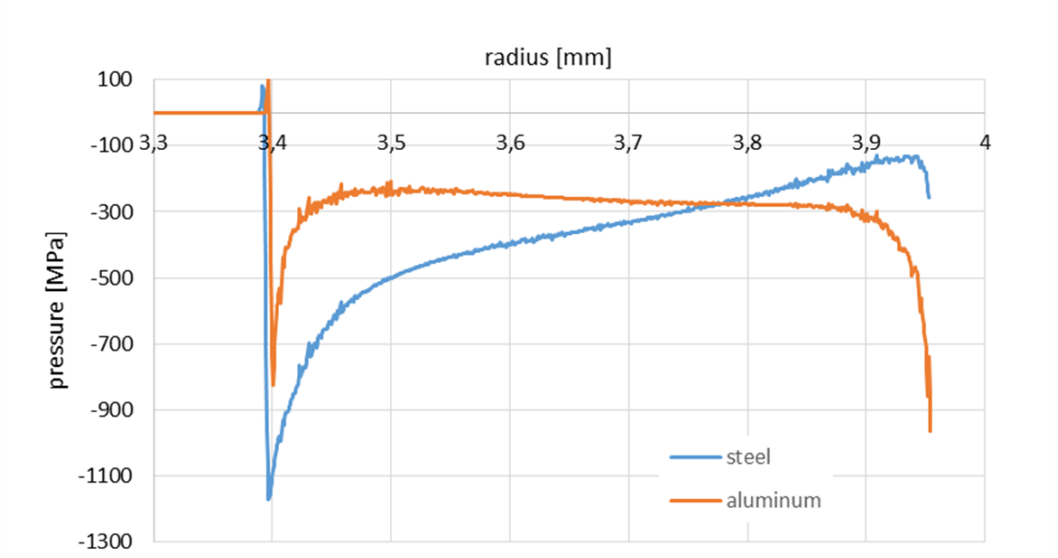

Figure 1.15 Contact pressure distribution in the thread region

For the two different materials of the threaded sleeve, it has been observed a different load distribution between the threads. Fig 1.16 The results obtained are similar to those reported in the literature [20].

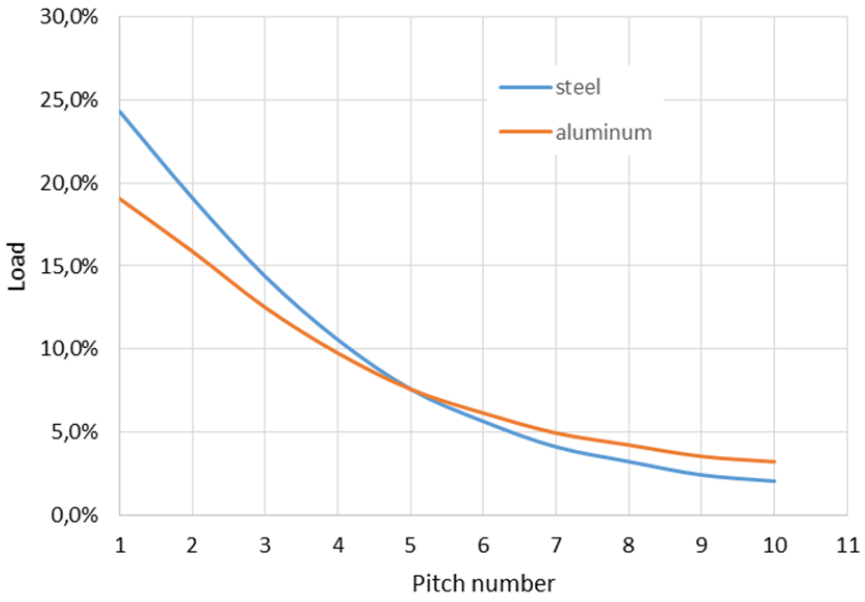

Figure 1.16 Load distribution in the first ten thread (90% of the total load). The first is the closest to the loaded face of the bushing

Each thread supports a different amount of load, but the trend of the pressure distribution is always similar. In fact, repeating the numerical integration for each thread the effective contact radius remain always the same. The difference between the different threads is negligible. Considering the results reported in Tab 1.3 the percent error introduced by using r_2 instead of the effective thread radius obtained by the numerical analysis is, inexistent for the steel sleeve. While for the aluminum sleeve the minor error are obtained using the mean radius r_{thm}.

Table 1.3. Error in the thread radius

material	Effective thread radius r^{eth} [mm]	mean geometric radius r^{thm} [mm]	teorical thread radius r^{th} [mm]	pich radius r^2 [mm]	error % re vs r^{th}	error % re vs rm	error % re vs r^2
42CrMo4	3,60	3,66	3,68	3,59	-1,71%	-2,10%	0,17%
EN AW 7075	3,68				0,46%	0,08%	2,30%

1.6 Discussion

Starting from the general equations proposed by Motosh and Shygley they were analyzed the effects of the pressure distribution and the speed on the thread and bearing radius following the consideration proposed by Nassar et al. In order to verify the equations proposed and clarify the real pressure distribution in the thread and in the underhead, some FEA analysis were performed. The result of this analysis have highlighted that for the hexagonal head screw, considering the mean geometrical radius of the underhead contact area is a good aproximation of the real condition as well as considering the pitch diameter instead of the effective thread diameter, at least when the screw and the nut are both in steel. When the nut is in aluminum the mean thread diameter, represent a better approximation.

1.7 References of the chapter

[1] D. Croccolo N. Vincenzi,(2011) Tightening Tests and Friction Coefficients Definition in the Steering Shaft of Front Motorbike Suspension, Strain 47, 337-342, DOI: 10.1111/j.1475-1305.2009.00694.x

[2] Sayed A. Nassar, Payam H. Matin, G. C. Barber, (2005) Thread Friction Torque in Bolted Joints, Journal of Pressure Vessel Technology 127, 387-393, DOI: 10.1115/1.2042474

[3]. VDI Handbuch Konstruktion 2230. (2001) Systematische Berechnung hochbeanspruchter Schrauberverbindungen Zylindrische Einschraubenverbindungen – Systematic calculation of high duty bolted joints – Joints with one cylindrical bolt, 1–94.

[4]. Niemann, G., Winter, H. and Hohn, B. R. (2005) Maschineelemente B.d I. Springer-Verlag, Berlin.

[5] Sayed A. Nassar, G. C. Barber, Dajun Zuo, (2005) Bearing Friction Torque in Bolted joints, Tribology Transaction, 48, 69-75, DOI: 10.1080/05698190590899967

[6] Shigley, J. E., and Mischke, C. R., 1989, Mechanical Engineering Design, 5th ed., McGraw-Hill, New York, Chap. 8.

[7] Juvinall, R. C., and Marshek, K. M., 2000, Fundamentals of Machine Component Design, 3rd ed., Wiley, New York.

[8] Motosh, N., 1975, "Load Distribution on Threads of Titanium Tension Nuts and Steel Bolts," ASME J. Eng. Ind., 97(1), pp. 162–166.

[9] Sayed A. Nassar, Xianjie Yang, (2007) Novel Formulation of the Tightening and Breakaway Torque Components in Threaded Fasteners, Journal of pressure Vessel Tecnology 129, 653-663, DOI: 10.1115/1.2767354

[10] Chiang, Y.; Nassar, S.A.; Barber, G.C., (2006) Multi-variable effects of fastening parameters on stress development at bolt threads, SAE Technical Papers 129, DOI: 10.4271/2006-01-1253;

[11] Rabinowicz, Ernest, 1965, Friction and Wear of Materials, Wiley, New York, pp. 60-61

International journal of material and product technology

[12] Sayed A. Nassar, Tianshu Sun, Qian (Beth) Zou, (2006) The Effect of Coating and Tightening Speed on the Torque-Tension Relationship in Threaded Fasteners, SAE Technical Papers 1252

[13] S. A. Nassar, H. El. Khiamy, G. C. Barber, Q. Zou, T. S. Sun, An Experimental Study of Bearing and Thread Friction in Fasteners, Jurnal of tribology 2005 127(2) pp.263-272 DOI: 10.1115/1.1843167

[14] Friedrich, C. , Koch, D. , Dinger, G. , Force transfer behavior of mechanically fastened structures in light weight design, Proceedings of IMECE 2008 ASME International Mechanical Engineering Congress and Exposition, Boston, MA; United States, Paper No. IMECE2008-66873, pp. 229-236; DOI:10.1115/IMECE2008-66873

[15] Kopfer, H. , Friedrich, C. , Gerhard, T. , Advanced design of screw joints with transverse loading and light materials , Proceedings of ASME 2010 International Mechanical Engineering Congress and Exposition British Columbia, Canada, Paper No. IMECE2010-38148, pp. 541-547; doi:10.1115/IMECE2010-38148

[16] 0. A. Olukoko, A. A. Becker, R. T. Fenner, Three benchmark examples for frictional contact modelling using finite element and boundary element methods ,1993, The Journal of Strain Analysis For Engineering Design 28 (4), pp. 293-301

[17] A Strozzi, A Baldini, M Giacopini, E Bertocchi, L Bertocchi, Normalization of the stress concentrations at the rounded edges of a shaft-hub interference fit, 2011 The Journal of Strain Analysis For Engineering Design 46 pp.1-14 DOI: 10.1177/0309324711403845

[18] D. Croccolo, M. De Agostinis and N. Vincenzi, Normalization of the stress concentrations at the rounded edges of a shaft–hub interference fit: extension to the case of a hollow shaft, 2012 The Journal of Strain Analysis For Engineering Design 47(3) pp.131-139 DOI: 10.1177/0309324712439982

[19] Kopfer H, Friedrich C, De Agostinis M, Croccolo D. Friction characteristics in light weight design focusing bolted joints. ASME 2012 International Mechanical Engineering Congress and Exposition, IMECE 2012; Houston (Texas); United States; 9 November 2012 through 15 November 2012; Code 100737.

[20] E. Dragoni, Effect of thread pitch on the fatigue strength of steel bolts, Proceedings of the Institution of Mechanical Engineers, Part C: Journal of Mechanical Engineering Science, 1997 211 (8), pp. 591-600 doi: 10.1243/0954406981521970

2. ANALYSIS OF THREADED CONNECTIONS FOR DIFFERENTIAL GEAR PINIONS

2.1 Introduction

The present analysis deals with the failure analysis of a pinion shaft belonging to a differential gear for offroad machinery applications, namely wheel loaders. The motivations of the study arise from some in-field failures, which resulted in the fracture of the pinion shaft, originated at an external groove located at the end of its threaded portion. The issue has been tackled by means of analytical, numerical and experimental tools. The observed failures have been demonstrated to be due to the in-service loosening of a ring nut, whose function is to preload the tapered rolling bearings, which support the shaft.

In a wheel loader the primary power from the diesel engine is split up between hydraulics and drive train: the first one is responsible for lift/tilt movements of the bucket, whereas the latter transfers power to the wheels. The typical layout of hydraulic and mechanical powertrain is applicable not only to wheel loaders but also to many other working machines in the fields of agriculture, forestry and mining. Many details, including also schemes and drawings are contained in [1, 2]. Moreover, some interesting historical issues with related powertrain schemes, regarding the development of hybrid wheel loaders are also reported in [3]. The studied pinion shaft transmits the torque from the engine to the drive wheels through the crown wheel of the differential gear. It is supported during rotation by two tapered single row rolling bearings that are axially preloaded by means of a ring nut, which in turn engages with an external thread, cut into the shaft tail end Fig. 2.1a. After tightening, the inner races of the bearings come in contact by means of a sleeve and some laminated shims. The tightening operation is performed in torque control, by means of an electric spindle.

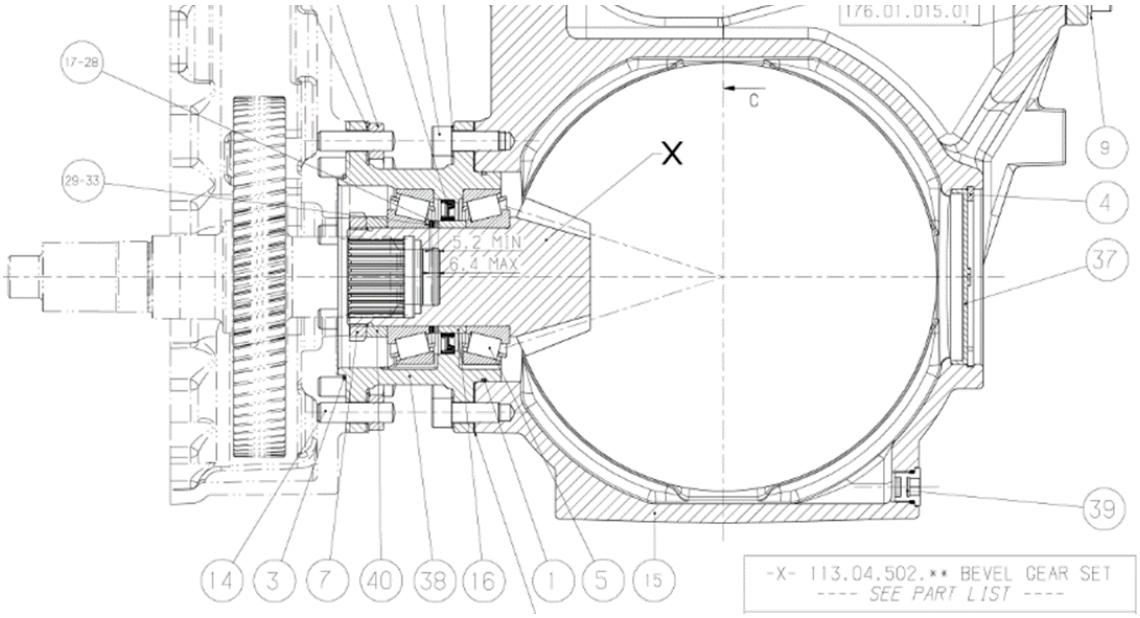

Figure 2.1a Pinion shaft assembly

An observation of the fracture surface of some failed shafts indicates that fracture always propagates along the cross section of the shaft, whereas final fracture occurs on a 45 inclined surface with respect to the shaft axis, as shown in Fig. 2.1b, where the cracked transverse section is highlighted, and the region of final failure is also marked.

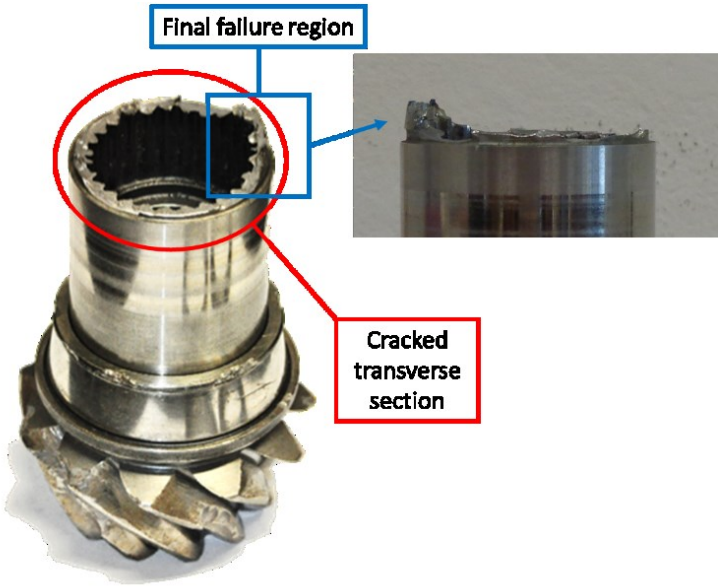

Figure 2.1b Failed pinion shaft

The inner splined that mates with the flywheel shaft is clearly visible by the tail side of the pinion shaft. The position of the cross section where failure occurs is well aligned along the shaft longitudinal axis to the groove at the end of the ring nut external thread. It must be pointed out that other similar groups did not experience complete failure, but an unexpected loosening of the ring nut, with resulting loss of bearing preload, was observed. The occurrence of the described breakage was the main motivation for this study, whose aim was to investigate the primary reason for the occurred failure. The investigation of the root cause of the observed ring nut loosening was a further point of discussion. It was finally important to state if this occurrence was likely to trigger the shaft complete failure and to indicate possible design improvements to overcome the described events. Considering the literature in the field of failure analysis, it must be pointed out that no studies are available, regarding similar fractures in a wheel loader pinion group. However, several investigations are reported on fatigue failures involving shafts in industrial applications. For instance, in [4] the failure of an extruder shaft is investigated by experimental in-field tests, material characterization and numerical models. The fracture of an agitator shaft in a pressure vessel is investigated in [5], where a careful analysis of the crack shape precedes numerical modeling. Analytical and numerical tools, as well as a careful fracture surface analysis, are finally used in [6], to explore the causes of the failure of a lift drive shaft operating under fatigue. The literature survey generally indicates that the combined use of experimental,

analytic and numerical tools along with a careful observation of the fracture surface is usually the most proper approach to tackle a failure analysis.

Based on the reported outcomes, after a detailed analysis of the fracture surface, strain gauge tests were performed to determine the actual state of load, a lumped parameter model was developed to determine a suitable stiffness scheme and numerical models were used to estimate the state of stress.

2.2 Materials and methods

Some failed pinions shafts have been observed by an optical multifocus microscope, in order to study the failure mechanism, as suggested by the approach followed in a previous study [7]. The static and fatigue dimensioning of the shaft has been assessed, under the assumption that the bearings were preloaded properly. The analysis of the shaft has been performed considering an Ultimate Tensile Strength of the material UTS = 850MPa and a Yield Strength Sy = 630MPa. The resistance against fatigue is assessed by means of the Haigh diagram. In order to accomplish this task, the duty cycle of the wheel loader [1] has been analyzed. The loads on the shaft have been evaluated, considering the powertrain geometry and the well-known formulas for spiral bevel gears [8, 9]. Analytical and numerical analysis have been carried out, in order to estimate the stress distribution generated by the preload at the threaded connection and the stress concentration factor at the external groove at the end of the shaft threaded portion. The axial stiffness of the tapered roller bearings was provided by the supplier [9]. Lab tests have then been performed with the aim of determining the mean friction coefficient in the screw connection and the actual preload force generated upon the ring-nut tightening [10, 11]. The tightening force has been measured by an instrumented sleeve, where strain gages (1-LY11-1,5/120 by Hottinger Baldwin Messtechnik, HBM, Germany) were connected in a full Wheatstone bridge. Data sampling was performed by a NI C-DAQ 9184 equipped by the bridge module NI 9237 at the frequency of 10Hz.

The same instrumented sleeve, assembled to the shaft, was then used for a further lab experimentation. The aim of this campaign was to get a full awareness about the bearing preload value and to assess if it was sufficient to warrant external load withstanding. The performed test consisted in the application of an external axial load over the pinion shaft, thus simulating the in-service load, by a standing press (by Italsigma, Forlì, Italy) with a 100kN capacity. The load was on-line measured and increased until the rear side bearing lost contact with its race, i.e. until the full loss of the initial preload. This event was detected by the continuous monitoring of the load on the instrumented sleeve: its constant trend after an initial increase indicated the loss of preload. A numerical model was finally developed, in order to estimate the torsional loads that, during the service, may be transmitted through the bearing inner races and the interposed spacer to the ring nut and that are likely to be an additional reason for the preload loss.

2.3 Results and discussion

The described problem has been initially tackled by the analysis of the fracture surface in the light of the actual in-service loads. Afterwards, the loads transmitted by the pinion to the shaft have been estimated, as well as the preload transmitted by the ring nut to the tapered bearings. The following step was the shaft fatigue assessment in its nominal design conditions. The possible occurrence of preload loss has been subsequently investigated by both numerical and experimental methods. Finally, the highly detrimental effect of preload loss has been discussed and the primary reason for the occurred failure has been determined. The chain of events that led to failure is presented considering also the faults observed in similar groups.

2.3.1 Fracture surface and in-service loads

A careful study of the fracture surface indicates that fracture substantially propagates perpendicularly with respect to the shaft axis. Considering an enlarged view of detail (1) of Fig. 2, a nucleation point, where the crack is likely to have initiated, can be observed; similar initiation points are visible in a number of teeth of the inner splined. The final fracture occurs on a 4 angled surface, which is visible at the top of detail (2) shown in Fig. 2.2. On the other hand, fatigue crack initiation points have not been detected on the shaft external surface. The maximum torque T_{max} is transmitted to the shaft during forward shoveling. However, this working condition is not highly frequent, considering the usual tasks performed by excavators. Conversely, a typical use condition is that summarized by the working cycle in Table 2.1 [1, 9], where the torque average values are much lower, approximately of 52%, with respect to T_{max}. The fatigue assessment was conducted in the worst situation, i.e. considering the highest value of torque, T_{max}, under a safe life design approach.

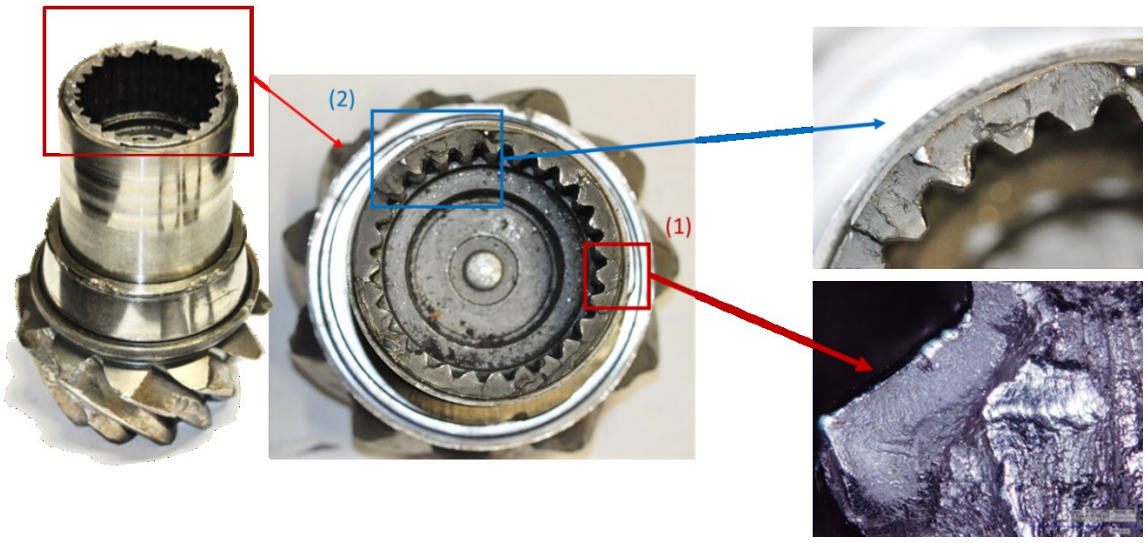

Figure 2.2 Shaft fracture surface

table 2.1. distribution of working conditions

CONDITION	RATE	TORQUE [Nm]
Digging	5%	1,007
Y-cycle (short)	30%	943
Y-cycle (long)	27%	882
Loadtransport	25%	399
Dozing forward	5%	1,767
Dozing reverse	2%	-926
Road driving	6%	397

2.3.2 Load transmitted to the shaft

The loads acting on the shaft have been calculated by means of the well-known formulas, equations. (2.1), (2.2) and (2.3) for the driving spiral bevel pinion shown in Fig. 2.3 [8, 9].In the following formulas the symbols F_{tp}, F_{ap} and F_{sp} respectively indicate the spiral bevel gear tangential, thrust and separating forces acting on the pinion. The pinion input torque and its mean diameter are respectively referenced as M and Dmp. Finally, the symbols γp, ϕp and Ψp are used for the bevel pinion pitch, pressure and spiral angles.

$$F_{tp} = \frac{2M}{D_{mp}} \tag{2.1}$$

$$F_{ap} = \frac{F_{tp}}{\cos\Psi_p}(\tan\phi_p \cdot \sin\gamma_p + \sin\Psi_p \cdot \cos\gamma_p) \tag{2.2}$$

$$F_{ap} = \frac{F_{tp}}{\cos\Psi_p}(\tan\phi_p \cdot \cos\gamma_p + \sin\Psi_p \cdot \sin\gamma_p) \tag{2.3}$$

As a consequence of the application of these three forces, both a bending and a torsional moment are generated on the pinion shaft. Considering shaft rotation, a rotating bending fatigue load arises from the bending moment: this load cycle can therefore be regarded as a symmetric alternate one, with one cycle being completed upon each rotation. The torsional moment is conversely basically constant, as it may experience a reversal, only following reverse gear insertions. However, the number of torque reversals is several orders of magnitude lower than that of shaft rotations. Finally, the thrust force and the preload force generated by the ring nut tightening also induces a constant normal load on the shaft, however the generated state of stress is generally much lower than the bending component. Consequently, the global fatigue cycle consists of both a constant (static) term, which depends on the torsional and axial loads, and of an alternate part related to bending. The corresponding normal and shear stresses were combined together, by the calculation of the von Mises equivalent stress.

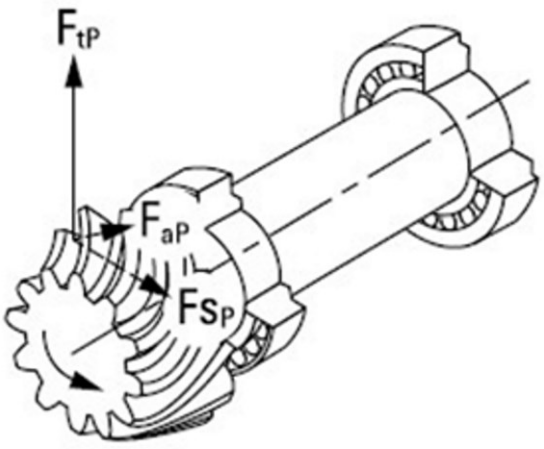

Figure 2.3 spiral bevel loads in the driving pinion

2.3.3 Experimental determination of ring nut preload

The preliminary knowledge of the friction coefficients at the ring nut underhead and in the threads is required, in order to compute the actual value of the induced preload force, as an effect of the controlled tightening torque. The estimation of a mean friction coefficient, which accounts for both frictions at the underhead and in the threads, is usually regarded as a valid alternative [11, 12]. This mean value can be computed as in equation (2.4) obtained from the equation (1.13) using d_2 as the effective thread contact diameter.

$$\mu_m = \frac{\frac{T}{F_v} - 0.16 \cdot p}{0.58 \cdot d_2 + 0.5 \cdot d_b} \tag{2.4}$$

Provided that the thread geometry and dimensions are known, the knowledge of the axial pre-load F_V is required, to achieve the estimation of the mean friction coefficient. For this purpose, an experimental campaign has been performed by a suitable strain gage instrumentation (Fig. 2.4) composed by a ring component that is involved in the tightening process. In-field testing led to the estimation of the preload force, which is generated by the tightening torque on the ring nut, according to the current assembly procedure of the group.

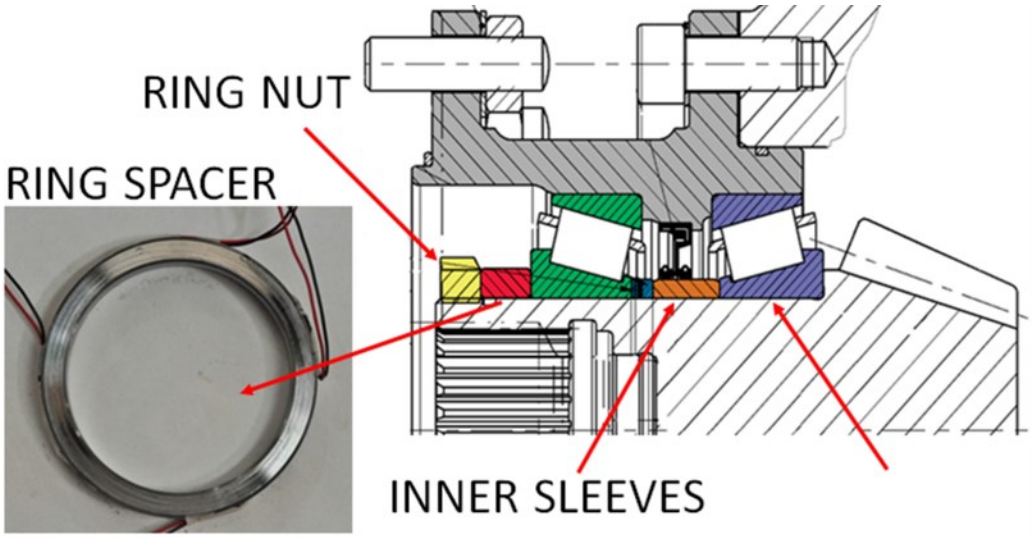

Figure 2.4 a ring spacer has been instrumented for the in-field determination of the axial preload upon tightening

Data processing led to the estimation of a mean friction coefficient μ_m between the values of 0.13 and 0.15, which can be regarded as a steady-state value after the third tightening. However, when considering the first two tightenings, we observed a remarkable scattering affecting the measured preload force for the same value of the tightening torque and in the same lubrication conditions [7]. The outcomes of the present experimentation are well highlighted in the diagram of Fig. 2.5.

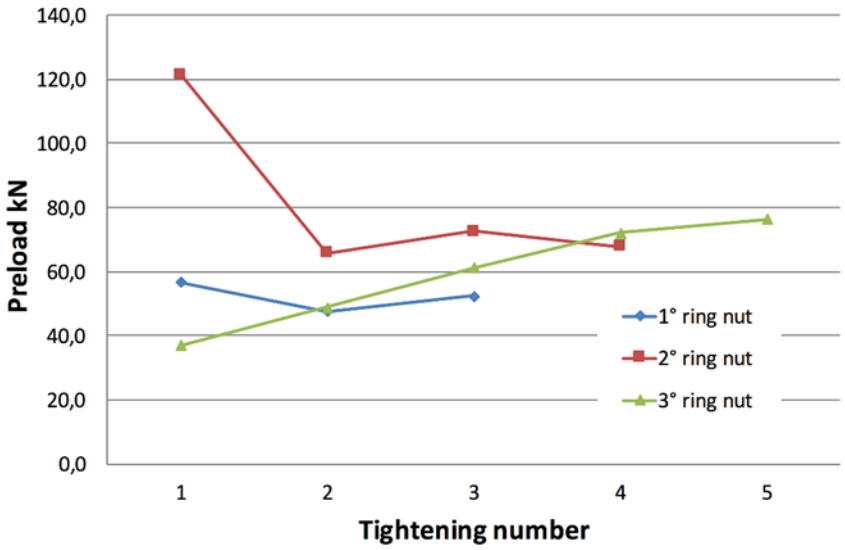

Figure 2.5 axial pre-load on the ring nut, plotted vs. the number of repeated tightenings (tests performed by three different ring nuts)

2.3.4 Shaft fatigue assessment in nominal design conditions

The static and fatigue shaft assessment has been performed under the assumption that the bearings are preloaded properly. In order to fulfil this task, the stress concentration factors in the region at the end of the ring nut thread, i.e. at the failure location, have been calculated under different load conditions, by Finite Element Analysis (FEA). The FEA analyses for the determination of the theoretical stress concentration factors have been carried out by means of the ANSYS code. Three different models have been prepared, one for each loading case. A two-dimensional, axisymmetric model has been used in the case of axial load. The element type chosen was PLANE183, yielding a total node count of approximately 2.500 nodes Fig. 2.6. This model converged to a solution with a tolerance threshold of 1% with an average element dimension in the refinement area (radius end) of d=0.1mm Fig. 2.7.

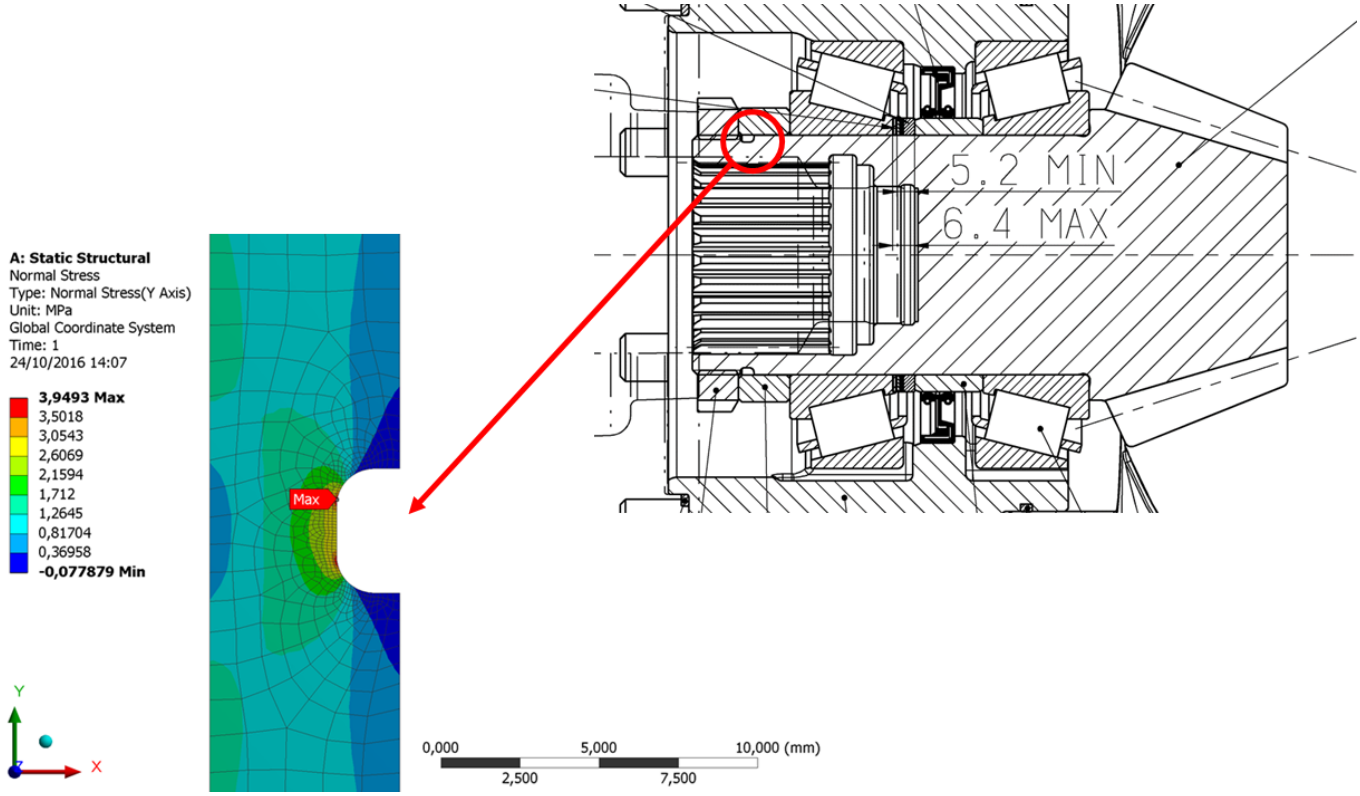

Figure 2.6 Axisymmetric model for the determination of Kt, axial load

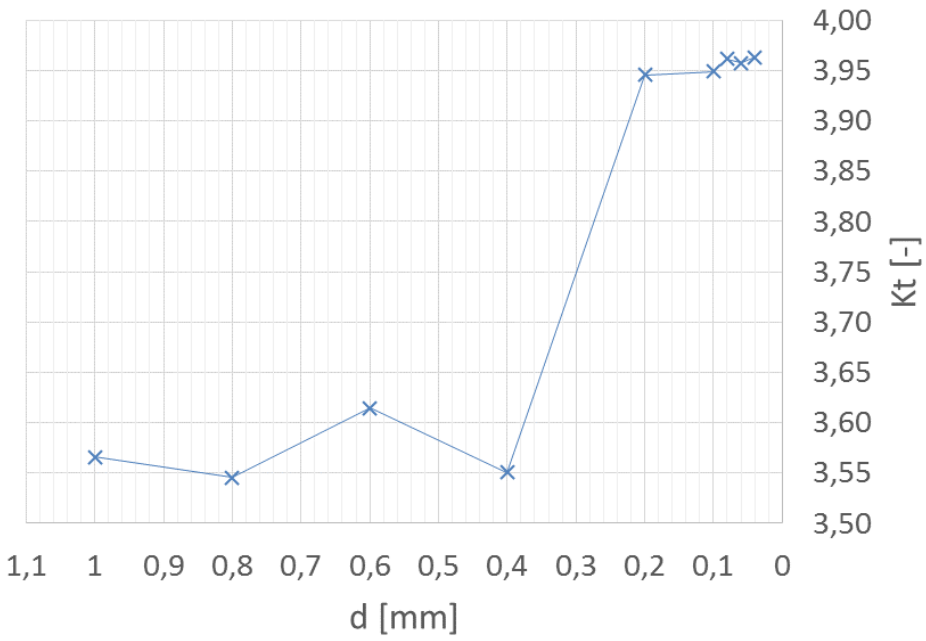

Figure 2.7 FEA convergence diagram, average element dimension in the refinement area in abscissa – axial load

In the case of bending load, the FEA model is three dimensional and the element type is a tetrahedral SOLID187: see Fig. 2.8. This model leverages a planar symmetry. Again, convergence (tolerance threshold 1%) is reached for an average element dimension in the refinement area of d=0.1mm and a total number of nodes of n=717.379: see Fig. 2.9.

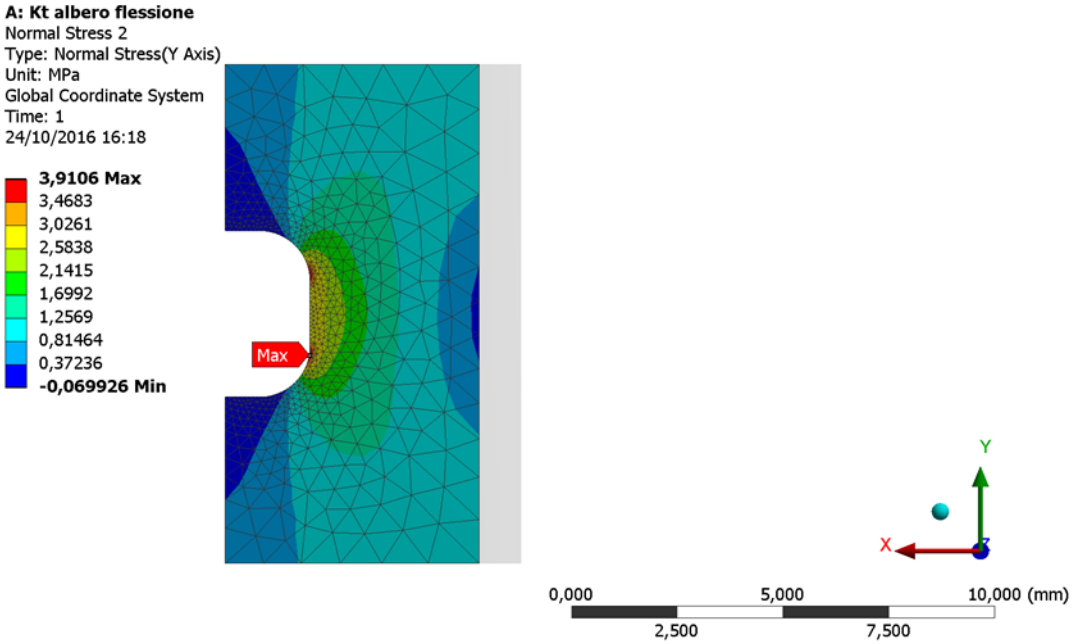

Figure 2.8 Model for the determination of Kt, bending load. Planar symmetry across XY axis.

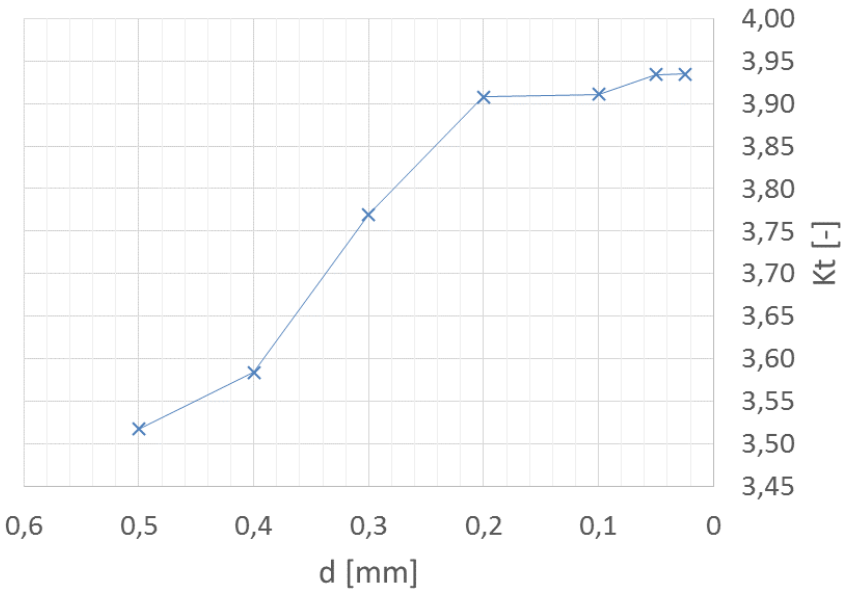

Figure 2.9 FEA convergence diagram, average element dimension in the refinement area in abscissa – bending load

Finally, the torsional case required a full three-dimensional model, made up of tetrahedral elements (SOLID187), as reported in Fig.2.10. According to the same criterium discussed above, convergence is found for an element average dimension in the refinement area of d=0.2mm Fig. 2.11. This choice leads to a total number of nodes of n=565.133.

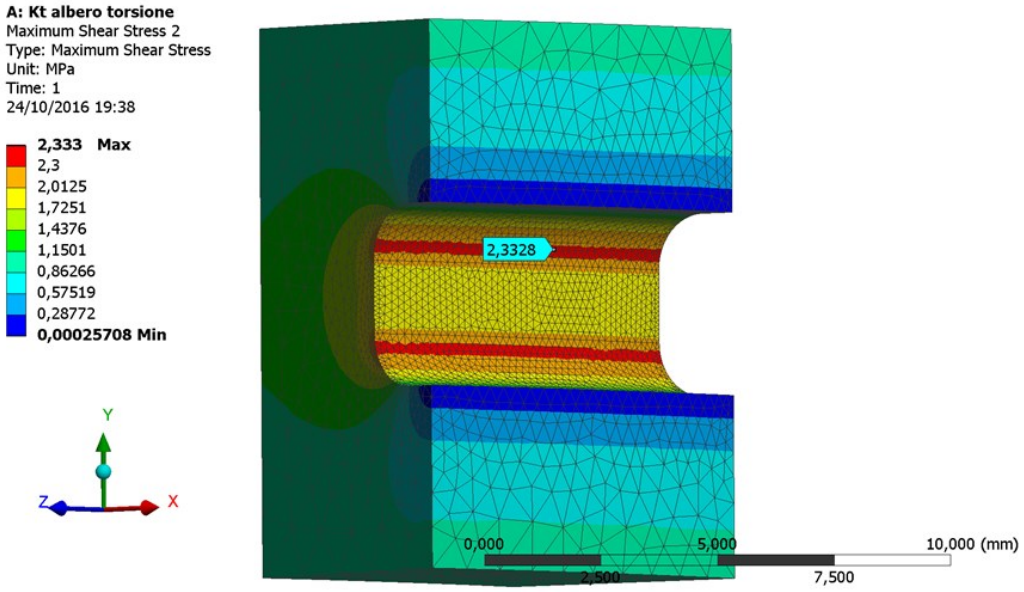

Figure 2.10 Model for the determination of Kt, torsional load.

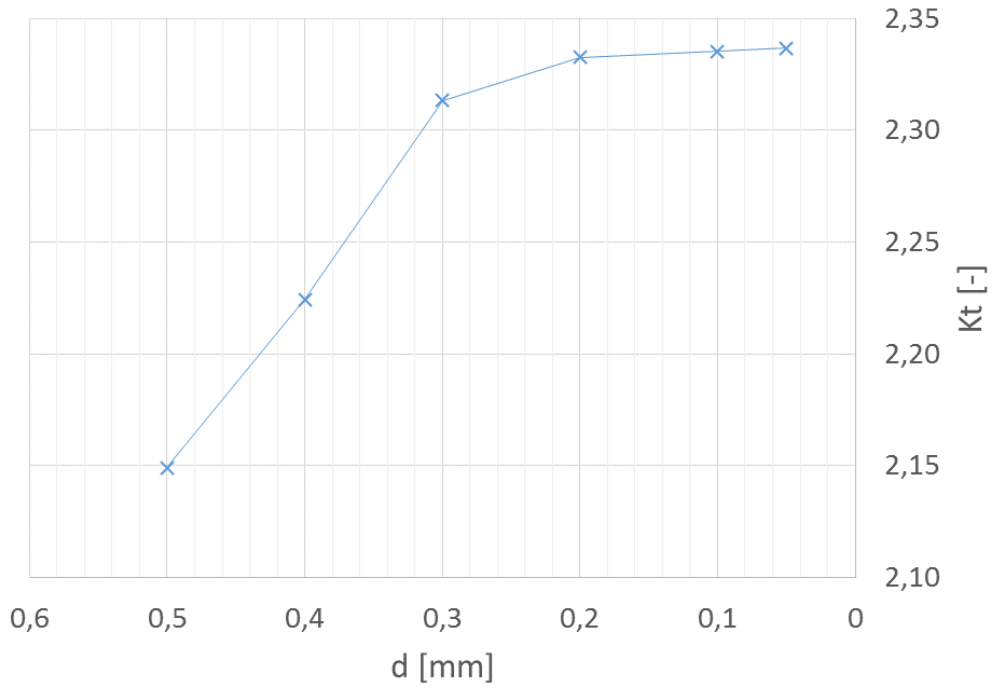

Figure 2.11 FEA convergence diagram, average element dimension in the refinement area in abscissa – torsional load

The theoretical stress concentration factors are reported in Table 2.1

Table 2.1 – Kt, Kf, q coefficients

LOAD TYPE	Kt (NET SECTION)	q	Kf
AXIAL	2.550	0.82	2.271
BENDING	2.503	0.82	2.232
TORSION	1.493	0.84	1.414

It is important to underline that the stress concentration factors reported in the Figures above are referred to the gross tubular section of the shaft. Hence, they are sensibly higher than those reported in Table 2.1 and used for the fatigue assessment: these are referred to the net section at the groove. The values of the stress concentration factors (Kt), along with those of the notch sensitivity q and of the fatigue concentration factors (Kf) are reported in Table 2. In particular, the values of Kt have been directly yielded by FEA, whereas the values of q and Kf have been post-processed, based on Pilkey et al; Niemann et al [13,14] and considering the material UTS. The fatigue response has been assessed, multiplying the nominal values of stresses by the aforementioned Kf coefficients, and subsequently plotting the Haigh diagram, to consider the material fatigue strength. The calculations indicate that the shaft is correctly designed against both static loads and fatigue in the infinite life domain. The related Haigh diagram is shown in Fig. 2.12, where the representative point for nominal constraining condition lies within the safe

region with a safety factor in the order of 1.2 under the hypothesis of the same load ratio maintained up to failure.

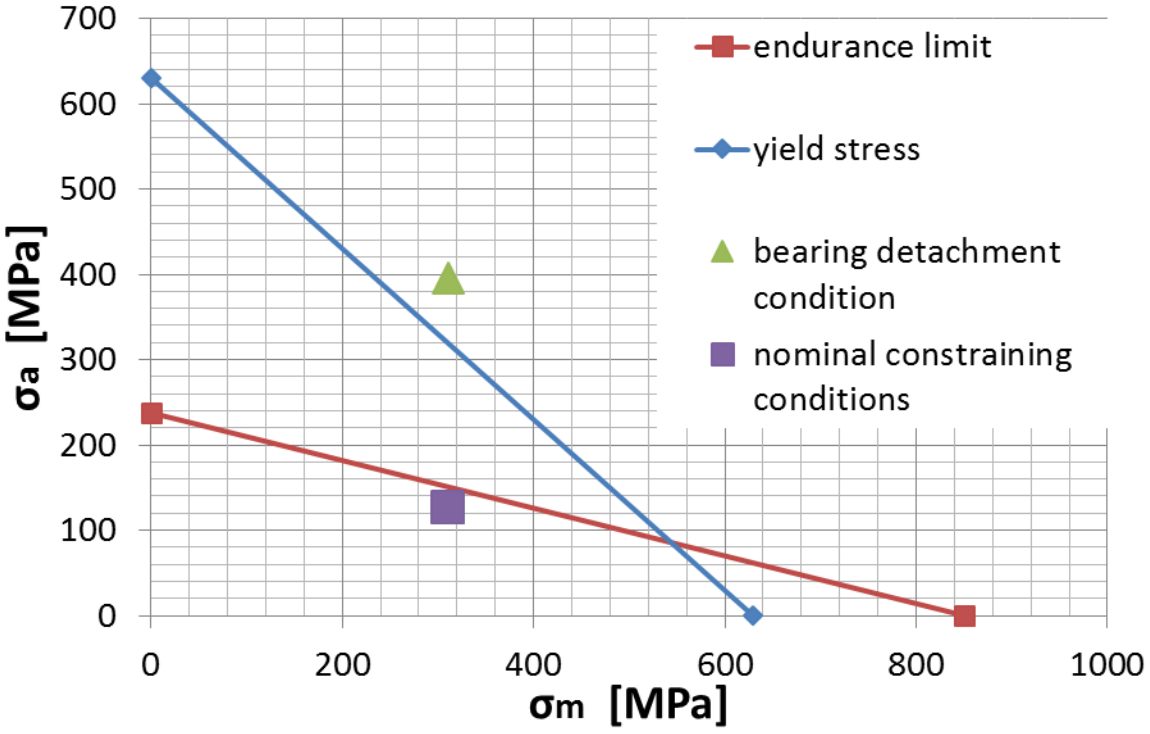

Fig. 2.12 Haigh Diagram in nominal working conditions (purple) and upon nut loosening (green)

It may be argued that this is a quite low values, however, it is necessary to remark that the fatigue assessment was conducted, considering the worst condition listed in Table 2.1, which occurs with quite a low rate in the machine life.

2.3.5 Occurrence of preload loss studied by experimental and numerical methods

A sketch of the pinion layout, with the machined internal hole, is shown in Fig. 2.13, where the strain gauge location is also highlighted. Further details of the experimental setting are also available in Fig. 2.14, where the holed pinion (a) and the shaft loading and constraining on the standing press (b) are depicted. The result of the calibration tests in terms of the strain-load relationship is shown in Fig. 2.15. This is based on the recorded data under ramp load increase

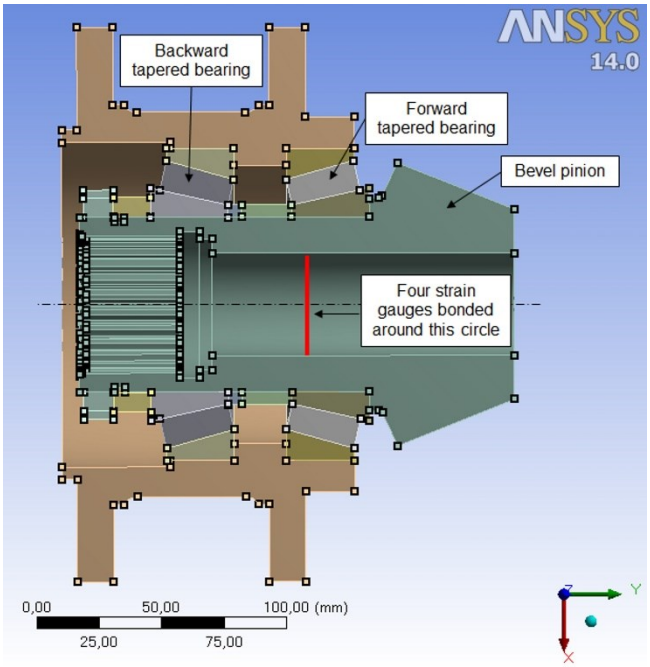

Fig. 2.13 Sketch of the machined pinion shaft, where the strain gauges locations are highlighted

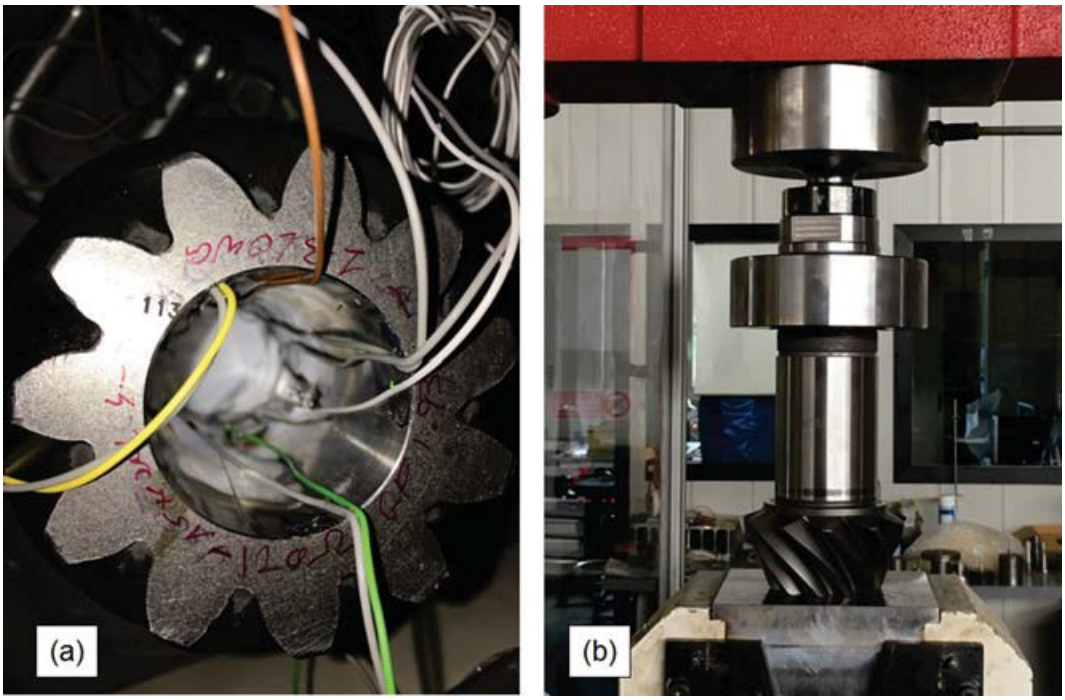

Fig. 2.14 (a) Holed pinion with the applied strain gauges; (b) Shaft loading and constraining on the standing press

and decrease. It can be remarked that the response linearity is very high, as confirmed by the linear correlation coefficient, being very close to one in the three replicated tests. Upon full assembly, a strain output in the order of 330μm/m has been recorded: based on the

aforementioned calibration relationship, it corresponds to an induced tensile load of 80kN on the shaft. The completely assembled pinion group (consisting of the shaft, the pinion bevel gear, the tightened ring nut and the preloaded tapered bearings) has been mounted on a standing press and suitably loaded, trying to simulate an in-service load on the powertrain. An axial load has been applied, acting directly on the pinion bevel gear, with simultaneous constraining of the shaft external body, as shown in Fig. 2.16.

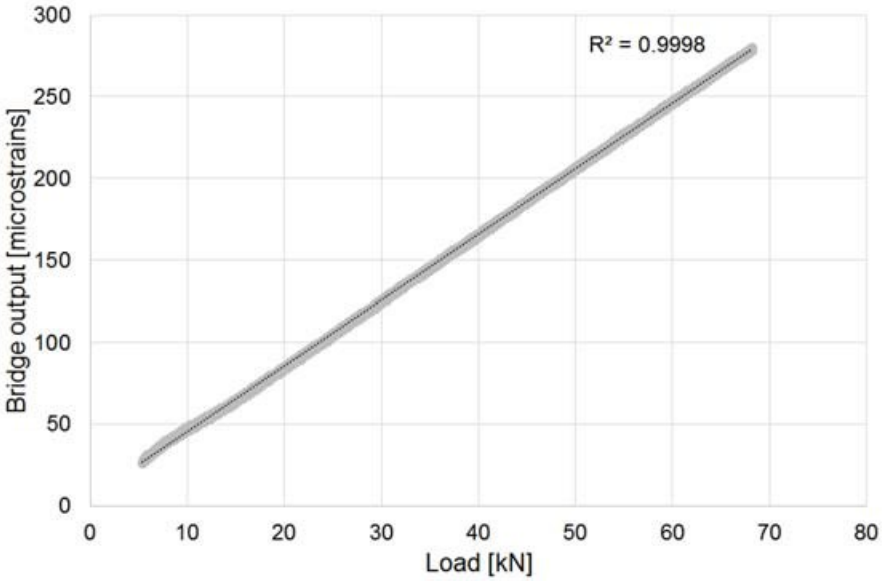

Fig. 2.15 Experimental calibration strain-load relationship

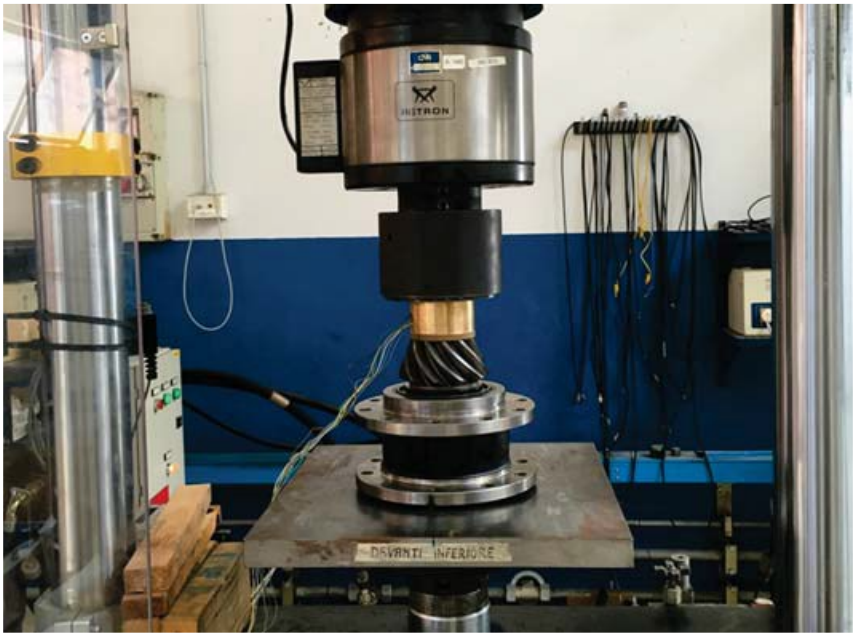

Fig. 2.16 Experimental setting during the detachment test

As described in Section 1, this state of load was also investigated by a FEA model, which was then validated by comparing the strain results. The outcome of the conducted validation is summarized in Fig. 2.17, where the outputs of FEA simulations are plotted versus the experimental results. As it can be observed, the dots are very close to the dashed line representing the ideal condition of a full numerical-experimental agreement: the depicted outcome indicates a good consistency, considering also that average error does not exceed 5%.

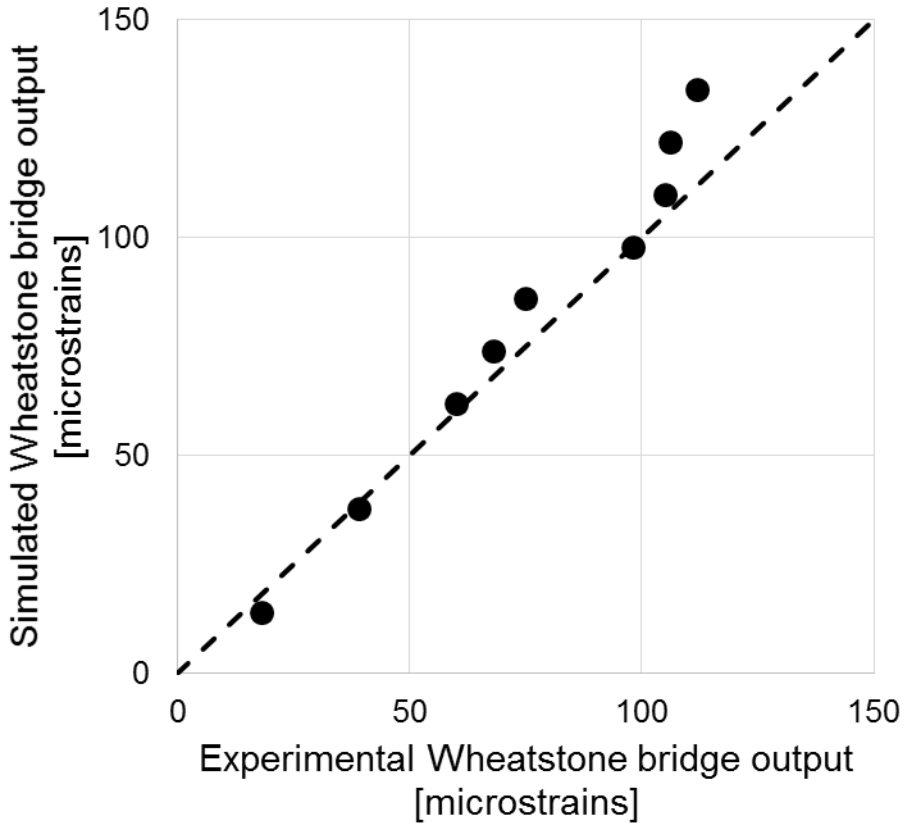

Fig. 2.17 Validation of the FEA model that accounts for the modified holed geometry andfor preload and external load effects

The main motivation for this further trial arose from the outcomes of both the aforementioned numerical model and a further analytical one, where the stiffnesses of the entire group parts were regarded as lumped parameters. The results yielded by the two models were consistent, indicating that preload significant drop could be expected under a load a bit higher than 15kN. A scheme of the lumped-parameter stiffness modelling is shown in Fig. 2.18. The performed tests confirmed the occurrence of detachment, indicated by the abrupt drop of the force on the shaft, followed by a sharp slope change with final constant trend. The related graph is shown in Fig. 2.19, where the axial force on the shaft, measured by the aforementioned instrumentation, is plotted vs. the force applied to the pinion. In particular, the shaft preload, initially around 80kN

in tension, is lowered, as the compressive force is gradually applied to the pinion. After an initial nearly constant trend, the load on the shaft linearly decreases until backward bearing detachment takes place. In this condition, for an applied load around 20kN, as an effect of the thrust load transmitted by the pinion, preload decreases under what can be regarded as its minimum threshold and is no longer sufficient to efficiently constrain the backward bearing that gets detached. When this event occurs, the entire load is withstood by the forward bearing and by the group case. The overall preload loss is around 15kN. This outcome proved to be well consistent with the aforementioned numerical and analytical predictions, which indicated that a preload loss was likely to occur under an axial load around 15 − 20kN. Further investigations have been carried out to get a complete awareness of the causes of ring nut loosening and of resulting preload loss. A FEA analysis of the pinion group indicated that the sleeve and the laminated shims mounted between the inner races of the bearings are responsible of a sort of torque bypass Fig.2.20

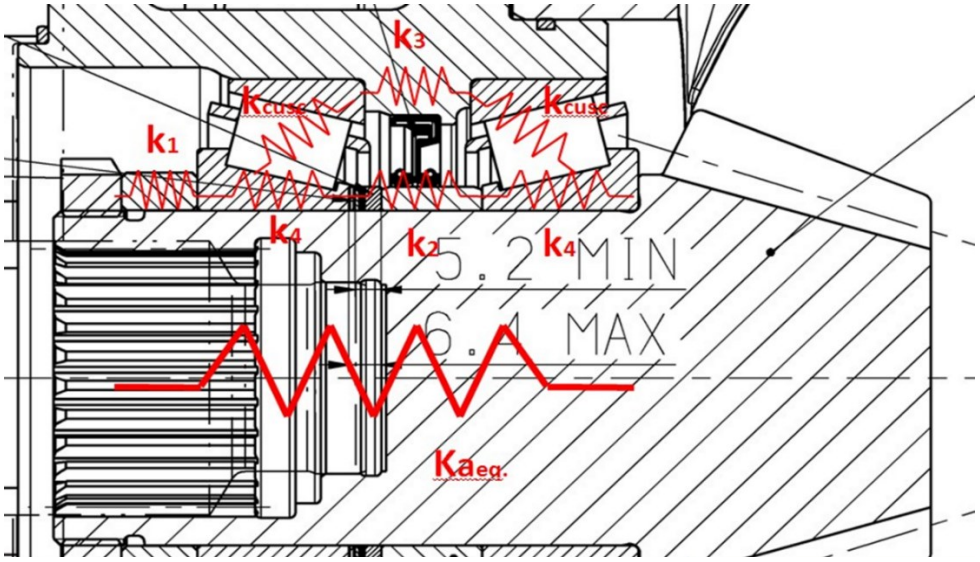

Fig. 2.18 Lumped-parameter stiffness model of the parts involved in the group

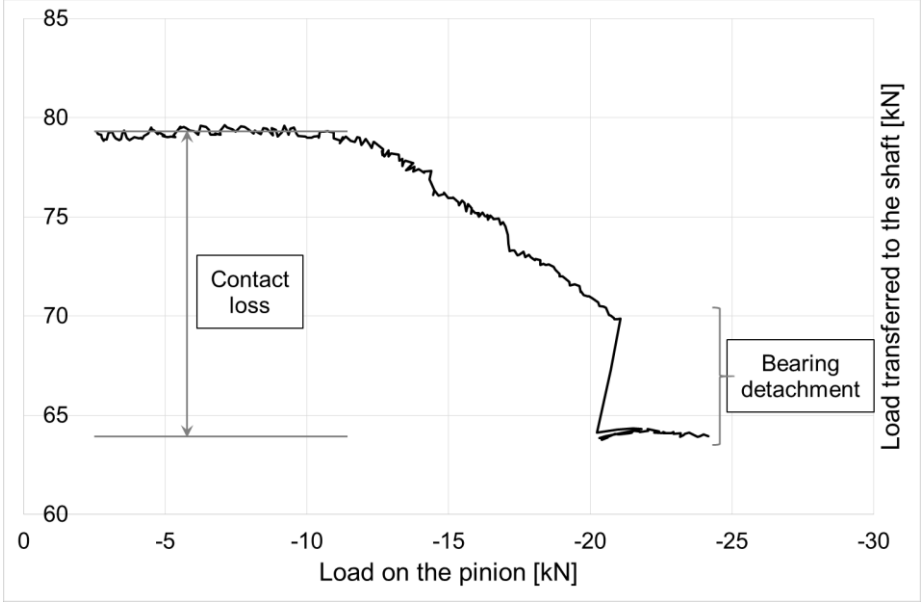

Fig. 2.19 Force transferred to the shaft vs. the axial load on the pinion

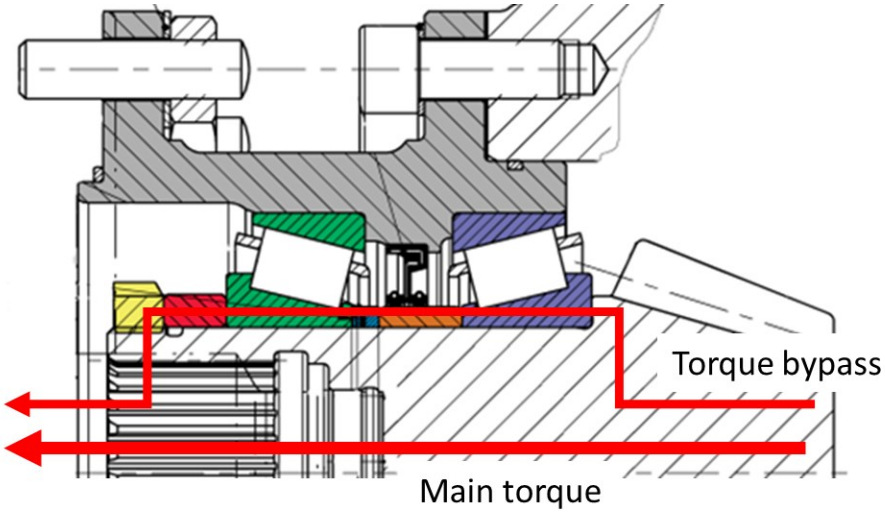

Fig. 2.20 Torque bypass between the head and the tail of the pinion shaft

This has the undesired feature of transmitting a fraction of the pinion head torque to the splined, passing through the ring nut. The analysis has been carried out in the extreme conditions of maximum clearance and maximum interference, starting from the nominal coupling tolerance between the pinion shaft, the bearing inner rings and the inner sleeves. While both interference and clearance conditions may be generated at the interface between the internal diameter of the bearing inner race and the shaft, the inner sleeves and the shaft are always coupled with radial clearance. In the case of a radial clearance between the internal diameter of the bearing inner race and the shaft a considerable amount of the pinion torque, up to 18%, is transmitted by the pinion to the ring nut, whereas in the case of interference the amount drops down, but remains present. This outcome is due to the occurrence that, as an effect of the friction coupling

between the inner rings and the shaft, a portion of the pinion torque is transmitted directly to the shaft and to its inner splined. The present phenomenon is well highlighted in Fig. 2.21, where the two curves account for the two described conditions: the blue one refers to clearance, whereas the green one is related to interference. It can be remarked that, for a given value of torque at the pinion (horizontal axis), the two curves yield different values of the torque transmitted to the ring nut. In particular, under the clearance condition a higher amount of torque is transmitted to the ring nut, whereas, under the interference condition a higher amount of torque flows directly to the shaft and is not transmitted to the inner sleeve.

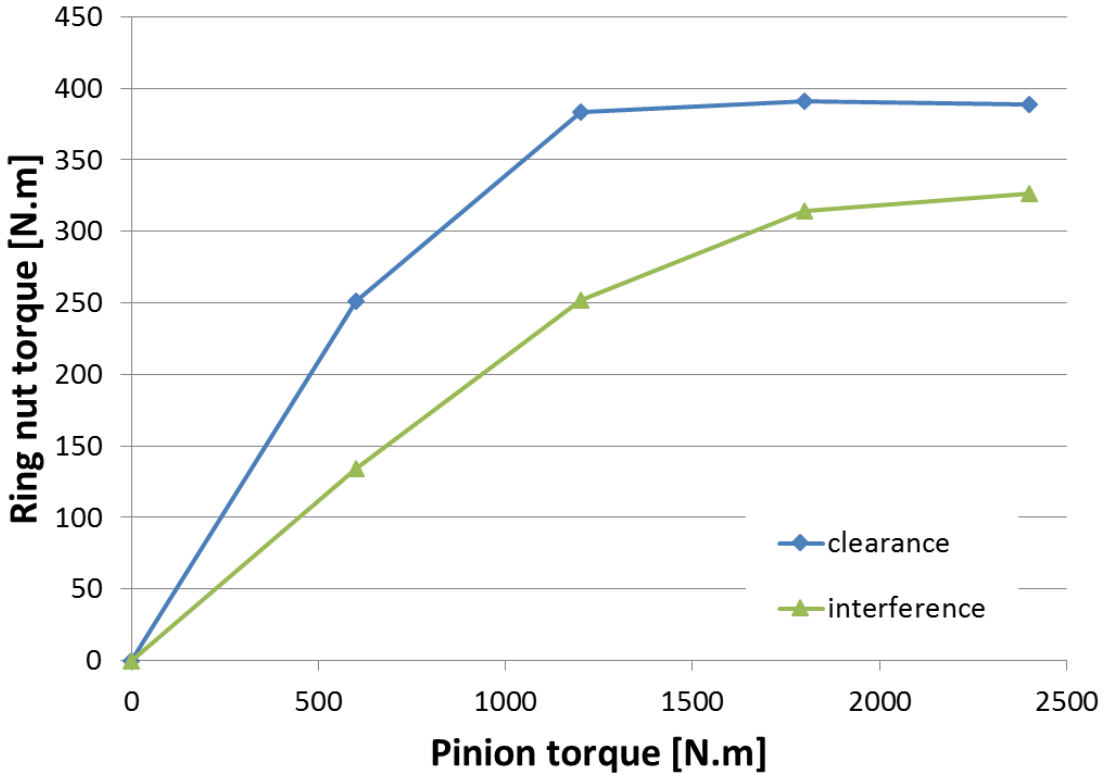

Fig. 2.21 Torque transmitted to the ring nut in the two (extreme) coupling configurations, as a function of the pinion torque

2.3.6 Effect of preload loss and primary reason for the observed failure

The torque transmitted to the ring nut, in combination with a certain amount of preload scatter due to the variability of the frictional conditions of the threaded parts, may lead to a sudden loosening of the nut, which in turn makes the axial preload of the backward bearing drop down to zero. Therefore, the described torque bypass occurrence seems to be the main reason for the unexpected ring nut loosening that was observed in some shafts. Nut loosening, with consequent loss of bearing preload and bearing detachment from the body is a very serious outcome. In fact, under the hypothesis that the rear side bearing becomes ineffective, the actual constraining of the pinion shaft would drastically change. Both static and fatigue assessments have been repeated in this new less constrained configuration and the conclusion is that the shaft would no

longer be able to withstand the fatigue loads generated by the duty cycle. This occurrence is well highlighted in the Haigh diagram in Fig. 2.12, where a bearing detachment condition representative point has been appended. This point lies in the unsafe region, which indicates that a fatigue failure is likely to occur in this condition. Therefore, this outcome indicates that the observed shaft failure must be surely investigated in the frame of the nut loosening observed in similar groups, since loosening and resulting bearing preload loss directly leads to fatigue failure.

2.4 Discussion

The main outcome of this work is that the mechanical group appears to be well designed against static and fatigue loads, considering the nominal load cycle and under the hypothesis of regular constraining at both bearings. However, under the same load conditions, if backward bearing detachment takes place, fatigue failure is likely to occur. In addition, the adoption of spacers (sleeves and shims) between the inner races of tapered rolling bearings may lead to an undesired torque transmission to the threaded nut applied to the pinion shaft tail. The pulsing torques transmitted to the ring nut, regardless of pinion rotation direction, may induce a long-term loosening of the ring nut. This event has the detrimental outcome of worsening the constraining conditions and increasing the state of load of the shaft. The fatigue assessment has indicated that in this modified condition the shaft is no longer able to withstand the actual loads: therefore, failure occurs. The torque bypass towards the ring nut is the primary reason for nut loosening, which, in turn, is the reason for preload loss, triggering the finally failure. A proof to this chain of events preceding failure can be provided by the ring nut loosening that was observed in some shafts. These groups were then refurbished before failure occurrence. Moreover, the remarked fluctuation of the preload forces, which is likely to be due to a dimensional scattering affecting the mounted ring nuts, amplifies the observed variability of the mechanical response of the studied group. This fluctuation is probably a further reason for preload loss and nut loosening. Considering the outcomes of the performed studies, in order to overcome the described problems and to improve the pinion shaft reliability, the use of mechanical or adhesive locking devices in combination with spacers is strongly suggested. Moreover, the analysis of the aspects which affect the friction coefficient and the repeatability of the tightening process is critical in order to ensure a correct preload of the tapered roller bearings.

2.5 Reference of the chapter

[1] Filla, R., 2013. “Optimizing the trajectory of a wheel loader working in short loading cycles”. In Proceedings of the 13th Scandinavian International Conference on Fluid Power, SICFP2013. Link¨oping, Sweden, June 3-5, 2013.

[2] Filla, R., 2009. “A methodology for modeling the influence of construction machinery operators on productivity and fuel consumption”. Lecture Notes in Computer Science, 5620, pp. 614–623.

[3] Wang, J., Yang, Z., Liu, S., Zhang, Q., and Han, Y., 2016. “A comprehensive overview of hybrid construction machinery”. Advances in Mechanical Engineering, 8(3), pp. 1–15.

[4] Pelaseyed, S., Mashayekhi, F., and Movahedi-Rad, A., 2015. “Investigation of the shaft failure connected to extruder”. Journal of Failure Analysis and Prevention, 15, pp. 775–781.

[5] Zangeneh, S., Ketabchi, M., and Kalaki, A., 2014. “Fracture failure analysis of AISI 304L stainless steel shaft”. Engineering Failure Analysis, 36, pp. 155–165.

[6] Ping, J., and Guang, M., 2008. “Investigation on the failure of the gear shaft connected to extruder”. Engineering Failure Analysis, 15, pp. 420–429.

[7] Croccolo, D., De Agostinis, M., and Vincenzi, N., 2012. “Influence of tightening procedures and lubrication conditions on titanium screw joints for lightweight applications”. Tribology International, 55, NOV, pp. 68–76.

[8] Niemann, G., Winter, H., and Hohn, B., 2005. Maschinenelemente: Band 2: Getriebe allgemein, Zahnradgetriebe - Grundlagen, Stirnradgetriebe. Springer- Verlag, Berlin, Germany.

[9] Timken, 2011. Timken Engineering Manual. Available on-line at http://www.timken.com/enus/ products/Documents/Timken-Engineering-Manual.pdf.

[10] Croccolo, D., De Agostinis, M., Fini, S., Morri, A., and Olmi, G., 2014. “Analysis of the influence of fretting on the fatigue life of interference fitted joints”. In ASME 2014 International Mechanical Engineering Congress and Exposition, Proceedings IMECE 2014, Vol. 2B, ASME. Montreal, Canada, November 14-20, 2014.

[11] De Agostinis, M., Fini, S., and Olmi, G., In Press. “The influence of lubrication on the frictional characteristics of threaded joints for planetary gearboxes”. Proc IMechE Part C, DOI: 10.1177/0954406215605863.

[12] Bickford, J., 2008. Introduction to the Design and Behavior of Bolted Joints: Non-Gasketed Joints, 4th ed. Taylor & Francis Group.

[13] Pilkey, W., Pilkey, D., and Peterson, R., 2008. Peterson’s Stress Concentration Factors, 3rd ed. Wiley, New Jersey, United States.

[14] Niemann, G., Winter, H., and Hohn, B., 2005. Maschinenelemente: Band 1: Konstruktion und Berechnung von Verbindungen, Lagern, Wellen. Springer-Verlag, Berlin, Germany.

3. Experimental investigation on the influence of lubrication on the frictional characteristics of threaded joints

3.1 Introduction

The threaded joints find one of their major advantages in the possibility to be easily assembled and disassembled for maintenance purposes. But the friction condition at every tightening can be very different as the behaviours reported in fig.3.5. The most widely used tightening approach consists in the use of a torque wrench, with tightening torque being applied to the screw head or to the bolt nut and being subsequently increased up to a desired value. The recommended values usually depend on the required preload force and on the estimated value for the total frictional coefficient (at the underhead and in the threads). However, uncertainties on friction may reflect in an overestimation or underestimation of the actual clamp force, with consequent crew yield or lack of safety of the joint [1]. For this reason, the frictional properties of threaded connections and the main factors that are likely to affect the tribological response have been the subject of several studies. For instance, the effects of oil lubrication and of surface finishing at the underhead along with that of the screw technological process have been experimentally studied with reference to motorbike suspensions [2]. A Design of Experiment assisted campaign indicated that lubrication and underhead anodizing are highly significant at reducing friction. The role of a suitable lubrication, when using Titanium alloy screws for lightweight structures in the automotive field, has also been investigated [3]. Experimentation indicated that the tribological response is significantly enhanced, when applying Interflon BV ceramic paste, even in the case of repeated tightening. The important role of friction and consequently of lubrication in lightweight design is also confirmed by the investigations focused on Aluminum alloy threaded connections [4]. The evolution of friction in repeated fastening has been the topic of other papers, e.g. [6], where the role of wear at the underhead is also emphasized. The importance of an accurate estimation and control of the preload entity in order to warrant the reliability of the threaded joint is also emphasized in [7-8]. The relationship between the applied tightening torque and the resulting preload has been studied as well by numerical three-dimensional models [9]. Friction again proved to have a great influence on the aforementioned relationship. Further studies deal with the effect of friction on the fatigue life of bolted connections [10] and with the effect of tightening speed [11].

Nowadays, there is an increasing interest in the development and application of suitable surface treatments or coatings with beneficial outcomes in terms of friction reduction. Regarding surface treatments, shot-peening may be cited: as an effect of shot impacts, micro dimples are created [12]. Tribometer tests indicated a significant reduction of friction, up to 40%, due to the increment of the contact points and to the generation of pockets for lubricant with consequent hydrostatic effect. Regarding coatings, some studies dealt with Diamond-like carbon (DLC) thin films. In particular, the tribological response of amorphous hydrogenated carbon films (a-C:H), hydrogen-free hard carbon films (a-C) and of Titanium-doped amorphous hydrogenated carbon films (a-C:H(Ti)) was the topic of the research in [13]. Pin-on-disc tests in both unlubricated and

lubricated conditions with continuous monitoring of friction and wear indicated that these coatings generally have a good response. Friction may be reduced even under 0.1, especially with the beneficial contribution of Ti doping. Further studies regard the tribological behavior of electrodeposited Zn–Ni coatings and of Zn- and Cd-based coatings. Experimental tests by tribometer confirmed a beneficial impact on both wear and friction even in dry conditions [14]. The effect of black oxidization was finally the topic of the study [15]. This type of coating is created by a process developed at the beginning of 1900 and is particularly suitable for the production of an attractive black finishing with positive outcomes from the points of view of corrosion resistance, lubricity and galling resistance [16]. Experimental campaigns reported in [17-19] reported a significant effect of black oxide surfaces at lowering friction. It must be pointed out that the aforementioned studies tackle the general application of the aforementioned treatments and coatings by tribometer tests: specific applications on threaded connections and related frictional tests involving screws are not present in the literature. The only exceptions are related to some works dealing with TiN, WC, TiC, TiCN and microcrystalline diamonds to be applied to abutment screws in the specific field of dental implants [20-22]. As far of lubricants are concerned, mineral oils have several industrial applications, for instance in gear units. When a liquid lubricant is used, the oil is usually spread on the entire screw, involving both the underhead and the threads. Whereas, the previously cited ceramic paste can be regarded as a solid lubricant used in the automotive fields, thanks to its stability even at high temperatures and to its efficiency even in case of multiple tightenings [3, 5]. In addition, it proves to be highly effective in applications with high pressure at the underhead [23] and in the threads to avoid stick-slip occurrence [3]. Several applications of the Interflon ceramic paste are mentioned in [24], where this lubricant was applied to different material screws used to fasten different material flanges. A further example of solid lubricant is Molybdenum disulfide (MoS2) that can be directly deposited on surfaces or can be regarded as an additive to be mixed up with liquid lubricants. It must be remarked that, as a solid lubricant is applied, it may be selectively spread on the entire screw or in some regions only. Regarding this point, the separate effects of lubrication at the underhead and in the threads are not reported in the literature. Finally, dry conditions are sometimes used for screws or bolts used for tightening gearboxes or machine cases, for which a limited amount of untightening and tightening procedures is expected during the overall life. Based on the literature survey, several coatings are generally available and are also promising from the point of view of the tribological response. However, their application on screws and bolts and the related outcome have been rarely investigated. The motivations to this work mainly arise from Refs. [14] and [15], dealing with Zinc-based coatings and with black oxidization: these treatments are commonly applied to screws, but there is a lack of knowledge on their actual effect on friction. Regarding lubricants, unlubricated, oil-lubricated and ceramic paste-lubricated conditions are compared, tackling also the issue of selective solid lubrication. This study deals with these topics, by an experimental approach on steel screws, following the recommendations of ISO 16047 [10]. A number of statistical methods, ranging from fractional factorial Design, to One and Two-way Analysis of Variance ANOVA and to pairwise tests has been used to tackle the aforementioned questions. In addition, a case study on the effect of repeated

tightening in a Planetary gearbox with and without the adoption of ceramic paste has been reported.

3.2 Effect of coatings and a suitable lubrication on the friction coefficient

3.2.1 Materials and methods

All the tests were performed on M14 X 2 8.8 class hexagonal head steel screws, with a length between 50 and 60 mm. Their technical features are summarized in Table 3.1. Moreover, for the sake of clarity a sketch of the threads with related dimensions is shown in Fig. 3.1.

Table 3.1. Main features of the tested steel crews

Symbol	Feature	Value	Unit
S_u	Ultimate Strength	800	MPa
S_y	Yield Strength	640	MPa
d	Nominal diameter	14	mm
d_2	Pitch diameter	17.70	mm
A_t	Stress area	115	mm^2
p	Pitch	2	mm

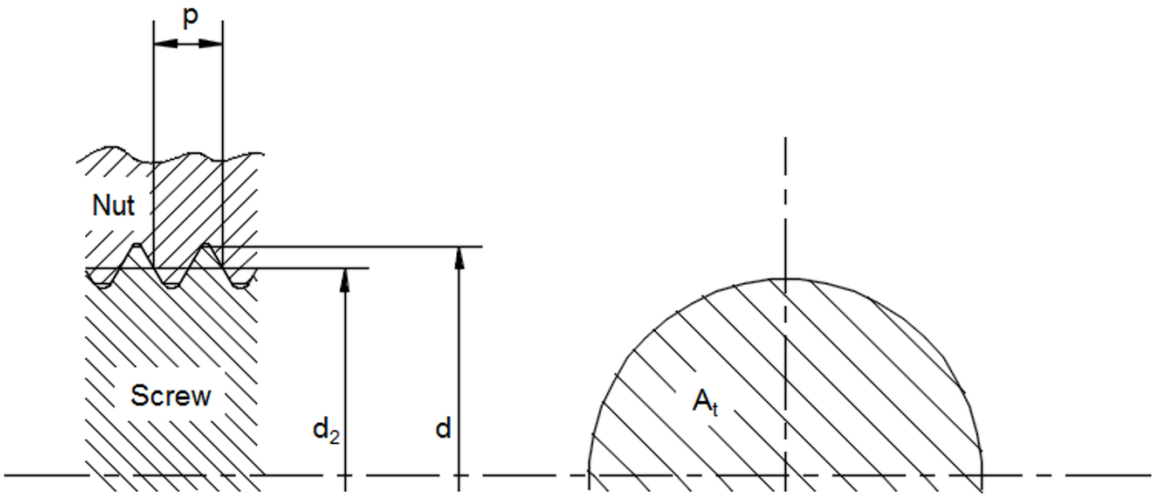

Fig. 3.1. A detail of the screw and nut threads with related dimensions

The performed trials were aimed at the determination of the total frictional coefficient, μ_{tot}, considering friction at the underhead and in the threads. The entire experimentation was carried out by a testing machine (Test GMBH, Model 201), capable of manually applying tightening torque and rotation on screw head with simultaneous measurement of both the applied torque and the resulting preload. The test bench was equipped by a torque and an axial load measuring devices, respectively with full scales of 1,100Nm and 300kN and with 0.5% accuracy. In addition, the testing device was provided with a steel test-bearing-plate (type HH) to be posed under the screw head, having a 30µm average roughness, 15.5 mm diameter holes and all the other features conformal to the recommendations of the aforementioned Standards. A rendering of the screw testing machine is shown in the section view in Fig. 3.2.

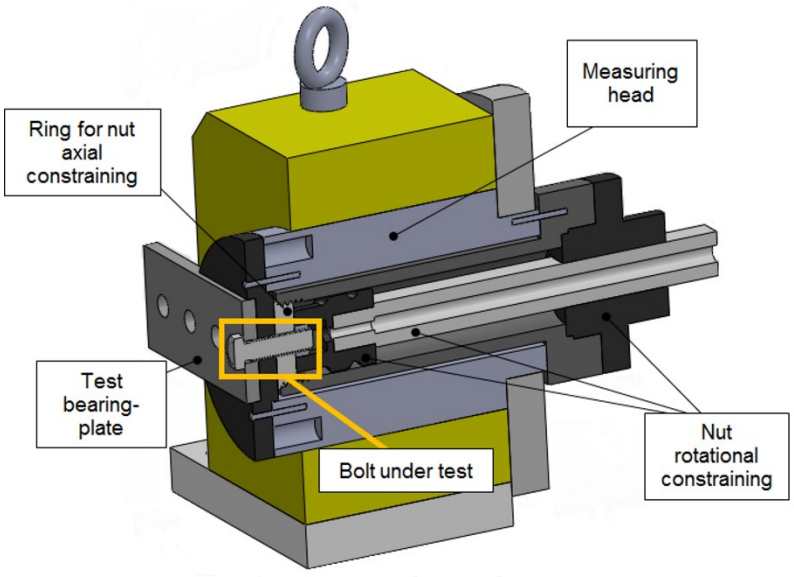

Fig. 3.2. A sketch of the test bench utilized in the experimental campaign

The tests were conducted by fixing the bolt nut and applying the tightening moment to the screw head by a wrench. It was applied at a constant rotational speed with on-line measurement of the induced axial preload. The tightening procedure was gradually incremented until preload increased up to 75% of the axial load at yield point (55,200N). The total frictional coefficient was then computed in this condition by Eq. (3.1), where T and F_v respectively indicate the tightening torque and then axial preload, p is the pitch, d_2 is the pitch diameter and D_b is the mean diameter at the underhead.

$$\mu_m = \frac{\frac{T}{F_v} - \frac{p}{2\pi}}{0.577 d_2 + 0.5 D_b} \tag{3.1}$$

This formula, available in [25], is based on the assumption that a total frictional coefficient, averaged between those at the underhead and in the threads, can be considered. Further details can be found in this Reference.
The experimental part was divided into three campaigns: a screening analysis was initially performed by the tool of the fractional factorial design assisted by the Taguchi method [26-27]. The use of the L8 magic square made it possible to arrange a campaign involving 5 factors, considering only 8 treatment combinations. Ten replications were performed for statistical evidence reasons, for an overall number of 80 experiments. It made it possible to individuate the two most significant factors, i.e., screw coating and lubrication. Afterwards, the analysis was deepened: the following campaign, based on a Two-Way ANOVA, involved the aforementioned factors with the aim of comparing their role on friction and of investigating a possible interaction between them. For this purpose, two different levels of lubrications were considered. The involved lubricants were a solid one consisting in a ceramic paste (Interflon Paste HT 1200) and a liquid one, consisting in an industrial mineral oil (Shell Omala S4 WE 320). The ceramic paste was spread both at the underhead and in the threads, whereas, for oil lubrication the entire screw was immersed into a bath containing the oil. All these procedures were performed by the same operator. The final campaign was then focused on the effects of lubrication. In this case, the effect of ceramic paste application, at the underhead or in the threads only, was compared to the effects of the oil and of the dry condition. For this purpose, the tools of One-Way ANOVA, of pairwise (Least Significant Difference and Newman-Keuls) tests and of orthogonality were used. The orders of all the tests were fully randomized, following the recommendations of the most widely known statistics manuals [26-27].

3.2.2 Preliminary screening analysis

A screening analysis was carried out first, to investigate the importance and the significance of a number of factors, and to determine which factors could be conversely neglected in the further analysis. The considered factors included the surface coating of the screw, the surface treatment of the washer located beneath the screw head, the state of wear of the washers, the coating of the nut, the lubrication of the joint. Two levels were considered for each factor: the considered factors along with the related levels are described and summarized in Table 3.2.

Table 3.2. Factors and related levels involved in the screening experiment

Factor	Low level (0)	High level (1)
A. Screw coating	Black oxidized	Zinc coated
B. Washer type	High strength	Zinc coated
C. Washer wear	New	Already used
D. Lubrication	Dry conditions	Full lubrication in oil
E. Nut treatment	Zinc coated	No coating

Table 3.3. Treatment combinations of the screening experiment and related notation

Yates notation	A. Screw coating	B. Washer type	C. Washer wear	D. Lubrication	E. Nut treatment
1	0	0	0	0	0
cde	0	0	1	1	1
be	0	1	0	0	1
bcd	0	1	1	1	0
ad	1	0	0	1	0
ace	1	0	1	0	1
abde	1	1	0	1	1
abc	1	1	1	0	0

As mentioned above, a number of ten replications was chosen to warrant sufficient evidence of the acquired data. This choice is due to the fact that the tightening operation usually has a great scatter in the results, due, for example, to the tightening speed, to a not constant lubrication and to the geometrical tolerance of the components involved in the assembly. As a consequence,

considering a full factorial design 25 with 10 replications would have required a number of 320 experiments to be run, which was considered to be too high for a screening test. Therefore, this number was lowered, by fractionating the experimental design. For this purpose, the technique of fractional factorial design was adopted: the L8 magic square by Taguchi made it possible to easily manage a 25-2 experiment with just 8 treatment combinations to be processed. Therefore, 80 trials were performed: a detail of the 8 treatment combinations, expressed according to the Yates notation is reported in Table 3.3 [26-27], where “0” and “1” are referred to the “low” and “high” levels of Table 3.2. For instance, the treatment combination in the first row was obtained, considering all the factors at their low levels, whereas the second one was obtained for the C, D and E factors at their high levels (A and B factors at their low level). The treatment combinations are indicated by the more compact Yates notation in the first column, Further details are available in Ref. [26]. The results retrieved for the mentioned combinations are collected in Table 3.4, in terms of the total frictional coefficient. The main effects of the five factors were determined according to the L8 by Taguchi and to the Yates Algorithm: they are shown in the bar graph in Fig. 3.3 along with their signs. Table 3.4. Results in terms of frictional coefficients determined for the 8 treatment combinations

Table 3.4. Results in terms of frictional coefficients determined for the 8 treatment combinations

	Treatment combinations							
	1	cde	be	bcd	ad	ace	abde	abc
Frictional coefficients μtot.	0.144	0.139	0.181	0.150	0.120	0.130	0.113	0.168
	0.131	0.133	0.171	0.139	0.118	0.147	0.110	0.147
	0.137	0.141	0.141	0.158	0.114	0.142	0.119	0.143
	0.130	0.128	0.144	0.149	0.125	0.137	0.120	0.146
	0.131	0.133	0.161	0.153	0.109	0.127	0.117	0.136
	0.153	0.145	0.169	0.153	0.138	0.157	0.124	0.177
	0.148	0.135	0.193	0.148	0.120	0.131	0.128	0.144
	0.150	0.136	0.167	0.153	0.129	0.128	0.121	0.139
	0.153	0.143	0.196	0.149	0.115	0.142	0.125	0.139
	0.138	0.126	0.194	0.154	0.132	0.147	0.119	0.153

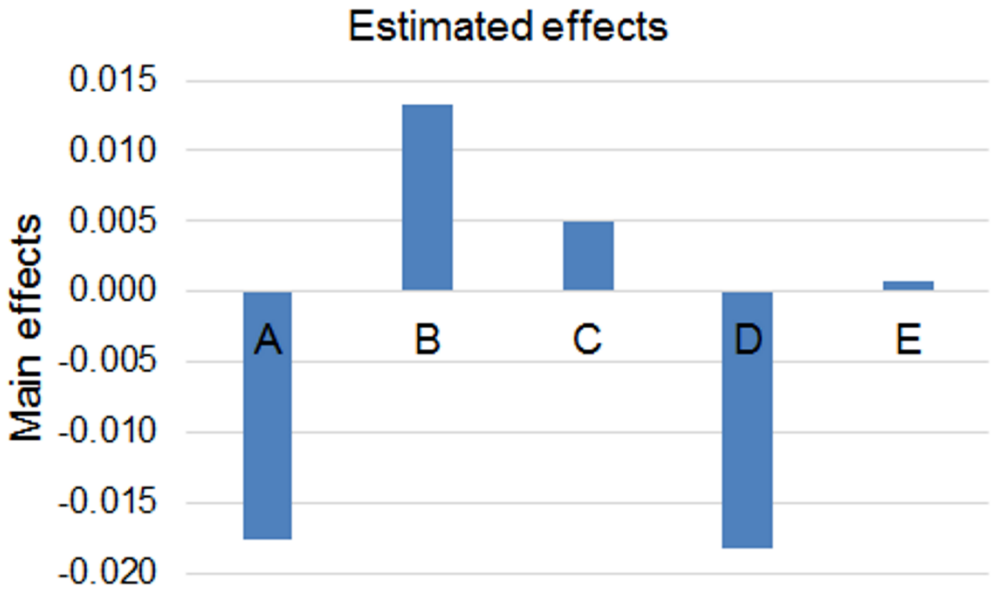

Fig. 3.3. Bar graph indicating the main effects of the investigated factors along with their signs

The results were then statistically processed by the tool of augmented ANOVA [26-27], used also in [28-30], to determine the significance of the five parameters. The results are reported in Table 3.5, where the acronyms SSQ, DoF, MSQ, Fcalc. and p.v respectively indicate Sum of squares, Degrees of freedom, Mean Squares, Fisher's ratio and p-value. The term Total indicates the total amount of variance, split into the effects of any single factor, the uncertainty-related term (Error) and a Residual. It must be pointed out that the Error term accounts for all the other factors, other than those in Table 3.2, that are likely to affect the frictional coefficient. In particular, the connection actual surface, contact geometry and external environment can be cited among these factors that, with their variations, may have an effect on the output variable, causing a noise commonly regarded as uncertainty. A sufficiently high number of replications, usually higher than 5, is necessary to reliably estimate uncertainty. Considering the widely accepted [26-27] 5% significance level, the parameters related to lubrication and to screw surface coating are highly significant and their effects are indeed the highest. Whereas, the effects related to the nut surface condition and to the washer previous use have a very low importance and are widely below the significance threshold. The effect of the washer type is also significant, even if it is lower than the other previously mentioned significant ones. A significance response indicates that the effect of those factors is evident, if compared to the uncertainty of the experiment: in other words, it can be separated from that of all the other aforementioned factors responsible of noise. Whereas, a not significance response indicates that the effect is confounded due to higher uncertainty. Based on these results, and considering also that the effect of underhead finishing has been already studied in literature (for example in [2]), the following campaigns were

focused on the determination of the effects of screw coating and of different lubrication procedures on the frictional response.

Table 3.5. Augmented ANOVA to determine the significance of the effects

	SSQ	Dof	MSQ	$F_{calc.}$	p-v
A	*0.00614*	*1*	*0.00614*	*53.16*	$3 \cdot 10^{-10}$
B	*0.00350*	*1*	*0.00350*	*30.28*	*5.42*
C	*0.00049*	*1*	*0.00049*	*4.25*	*0.043*
D	*0.00668*	*1*	*0.00668*	*57.83*	$8 \cdot 10^{-11}$
E	$9.6 \cdot 10^{-6}$	*1*	$9.6 \cdot 10^{-6}$	*0.083*	*0.77*
Residual	*0.00269*	*2*			
Error	0.00832	72	0.00012		
Total	0.02784	79			

3.2.3 Experimental results

As mentioned in the Introduction Section the following campaigns were aimed at studying the combined effects of screw coating and of lubrication and at a more detailed investigation on lubrication. The first campaign was framed within a two-factor ANOVA with six treatment combinations and ten replications each for a total of 60 experiments. No washer was used: the bolts were tightened, by torque application to the screw head posed on the test bench bearing-plate. The high strength (class 8) zinc coated nut was maintained constrained during the tightening procedure. The bearing-plate hole was changed after each trial. The results are collected in Table 6. As mentioned, the second campaign was focused on the effect of lubrication: this was regarded as single factor and was studied at different levels by the tools of a One-way ANOVA. In particular, five levels were considered with ten replications each for a total amount of 50 tests. The aforementioned levels corresponded to full (at the underhead and in the threads) Interflon lubrication, Interflon lubrication at the underhead only, Interflon lubrication in the threads only, full lubrication in Oil and dry conditions. The undernut was always lubricated (by Interflon or Oil). Black oxidized screws with related heads posed on the aforementioned steel

bearing-plate were used for the experiment. No washer was used and the substrate of the bearing-plate was new for each trial. The related results are summarized in Table 3.7.

Table 3.6. Results in terms of frictional coefficients related to lubrication and screw coating effects

		Lubrication		
		Dry cond.s	Oil	Interflon
Screw coating	Black oxidization	0.144	0.168	0.120
		0.166	0.157	0.122
		0.219	0.163	0.112
		0.155	0.176	0.112
		0.162	0.170	0.116
		0.208	0.150	0.121
		0.143	0.145	0.128
		0.188	0.146	0.126
		0.177	0.170	0.122
		0.182	0.134	0.113
	Zinc-coating	0.134	0.103	0.099
		0.139	0.127	0.094
		0.147	0.133	0.105
		0.145	0.092	0.098
		0.161	0.105	0.095
		0.151	0.112	0.093
		0.137	0.102	0.100
		0.134	0.116	0.098
		0.175	0.118	0.094
		0.128	0.113	0.097
		0.134	0.103	0.099

Table 3.7. One factor ANOVA involving Interflon or Oil full or partial lubrications

	Full lubr. in Interflon	Interflon lubr. underhead+ undernut	Interflon lubr. threads+ undernut	Full lubr. in Oil	Dry conditions
	0.120	0.139	0.164	0.168	0.145
	0.122	0.139	0.169	0.157	0.166
	0.112	0.152	0.162	0.163	0.219
	0.112	0.138	0.175	0.176	0.155
	0.116	0.136	0.170	0.170	0.162
	0.121	0.163	0.171	0.150	0.213
	0.128	0.137	0.191	0.145	0.142
	0.126	0.141	0.151	0.146	0.195
	0.122	0.132	0.155	0.170	0.184
	0.113	0.152	0.184	0.134	0.182
Column Means	0.1193	0.1429	0.1691	0.1579	0.1763

3.2.4 Discussion

The results of the first campaign, detailed in Table 3.6, where processed by the tool of two-way ANOVA to determine the significance of the two factors and of their interaction. The output is reported in Table 3.8, where the acronyms SSBR and SSBC, respectively indicate “Sum of Squares Between Rows” and “Sum of Squares Between Columns”. These two terms are respectively related to the impacts of the “row” and of the “column” factors, i.e. Screw coating and lubrication, considering again Table 6. The other acronyms retain the same meanings as in Table 3.5. The results indicate that the two factors are highly significant. Their interaction is also significant at the 5% significance level, even if it is much weaker (it turns to be negligible at a 3% significance level). The results can be commented in the light of the bar graph in Fig. 3.4, where

the excursion intervals of the results, from minimum to maximum values are also sketched. Zinc coating generally has the effect of significantly lowering the frictional coefficient, by an amount of approximately 20%. Its effect is similar in all the studied lubrication conditions, i.e. for dry contact surfaces, with Oil and Interflon lubrications. This similarity of the effects confirms that a not strong interaction is present. Regarding lubrication, Oil lubrication leads to a drop of the frictional coefficient by about 15%, whereas Interflon lubrication makes it possible to achieve a further drop by 17%, corresponding to a total drop by 32%. Therefore, on one hand, solid lubricant proved to be more effective than liquid one, consistently with the results of [3]. On the other hand, black oxides and Zinc coating are both effective at reducing friction, but zinc coating has a more beneficial effect. This effect can be related to surface smoothening or to the shearing of the treated surface. A brief remark must be finally made, regarding the possible effect of the initial smearing state and of the screw-structure interaction on the final actual lubrication and on its overall effect. This point is often a key issue, as serious failures [31] may arise from a not proper application of a lubricant, resulting in too high or too low preload. All the screws were lubricated by the same operator and the results exhibit a remarkably decreasing scatter, when comparing the frictional response in dry conditions to that under Oil and, especially, Interflon lubrication. This occurrence indicates that, despite the aforementioned issues, a final uniform lubrication can be obtained anyway. This positive outcome and stable behavior of the applied liquid and solid lubricants is also testified by their uniform response under repeated tightenings [3, 5]. Regarding the ceramic paste, it is worth remarking that, on one hand the smearing procedure must be performed manually, but, on the other one, visual inspection is usually sufficient to make sure of the correct lubricant application. This check is even facilitated by the color contrast between the ceramic paste and the screw surface.

Table 3.8. Two-factor ANOVA to determine the significance of the effects of screw coating and of lubrication

	SSQ	DoF	MSQ	$F_{calc.}$	p-v
SSBR	0.0263	2	0.0132	64.13	$5 \cdot 10^{-15}$
SSBC	0.0157	1	0.0157	76.63	$6 \cdot 10^{-12}$
SSI	0.0016	2	0.0007	3.62	0.03
Error	0.0111	54	0.0002		
Total	0.0546	59			

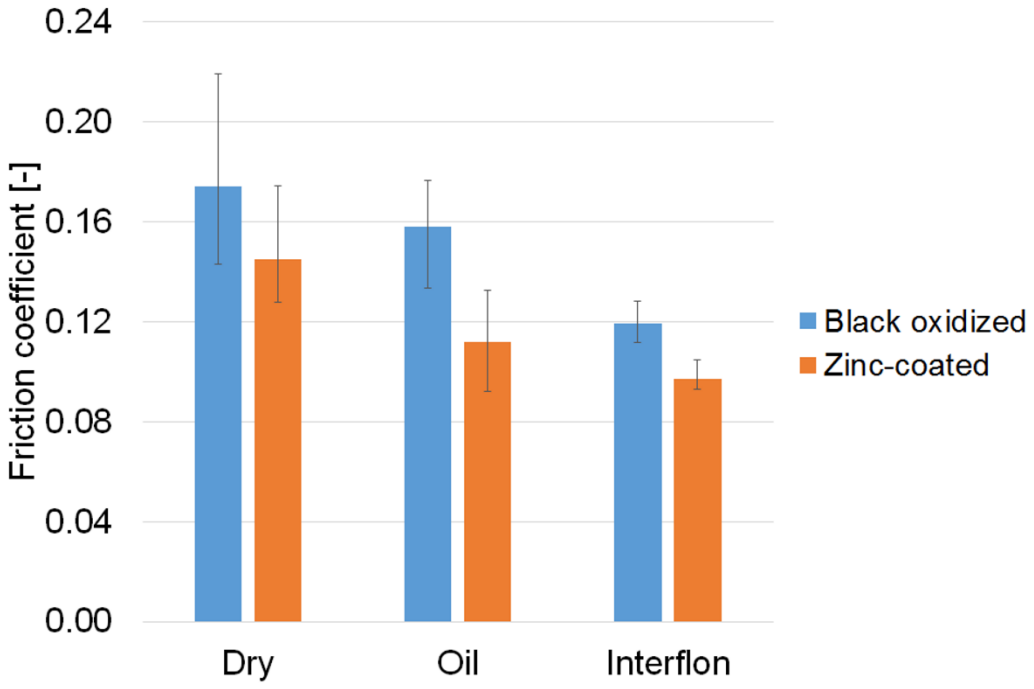

Fig. 3.4. Bar graph indicating the effects of screw coating and of lubrication on friction

The final step consisted in the detailed analysis of lubrication. The results in Table 3.7 were processed by One-way ANOVA: the output is reported in Table 3.9, which confirms, as expected, the high significance of the studied factor. Its effect is related to the term SSBC, acronym of "Sum of Squares Between Columns", indicated in the first row of the Table.3.9

Table 3.9. One-factor ANOVA in the investigation of the effect of lubrication

	SSQ	DoF	MSQ	$F_{calc.}$	p-v
SSBC	**0.0207**	**4**	**0.00517**	**21.80**	**$5 \cdot 10^{-10}$**
Error	**0.0107**	**45**	**0.00024**		
Total	**0.0314**	**49**			

The analysis was therefore deepened with the aim of allocating the sources of variance. In particular, it was interesting to compare the effect of the ceramic paste lubrication, when the lubricant is applied to the entire screw or just at the underhead or in the threads. The related response needed to be compared to that in dry condition or in Oil full lubrication. For this purpose, the tool of pairwise tests was used. In particular, two test types were applied: the Least Significant Difference (LSD) and the Newman-Keuls Test. The first one compares the difference of two column means (considering the results in Table 7) to a fixed threshold. It depends on the

Mean Squares Error (MSE), namely the ratio between the Error term in Table 3.9 and its degrees of freedom, and on the number of replications. The second one adopts a variable threshold, which increases, as the difference between column means increases [26]. From this point of view, this second test, which adopts a generally higher threshold, is more reliable, when pointing out significant differences. The fixed threshold for the first test, namely the LSD, is computed in Eq. (3.2), where R indicates the number of replicated tests, 10. Whereas, the threshold for the Newman-Keuls Test (NKD) is indicated in Eq. (3.3), where q is a coefficient provided by Ref. [26]. This coefficient assumes different values, depending on the number of steps separating the column means, when they are ordered in increasing order. This occurrence makes it possible to have a variable threshold. For the sake of clarity, column means are appended at the bottom row of Table 3.7. The results of the comparisons along with the considered thresholds are reported in Table 3.10.

$$LSD = t \cdot \sqrt{MSE} \cdot \sqrt{\frac{2}{R}} \tag{3.2}$$

$$NKD = q \cdot \sqrt{\frac{MSE}{R}} \tag{3.3}$$

Table 3.10. Pairwise Tests by LSD and Newman-Keuls methods

	Difference of column means	LSD threshold	NKD threshold	Significant (Y/N)
(Interflon lubr. underhead+undernut) vs. (Interflon lubr. threads+undernut)	**0.0262**	**0.0139**	**0.0172**	**Y**
(Interflon lubr. threads+undernut) vs. (Dry conditions)	**0.0072**	**0.0139**	**0.0142**	**N**
(Interflon lubr. underhead+undernut) vs. (Dry conditions)	**0.0334**	**0.0139**	**0.0190**	**Y**

Considering in particular the Interflon lubrication, the frictional response with lubrication at the underhead only, was compared to that when only the threads are lubricated. Both the tests indicate that the differences are significant. Afterwards, the response with lubrication in the threads only was compared to that in dry conditions. In this case, the measured friction coefficients are quite close and the difference of column means is below the thresholds for both tests. Whereas, when comparing the response with lubrication at the underhead to that without lubrication, a significant difference is indicated by the LSD Test. It can be remarked that the Newman-Keuls Test, which is more reliable, since it considers a much higher (about 37%) threshold (0.019 vs. 0.013), was consistent to confirm this result. This is an interesting outcome that indicates that Interflon lubrication in the threads retains a much lower importance than that at the underhead. Conversely, lubrication at the underhead is essential to reduce friction affecting the bolt preload. This outcome indicates that the tribological response upon tightening is steered more by the contact at the underhead rather than by the contacts in the threads. This contact is generally affected by the actual roughness of the surface at the underhead. Therefore, friction at the underhead is the main responsible of torque dissipation, i.e, of the amount of tightening torque that is lost due to friction and is not converted into axial preload. As a matter of the fact, lubrication at the underhead and limited friction between the mating surfaces provide the benefit of significantly lowering the amount of dissipated torque, thus allowing a much higher torque to be transferred to the shank and converted into axial preload.

The same tool of pairwise tests indicates that Interflon lubrication, even when carried out at the underhead only, is more effective than Oil lubrication. These results can be summarized by the bar graph in Fig. 3.5, where solid vertical lines indicate significant differences between the adjacent distributions, the bar extensions are proportional to mean values and excursion ranges from minimum to maximum values are added. The results of the pairwise tests were finally refined by the tool of orthogonality (used also in [28-30]), which made it possible to split the sources of variance in the performed experiment. The results of this analysis are summarized in the cake diagram in Fig. 3.6.

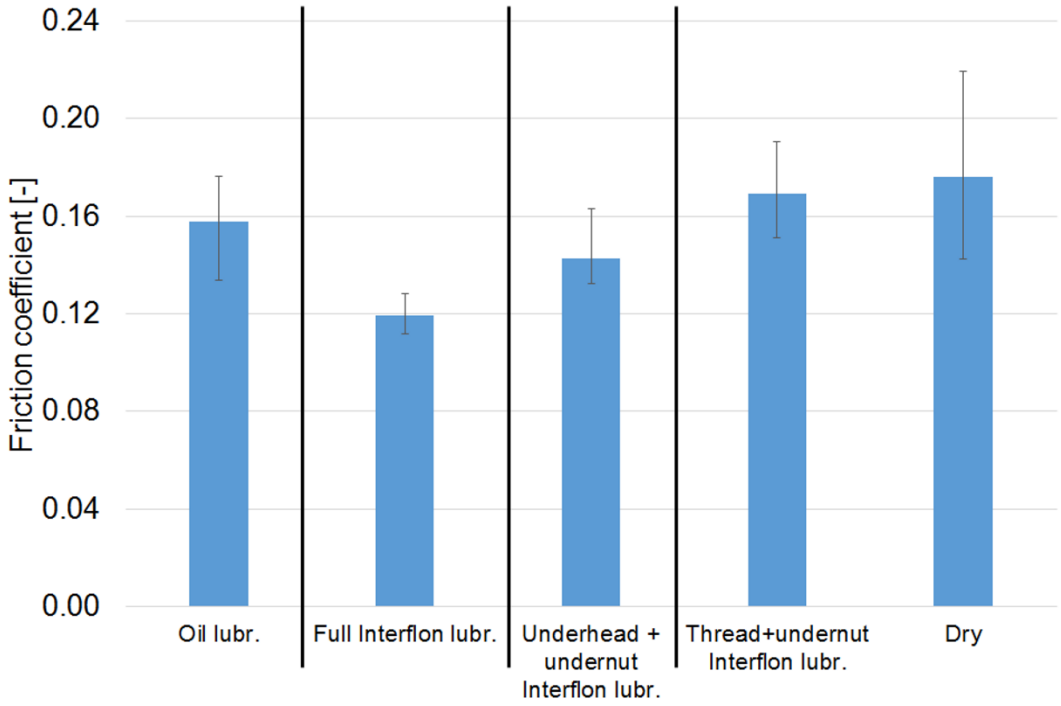

Fig. 3.5. Bar graph indicating the results at different levels of lubrication along with their excursion ranges

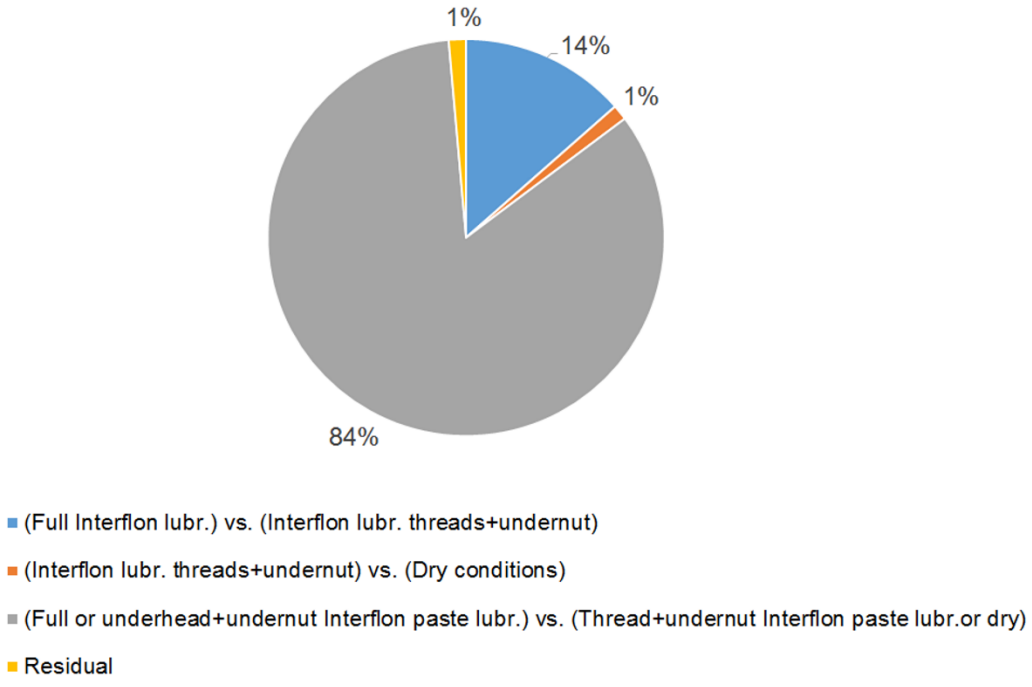

Fig. 3.6. Cake diagram summarizing the sources of variance determined by its orthogonal decomposition

Considering the outputs of the pairwise tests, the results under full Interflon lubrication and under underhead lubrication were merged together and compared to those in Dry conditions or with lubrication in the threads only. The results in these conditions were also regarded as merged together. It can be pointed out that the largest amount of variance, 84% of the total, is related to this contribution. Another, much smaller, source of variance is related to the response under full lubrication and with lubrication at the underhead only. Very small and not significant slices correspond, finally, to a residual and to the response in dry conditions vs. that with lubrication in the threads only. The results of the augmented ANOVA are reported in Table 3.11.

Table 3.11. Augmented ANOVA in the investigation of the effect of lubrication

	SSQ	DoF	MSQ	$F_{calc.}$	p-v
SSBC	0.0207	4	0.00517	21.80	$5 \cdot 10^{-10}$
(Full Interflon lubr.) vs. (Interflon lubr. threads+undernut)	*0.0028*	*1*	*0.0028*	*11.79*	10^{-3}
(Interflon lubr. threads+undernut) vs. (Dry conditions)	*0.0003*	*1*	*0.0003*	*1.09*	*0.30*
(Full or underhead+undernut Interflon paste lubr.) vs. (Thread+undernut Interflon paste lubr.or dry)	*0.0173*	*1*	*0.0173*	*73.11*	$5 \cdot 10^{-11}$
Residual	*0.0003*	*1*	*0.0003*	*1.23*	*0.27*
Error	0.0107	45	0.00024		
Total	0.0314	49			

3.3 Effect of a suitable lubrication on the friction coefficient for repeated tightening operations

In the previous paragraphs the effect of a suitable lubrication with a ceramic paste it is taken into account for different coating of the fasteners. In order to evaluate the effect of the same lubrication condition on the friction coefficient for a repeated tightening, it was analyzed the case of a Planetary gear boxes. The present work has been carried out by means of both numerical finite element analyses and experimental stress analysis techniques.

3.3.1 Introduction

Planetary gearboxes generally consist of a ring gear, which is connected with the input and output flanges by means of several screws, equally spaced along the diameter. These screws must provide enough axial preload to the parts in order to allow the assembly withstanding the design breakaway torque. The axial preload is easily found, provided that the geometry of the screw and the friction coefficients in the thread and in the underhead are known. How is reported in the previous paragraphs the friction coefficient have a strong impact on the performance of the threaded joints, and are in turn affected by several parameters as: (i) the materials in contact [24,32-35], (ii) the wear or corrosion of the surfaces [2,6,36], (iii) their state of lubrication [3,31,37,38], (iv) the coating characteristics [39] and (v) the tightening speed [40]. Moreover, the literature reports that a better exploitation of the screw material may be achieved, if the coefficients of friction take values within a certain interval [41]. Due to manufacturing reasons, simultaneous torque–angle control [37,42] or more sophisticated means (e.g. that reported in Heyman and Chern [43]) to assess the achievement of a correct preload during assembly are not feasible for the particular gearbox that was the object of this investigation. Therefore, since the tightening torque remains the only controlled parameter during the assembly procedure, it is mandatory to characterize the friction coefficients accurately. Other than this, maintenance operations introduce one more issue: in fact, the wearing conditions and, consequently, the friction coefficients experience significant changes through repeated tightenings. Due to this occurrence, the axial preload is expected to encounter strong fluctuations, although the retightening torque is retained constant. As a consequence, loosening in operation conditions is likely to occur, which may lead to undesired relative displacement between the ring gear and the flanges and sometimes induce more serious failures. [44] The present research aims at characterizing the evolution of the coefficient of friction through multiple tightenings, in the presence or absence of lubricants. An instrumented sleeve is used for measuring the screw preloading force during repeated tightenings Fig. 3.7. The mean friction coefficient of the joint is then calculated back, by means of a widely known formula [3,36], as a function of the geometry, the preload torque estimated by a torque wrench and the axial preload value measured by the instrumented sleeve. The tests have been carried out considering both dry and lubricated surfaces, over a set of five re-tightening operations.

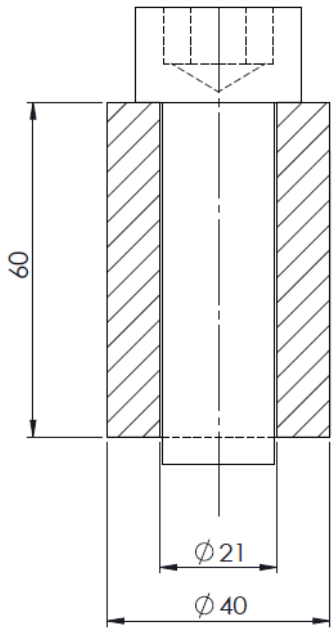

Figure 3.7: Sketch of the specimen for the evaluation of the screw initial preload F_V.

As detailed in [2,3] the instrumented sleeve must be interposed between the screw underhead and the flange. In order to recreate the actual boundary conditions in terms of frictional behavior of the underhead, the specimen shall be manufactured with the same material, roughness and surface treatment of the flange. In the present case, the flanges are manufactured with cast iron EN GJS 500-7U(EN 1563:1997,22 see Table 3.12), whereas the ring gear is made of steel. The flanges have a mean roughness Ra 5 µm and a mean hardness HB_{30} 240. The parts are joined together by means of twenty M20, L 160 mm, class 12.9 (ISO 898-1: 1993[46]) black oxidized socket head screws, whose characteristics are summarized in Table 3.12.

Table 3.12: Cast iron EN GJS500 - 7 properties, according to [45]

S_u	**Ultimate strength**	**500**	**MPa**
S_y	**Yield strength**	**320**	**MPa**
A%	**Elongation at break**	**7**	**-**
Y	**Young's modulus**	**169**	**GPa**
v	**Poisson's Ratio**	**0.275**	**-**
HB	**Brinell hardness**	**>180**	**-**
ρ	**Density**	**7,200**	**kg/m³**

Table 3.13: Screw characteristics, according to [46-47]

S_u	Ultimate strength	1,200	MPa	[23]
S_y	Yield strength	1,080	MPa	[23]
d	Nominal diameter	20	mm	[24]
d_2	Pitch diameter	18.376	mm	[24]
A_t	Stress area	245	mm^2	[23]
p	Pitch	2.5	mm	[24]

3.3.2 Finite elements analysis

In order to assess the overall behavior of the joint before the experimental tests, a finite elements analysis has been performed on the gearbox. The primary purpose of such analysis was correlating the preload applied to the screws to the strain measured on the external surface of the planetary gear. The secondary aim of the FEA analysis was to assess whether the bolt preload chosen for the experimental tests would be suitable, considering the mechanical characteristics of the assembly. The FEA model has been developed in ANSYS Workbench R.12.

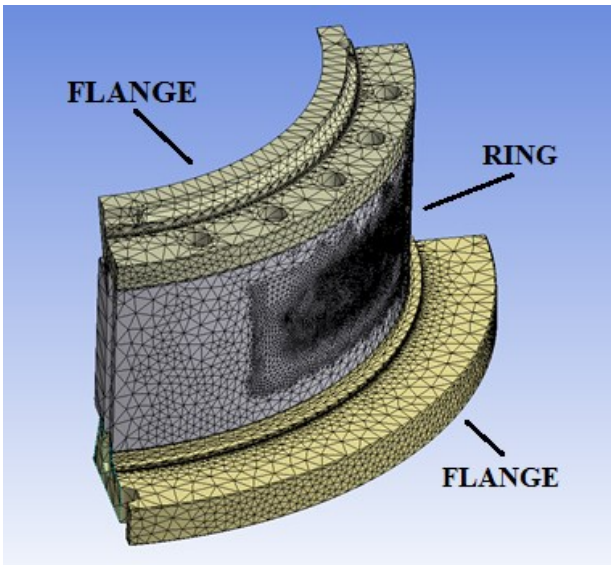

Figure 3.8: Mesh of the FEA model (quarter geometry)

The geometry of a quarter of the gearbox has been used, leveraging the double planar symmetry of the structure. It was analyzed a quarter of this in order to considering the effect of all screws in a specific point. The strain distribution in the gearbox is not homogeneous in the thickness. The model has been meshed with four-node tetrahedral elements (SOLID187 in the Ansys nomenclature). The mesh is shown in Fig. 3.8: a refinement window can be seen in the central area of the external surface of the ring. The general element size is a=5mm, whereas in the refinement window it drops down to a'=1mm. The overall number of nodes is n=270,506.

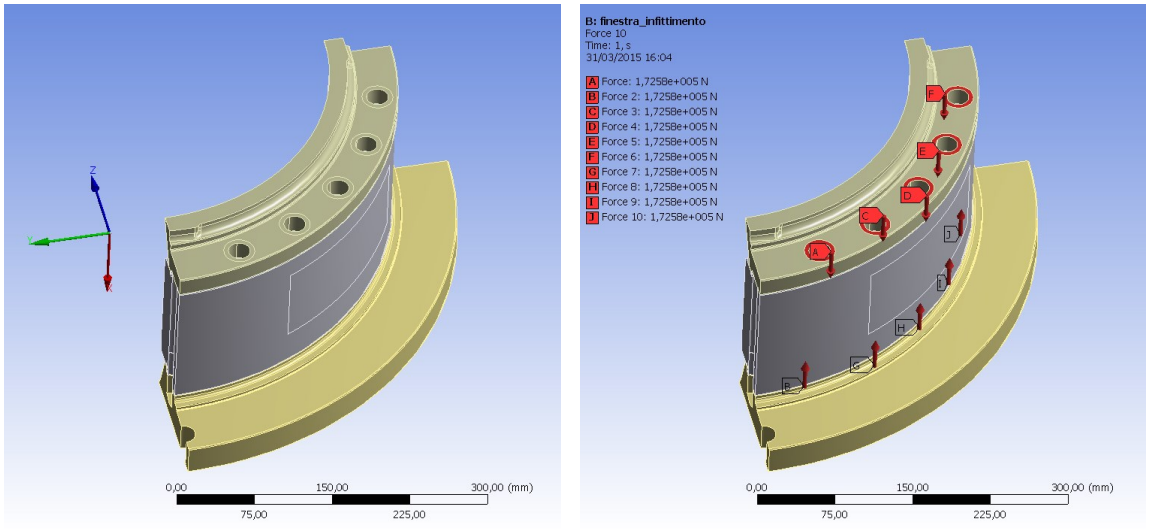

(a) (b)

Figure 3.9: (a) Coordinate system, (b) load application

The contacts between the upper flange and the ring and between the ring and the lower flange are set as bonded, pure penalty, with the normal stiffness controlled by the software. The coordinate system is shown in Fig. 3.9 (a), whereas the loads can be seen in Fig. 3.9 (b). The preload set on each screw M20 TCEI 12.9, equal to Fv = 172,580N, has been simulated by the application of two equal forces Fv, sharing the same line of action, but opposite in sign. The forces represented by the downwards pointing arrows in Fig. 3.9 (b) are applied to an annular region, and represent the forces transmitted to the upper flange by the head of the screw. The upwards pointing arrows in Fig. 3.9 (b) indicate the forces applied to the threaded portion of the lower flange of the gearbox. The lower flange is externally constrained by means of a frictionless constraint applied to its base surface. The application of the aforementioned forces F_v leads to the state of stress depicted in Fig. 3.10, which refers to the normal stresses along the x axis in the gearbox.

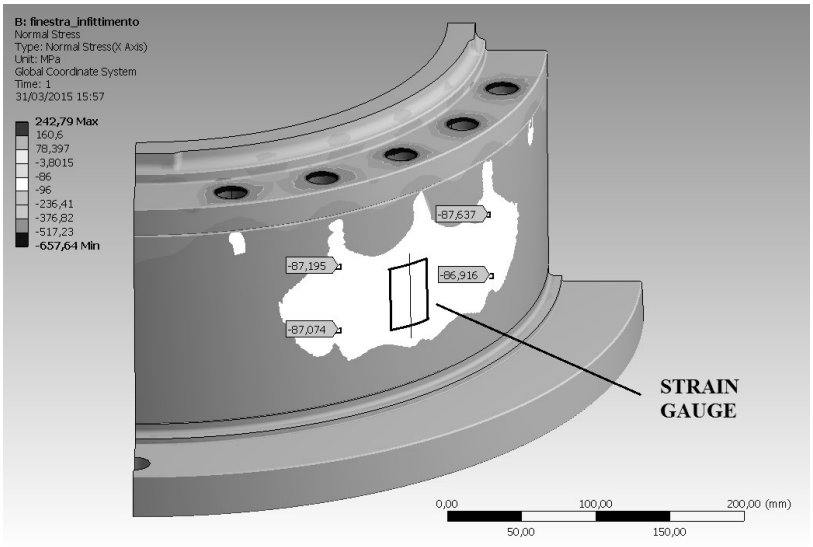

Figure 3.10: σ_x stresses generated by the screw preload F_v

In Fig. 3.10, the area where the values of the stresses σ_x fall within the range [- 96 MPa; -86 MPa] is shown in white color, whereas the flags indicate some local values of σ_x. During the experimentation, a strain gauge will be applied on the external surface of the ring, with its main axis aligned with the axis of the ring (x-axis), as shown in Fig. 3.10. The signal of this strain gauge is sampled, in order to have an additional reading of the screws preload values: this arrangement allows to double check the correct reading of the sleeve specimens directly in the field. The sleeve specimen shown in Fig. 3.7 is instrumented by a quarter-bridge strain gauge, applied to its external cylindrical surface, with the main axis aligned with the screw axis. In order to obtain an accurate measurement of the force acting on the screw through the axial strain of the sleeve, it

is mandatory that such axial stress/strain state exhibits a uniform distribution over the entire section at the measurement point on the sleeve.

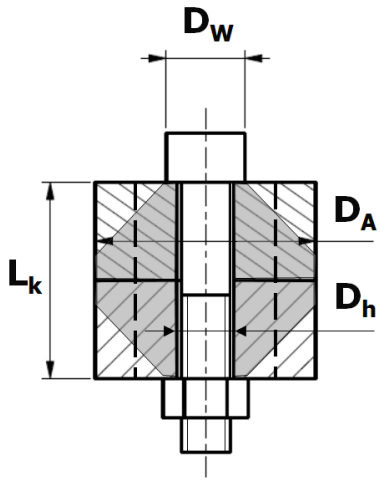

Figure 3.11: Equivalent compressed area.

Referring to Fig. 3.10 and Fig. 3.11, D_W=30mm is the screw head external diameter, D_A=40mm is the external diameter of the bushing, D_h=21mm is the hole diameter and L_k=60mm is the length of the bushing. In the present case, $D_W < D_A < D_W + L_k$, hence the equivalent compressed area of the joint can be calculated, according to [48], by means of the following expression:

$$A_{eq} = \frac{\pi}{4} \cdot \left(D_W^2 - D_h^2\right) + \frac{\pi}{8} \cdot D_W \cdot \left(D_A - D_W\right) \cdot \left[\left(\sqrt[3]{\frac{L_k \cdot D_w}{D_A^2}} + 1\right)^2 - 1\right] \cong 733 mm^2 \tag{3.4}$$

If a more accurate estimation is needed, some alternative formulations may be found in [26]. By comparing the value obtained by Eq. (3.4), to the nominal sectional area of the specimen:

$$A_n = \frac{\pi}{4} \cdot \left(D_A^2 - D_h^2\right) \cong 910 mm^2 \tag{3.5}$$

According to this quite rough estimation, it can be observed that about twenty percent of the volume of the specimen remains uncompressed. Alternatively, according to [32], the angle of the substitutional deformation cone ϕ_E can be evaluated as follows:

$$\varphi_E = \arctan\left[0.348 + 0.013\ln(\beta_L) + 0.193\ln(y)\right] \quad (3.6)$$

Eq. (3.6) holds true in the case of cylindrical tapped thread joint, where L_W is the length of the sleeve specimen. Symbol $\beta_L=L_k/D_w$ represents the length ratio of the joint, whereas $y=D_A/D_W$ is its diameter ratio. In the present case, $\beta_L=2$ and y=1.33, therefore $\phi_E=22.4°$. It must be pointed out that the substitutional deformation cone angle is not identical to the angle formed by the screw axis and a segment connecting the outermost point of the bearing area in the underhead with the point at the external surface of the sleeve at which the y-axis pressure equals zero [32]. Nonetheless, it can be verified by means of FEA that such angle well defines a volume in which the y-axis pressure stays below 10% of the nominal contact pressure $p_n=F_V/A_n$. In order to proceed with a FEA simulation, the specimen has been modeled in two dimensions, imposing the axial symmetry of the model around y-axis (Fig. 3.12). The geometry has been meshed with eight-node elements (PLANE 183) for a total amount of about 18,000 nodes with an average size of 0.5mm. The screw-bushing contact is managed by a frictionless, pure penalty, contact formulation. The screw preload is simulated by a force applied at the lower end of the shank, equal to F_v=172,580N. The resulting normal stress distribution along the y-axis is shown in Fig. 3.12. It can be seen that, about one third L_k underneath the screw – bushing contact surface, the stresses are: (i) uniformly distributed over the whole section and (ii) equal to $p_n=F_V/A_n$=190MPa. Looking at Fig. 3.12, one can appreciate how the uncompressed volume (pressure below 10% of the nominal contact pressure p_n) is actually delimited by a paraboloid of revolution (and not a straight segment) connecting the outermost point of the screw head with the external surface of the sleeve: this occurrence is in good agreement with [32]. For the sake of an accurate strain reading, it can be concluded that the strain gauge shall be positioned at half the length of the sleeve or below.

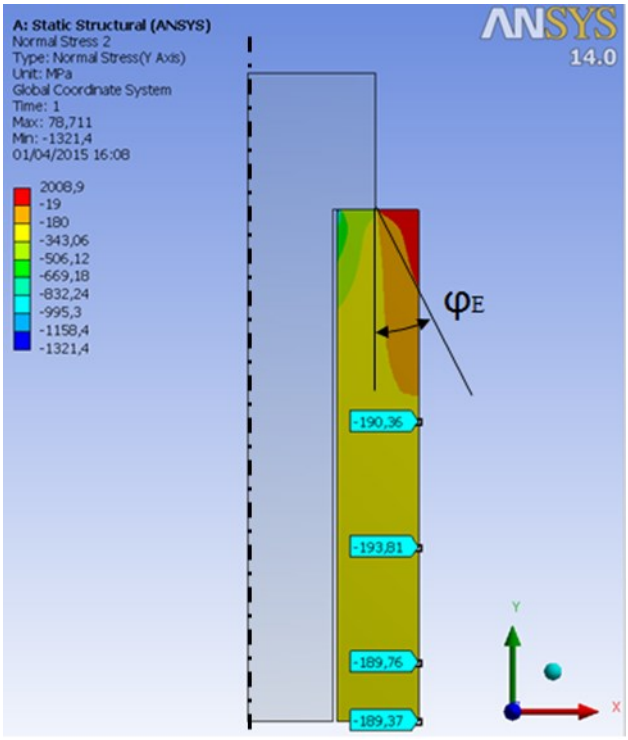

Figure 3.12: σ_y stress distribution along the sleeve specimen, substitutional deformation cone angle ϕ_E.

3.3.3 Experimental test

A total amount of six specimens has been manufactured and instrumented, each underwent three equally spaced (120°) roughness measurements on both faces. This task has been performed by means of a roughness meter Zeiss Handysurf E-30A. The results are reported in Table 3.14. The upper face of the specimen is the one which mates with the screw underhead: this face is identified in the following by capital letter “A”, whereas the face at the opposite end is called “B”.

Table 3.14: Underhead roughness measurements.

Specimen ID		1	2	3	4	5	6
SIDE	MEASUREMENT	Ra [µm]	Ra [µm]	Ra [µm]	Ra [µm]	Ra [µm]	Ra [µm]
A	1st	5.3	5.1	3.9	4.2	5.5	4.9
A	2nd	6.3	4.2	3.7	3.5	5.4	5.6
A	3rd	5.6	4.3	4.2	3.9	5.4	5.5
	MEAN	5.73	4.53	3.93	3.87	5.43	5.33
	STD DEV	0.51	0.49	0.25	0.35	0.06	0.38
	GRAND MEAN	4.81					
B	1st	3.4	5.8	5.5	7.7	4.3	5.6
B	2nd	3.8	6.3	5.9	8	3.4	4.9
B	3rd	3.8	6	6.2	8.1	3.8	5.1
	AVERAGE	3.67	6.03	5.87	7.93	3.83	5.20
	STD DEV	0.23	0.25	0.35	0.21	0.45	0.36

From the data in Tab. 3.14, it can be concluded that the grand mean of the surface roughness of the specimens' face "A" is R_{a_M}=4.81µm, which is in good agreement with the roughness values prescribed for the gearbox flanges. As a means to assess the conformity of the specimen material with the requirements reported in Tab. 1, hardness measurements have been performed on three randomly selected bushings. The samples have been taken on the "B" face of the sleeve, so as not to impair the surface characteristics of the "A" side. The results are summarized in Table 3.15.

Table 3.15: Brinell hardness test HB_{30}.

	Hardness HB_{30}	Avg. Hardness	Std. Dev.
Test 1	233		
Test 2	242	242	9
Test 3	251		

By comparing the data of Tab. 3.15 with the data reported in Tab. 3.12, it can be concluded that the specimen material conforms to the specifications contained in [45]. Fig. 3.13 shows the test arrangement, during screw preloading. The specimens have been instrumented by means of strain gauges made by Vishay Micro measurements, model CEA-06-375UW-350Ω, with a grid length of 9.53mm.

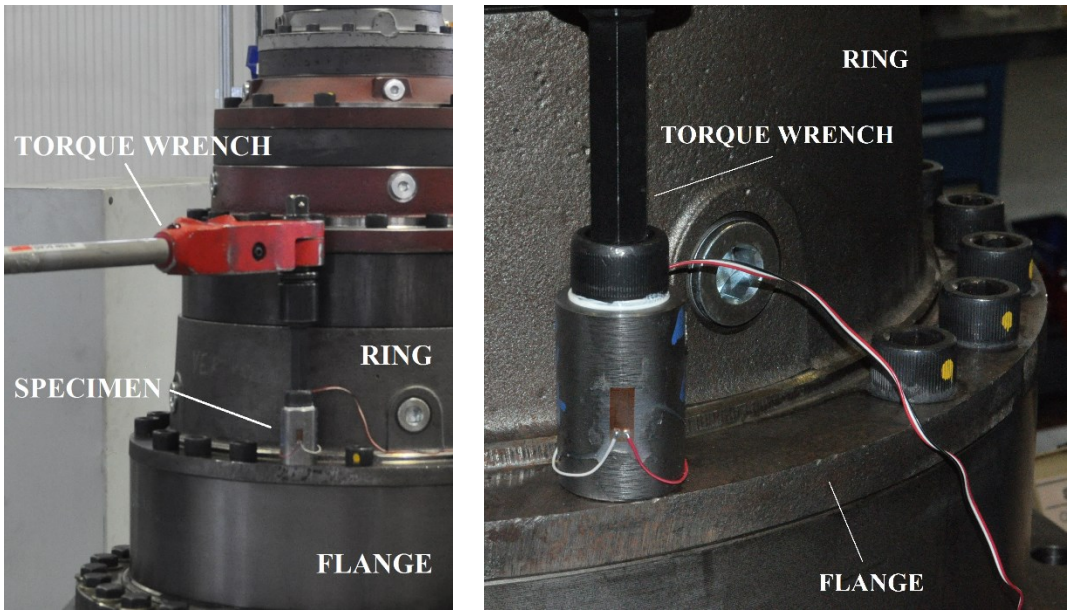

(a) (b)

Figure 3.13: Test arrangement (a) overall view (b) close up of the specimen

As for the numerical – experimental correlation, the axial stress on the outer surface of the gearbox has been sampled by means of a strain gauge made by HBM, model 1-LY43-10-350Ω, with a grid length of 10mm. This sensor has been applied with the main grid axis aligned with the gearbox axis, as shown in Fig. 3.14. All the strain gauges have been sampled by means of the control unit Vishay P-3500.

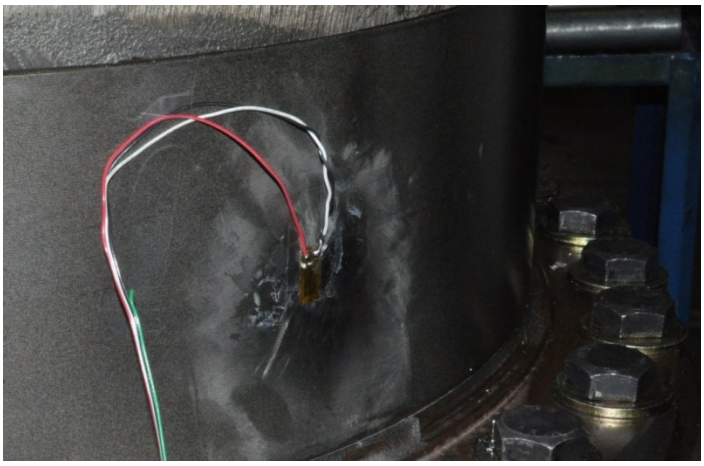

Figure 3.14: Position of the strain gauge at the outer surface of the ring

In the case of dry surfaces, the upper face of the load cell and the threaded portion of the screw have been degreased by means of cleaner Loctite 7063. In the case of tightening with ceramic paste HT1200, the surfaces have been cleaned by means of Loctite 7063, and then greased with ceramic paste on the screw thread and underhead, as shown in Fig. 3.15.

Figure 3.14: Application of the ceramic paste

The application of the paste has been performed before the first tightening and never repeated for subsequent tightenings. The sleeve has then been mounted between the screw underhead and the flange of the gearbox, as indicated in Fig. 3.13. In order to account for the extra-length due to the sleeve, a longer screw (L=220mm) had to be used. All the other characteristics of this longer screw are identical to those of the original screw. During the tightening operation, the screw-sleeve assembly is connected in series [32, 2, 36], hence, the knowledge of the axial strain of the sleeve (whose geometrical and material parameters are known) easily leads to the initial preloading force of the screw. Provided that the tightening torque is simultaneously measured

by means of a torque wrench, it is then possible to compute the mean friction coefficient μ_m of the joint by means of Eq. (3.7):

$$\mu_m = \frac{\frac{T}{F_V} - 0{,}159 \cdot p}{0{,}577 \cdot d_2 + 0{,}5 \cdot D_b} \tag{3.7}$$

Symbol T in Eq. (3.7) represents the preloading torque, whereas F_V is the initial preload, p is the pitch, d_2 is the mean diameter of the threaded portion of the screw and D_b is the mean diameter of the underhead. The aim of the experimental campaign was to measure the mean friction coefficient of the joint, both for dry and lubricated surfaces of the thread and of the underhead. The evolution of the mean friction coefficient over a set of five consecutive tightenings has been studied as well. Therefore, the influence of lubrication on the surface wearing behavior has been determined, when multiple re-tightenings take place. The test sequence has been arranged as follows:

1. Five consecutive dry tightenings of a single screw at T=400Nm, sleeve specimen number 1;
2. Five consecutive dry tightenings of a single screw at T=400Nm, sleeve specimen number 2;
3. Five consecutive dry tightenings of a single screw at T=400Nm, sleeve specimen number 3;
4. Five consecutive tightenings with ceramic paste of a single screw at T=400Nm, sleeve specimen number 4;
5. Five consecutive tightenings with ceramic paste of a single screw at T=400Nm, sleeve specimen number 5;
6. Five consecutive tightenings with ceramic paste of a single screw at T=400Nm, sleeve specimen number 6;
7. Tightening of the whole set of twenty screws, at T=687Nm, repeated twice, with application of ceramic paste and acquisition of the strain at the ring gearbox, for the numerical – experimental correlation.

All the tests, except the last one, have been performed at a preloading torque of 400Nm by means of a hand operated torque wrench made by Torqueleader, model 400, with three replications for each lubrication condition. The single screw tightening, as described in steps from 1 to 6 has been performed with the remaining screws of the gearbox being fully tightened. It is

then important to point out that each replication has been performed with a new screw-specimen pair, so that the current results were not affected by the tests at the previous steps. For actual manufacturing operations, the specified preloading torque of the gearbox screws is T=687Nm, while most of the tests have been performed at 400Nm. This choice is due to the issue that tightening at T=687Nm is not feasible with the hand operated torque wrenches that were available at the test facility. In fact, the actual components are assembled by means of impact wrenches. Since the influence of the tightening speed and of the preload level on the friction coefficients may not be negligible [38, 40], the test listed at point 7 has been conceived as a double check of the previously calculated friction coefficients (at reduced torque level and tightening speed) for the case of lubricated joint. In other words, the strain gauge on the ring allows to verify that, when T=687Nm is achieved by means of an impact wrench and μ_m is assumed equal to the mean value calculated based on the outcomes of the previous tests, the actual preload of the screws is suitably close to the value calculated by means of Eq. (3.8):

$$F_V = \frac{T}{(0{,}159 \cdot p + 0{,}577 \cdot \mu_m \cdot d_2 + 0{,}5 \cdot \mu_m \cdot D_m)} \tag{3.8}$$

3.3.4 Results

The data obtained by the experimental investigation are collected into the bar graphs of Fig. 3.15(a) and (b). Each graph has scatter bands reporting maximum and minimum measured values. The dry joint has a mean friction coefficient (average of three measurements) of μ_m=0.311 at first tightening, which grows up to μ_m=0.394 at fifth tightening. Over five re-tightening operations, the increase is in the order of 27% with a peak up to 38%. The paste lubricated joint has a mean friction coefficient (average of three measurements) of μ_m=0.162 at first tightening, which slightly decreases at μ_m=0.153 at fifth tightening, corresponding to a negligible variation of about 6% over the entire set of re-tightening operations. This outcome can be easily confirmed also by the analysis of the variance of the results (ANOVA) [2, 26, 28, 50–55] at a very high confidence level (around 90%): thanks to paste lubricating effect, the tribological behavior is made independent of the retightening operation. Considering the graphs reported in Fig. 3.15, it is interesting to highlight that lubrication yields an additional beneficial effect in terms of a remarkable reduction of the scattering. From the quantitative point of view, the ‘‘Sum of Squares Within’’ (SSW) term, which is the estimator of uncertainty in the ANOVA, is decreased by a factor 60 (for the same number of degrees of freedom), as an effect of the paste application. As for the preload values, that of the dry screw has a mean value of 53kN at first tightening which drops down to approximately 42kN at fifth tightening. The evolution of the initial preload of the screw in the dry condition is highlighted by triangular indicators in Fig. 3.16.

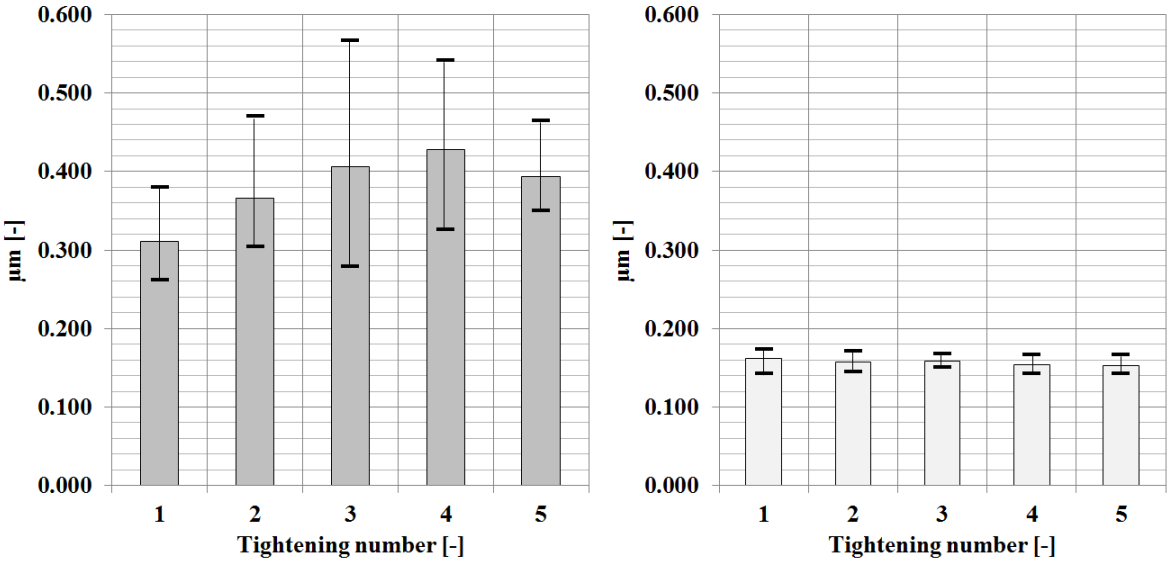

Fig. 3.15: Mean friction coefficient evolution for (a) dry and (b) paste lubricated joint

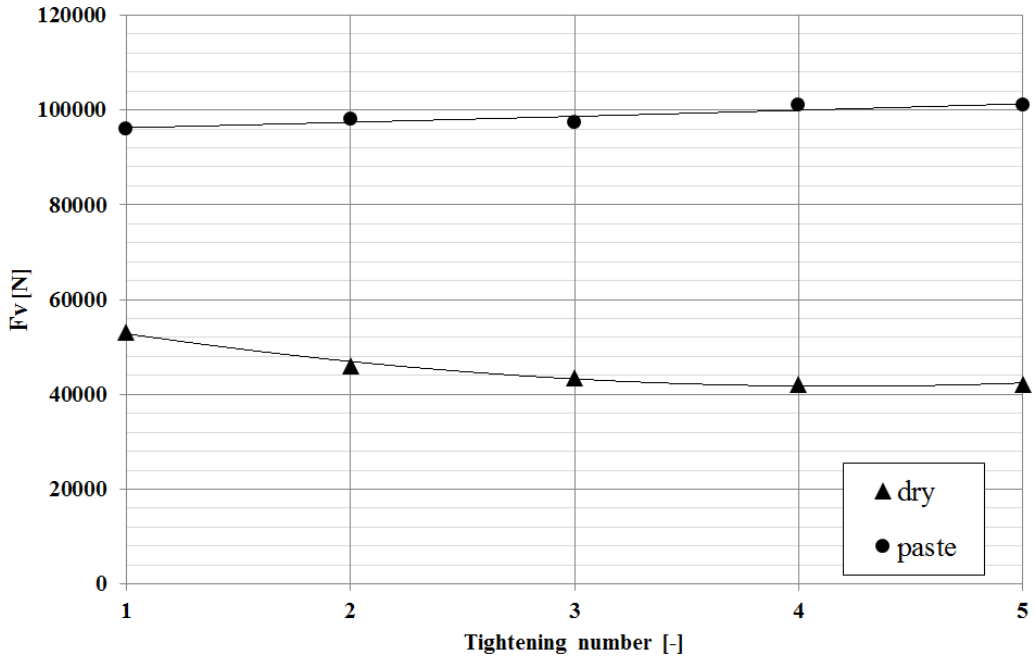

Figure 3.16: Initial preload evolution across a set of five re-tightening operations: dry and lubricated conditions

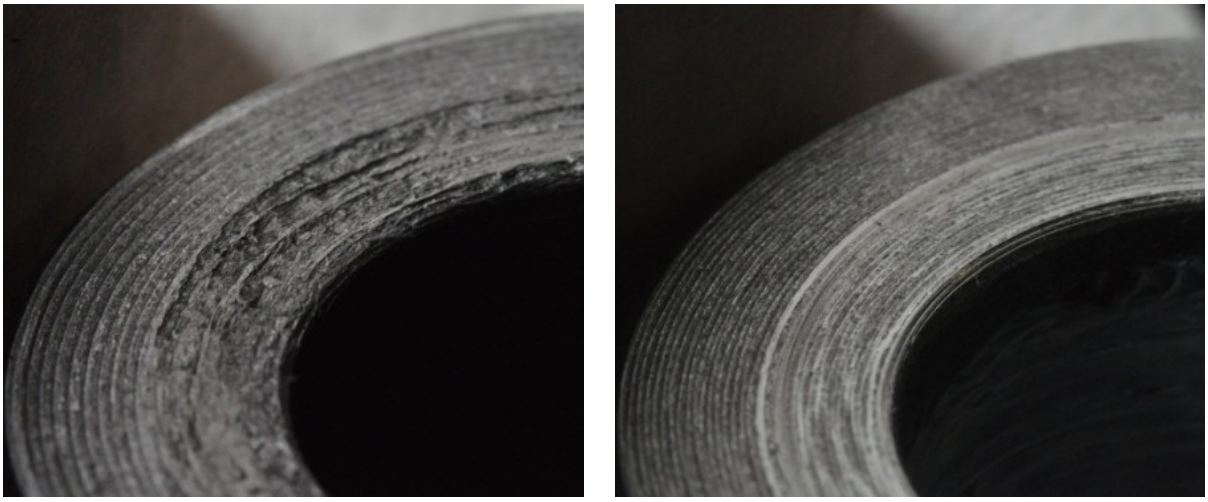

(a) (b)

Figure 3.17: (a) Sleeve surface after dry tightening, (b) Sleeve surface after tightening with ceramic paste

The underhead contact area of the sleeve (surface “A”) exhibits remarkably different wear patterns, depending whether the joint is lubricated or not. The two pictures in Fig. 3.17 (a) and (b) represent a sleeve underhead surface, which operated in the dry condition and a sleeve underhead surface treated with ceramic paste respectively. Across five re-tightening operations, the ceramic paste treated surface undergoes far less degradation with respect to its homologous operated in the dry condition. The large pits visible in Fig. 3.17 (a) are due to a noticeable amount of material removal, as it can be appreciated in Fig. 3.18. This image refers to a sleeve that operated in the dry condition across five re-tightenings, just after screw removal: the large amount of iron debris can be clearly seen.

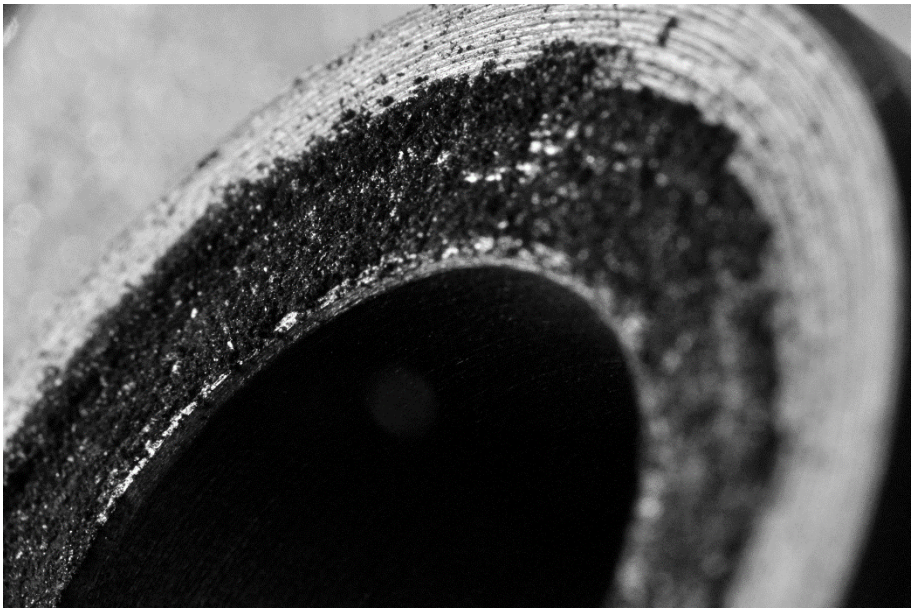

Fig. 3.18 Large amount of iron debris just after five re-tightenings and screw removal

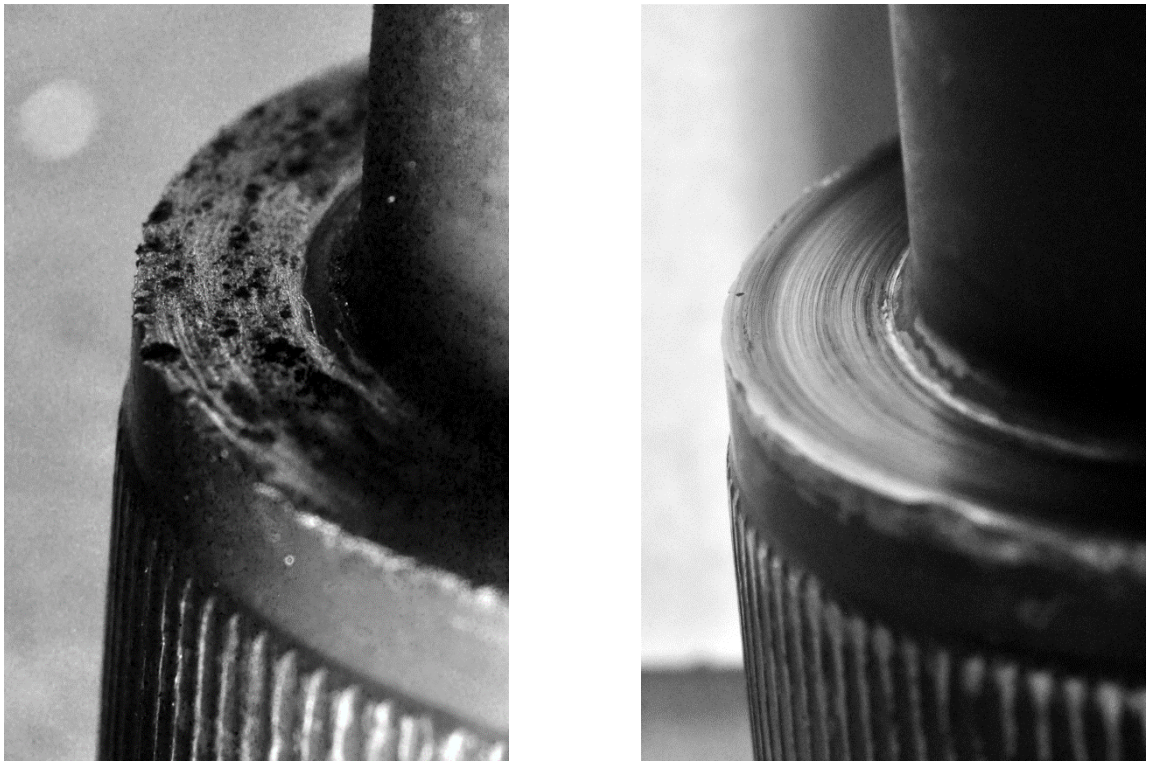

(a) (b)

Fig. 3.19 Screw underhead after operation: (a) dry tightening, (b) tightening with ceramic paste

As a matter of the fact, a screw counterface, which operated in the dry condition for five re-tightenings exhibits a noticeable amount of material transfer from the cast iron surface to the steel surface, as shown in Fig. 3.19 (a). Such occurrence is in quite good agreement with the findings of Riahi and Alpas [56], who identified a similar behavior in the case of severe sliding wear of grey iron – steel pairs. On the contrary, the paste lubricated steel surface shown in Fig. 3.19 (b) displays no material transfer. As far as the validation test (#7 in the list above) is concerned, a friction coefficient being equal to the mean value at first tightening (μ_m=0.162) is initially assumed. Then, a tightening torque of T=687Nm is assigned to the twenty screws of the gearbox, by means of an impact wrench. Based on these assumptions, Eq. (3.8) gives F_V=166kN: if the coefficient of friction was estimated correctly, this force should be acting on each screw. For such a value of F_V, the FEA model forecasts a normal stress along the x-axis of 87MPa at the application point of the strain gauge. During the test, σ_x=100MPa has been sampled. The error, in the order of 13%, substantially validates the previously calculated friction coefficients.

3.3.5 Discussion

The dry joint exhibited a remarkable increase of the friction coefficient, associated with a proportional decrease of the initial preload, due to a severe degradation of the mating surfaces. The addition of a ceramic paste proved to yield beneficial effects, since it leads to a significant decrease of the friction coefficient value, with consequent remarkably higher values of the preload. Moreover, the lubricated joint shows a constant friction coefficient over the entire set of repeated tightenings, with a much reduced scattering. This occurrence is due to the capability of the lubricant of preserving the iron surface from material removal, which in turn leads to severe wear.

3.4 Reference of the chapter

[1] Fukuoka T, Nomura M, Kawabayashi H. A new experimental approach for measuring friction coefficients of threaded fasteners focusing on the repetition of tightening operation and surface roughness. ASME 2013 Pressure Vessels and Piping Conference, PVP 2013; Paris; France; 14 July 2013 through 18 July 2013; Code 102840.

[2] Croccolo D, De Agostinis M, Vincenzi N. Failure analysis of bolted joints: Effect of friction coefficients in torque-preloading relationship. Eng Fail Anal 2011; 8: 364-373.

[3] Croccolo D, De Agostinis M, Vincenzi N. Influence of tightening procedures and lubrication conditions on titanium screw joints for lightweight applications. Tribol Int 2012; 55: 68-76.

[4] Hoernig T, Friedrich C. Thread reinforcement of screw connections in lightweight design. ASME 2014 International Mechanical Engineering Congress and Exposition, IMECE 2014; Montreal; Canada; 14 November 2014 through 20 November 2014; Code 111737.

[5] De Agostinis M, Fini S, Olmi G. The influence of lubrication on the frictional characteristics of threaded joints for planetary gearboxes. Proc IMechE Part C: J Mechanical Engineering Science 2016; 230 (15): 2553-2563.

[6] Eccles W, Sherrington I, Arnell RD. Frictional changes during repeated tightening of zinc plated threaded fasteners. Tribol Int 2010; 43: 700-707.

[7] Hermansson TO. Quality assured tightening of screw joints. P I Mech Eng C-J Eng 2016; 230 (15): 2588-2594.

[8] Persson E, Roloff A. Ultrasonic tightening control of a screw joint: A comparison of the clamp force accuracy from different tightening methods. P I Mech Eng C-J Eng 2016; 230 (15): 2595-2602.

[9] Yu Q, Zhou H, Wang L. Finite element analysis of relationship between tightening torque and initial load of bolted connections. Adv Mech Eng 2015; 7 (5): 1-8.

[10] Chakherlou TN, Razavi MJ, Abazadeh B. Finite element investigations of bolt clamping force and friction coefficient effect on the fatigue behavior of aluminum alloy 2024-T3 in double shear lap joint. Eng Fail Anal 2013; 29: 62-74.

[11] Zou Q, Sun TS, Nassar SA, Barber GC, Gumul AK. Effect of Lubrication on Friction and Torque-Tension Relationship in Threaded Fasteners. Tribol T 2007; 50 (1): 127-136.

[12] Mitrovic S, Adamovic D, Zivic F, Dzunic D, Pantic M. Friction and wear behavior of shot peened surfaces of 36CrNiMo4 and 36NiCrMo16 alloyed steels under dry and lubricated contact conditions. Appl Surf Sci 2014; 290: 223-232.

[13] Ronkainen H, Varjus S, Holmberg K. Friction and wear properties in dry, water- and oil-lubricated DLC against alumina and DLC against steel contacts. Wear 1998; 222: 120-128.

[14] Sriraman KR, Strauss HW, Brahimi S, Chromik RR, Szpunar JA, Osborne JH, Yue S. Tribological behaviour of electrodeposited Zn, Zn–Ni,Cd and Cd–Ti coatings on low carbon steel substrates. Tribol Int 2012; 56: 107-120.

[15] Hager CH Jr., Evans RD. Friction and wear properties of black oxide surfaces in rolling/sliding contacts. Wear 2015; 338-339: 221-231.

[16] Farrell R Jr.. Blackening of ferrous metals. Met Finish 2007; 105 (10): 390-396.

[17] Scherb BJ, Zech J. A study on the smearing and slip behaviour of radial cylindrical roller bearings, Sonderdruck/Schriftenreihe der Georg-Simon-Ohm-Fachhochschule Nürnberg 2001; 1-20.

[18] Mihailidis A, Salpistis C, Panagiotidis K, Sachanas C, Gatsios S, Hoffinger C, Bakolas V. Wear and smearing resistance of black iron mixed oxide coated steels, Int J Surf Sci Eng 2010; 4 (4-6): 337-359.

[19] Evans R, Hager C, Kang Y, Doll G. Comparison of black oxide and tungsten carbide reinforced diamond-like carbon (WC/a-C:H) surface treatments for rolling element bearings. Tribol Trans 2015; 58: 444-453.

[20] Elias CN, Figueira DC, Rios PR. Influence of the coating material on the loosing of dental implant abutment screw joints. Mat Sci Eng C-Biomim 2006; 26: 1361-1366.

[21] Jeong Y-H, Lee C-H, Chung C-H, Son M-K, Choe H-C. Effects of TiN and WC coating on the fatigue characteristics of dental implant. Surf Coat Tech 2014; 243: 71-81.

[22] Xie Y, Zhou J, Wei Q, Yu ZM, Luo H, Zhou B, Tang ZG. Improving the long-term stability of Ti6Al4V abutment screw by coating micro/nano-crystalline diamond films. J Mech Behav Biomed Mater 2016; 63: 174-182.

[23] Stephen JT, Marshall MB, Lewis R. An investigation into contact pressure distribution in bolted joints. P I Mech Eng C-J Eng 2014; 228 (18): 3405-3418.

[24] Kopfer H, Friedrich C, De Agostinis M, Croccolo D. Friction characteristics in light weight design focusing bolted joints. ASME 2012 International Mechanical Engineering Congress and Exposition, IMECE 2012; Houston (Texas); United States; 9 November 2012 through 15 November 2012; Code 100737.

[25] International Organization for Standardization ISO 16047:2005(E). Fasteners - Torque/clamp force testing. Geneva, Switzerland; 2005.

[26] Berger PD, Maurer RE. Experimental design with applications in management, engineering and the sciences. Belmont, CA: Duxbury Press; 2002.

[27] Montgomery DC. Design and analysis of experiments. New York: Wiley; 2001.

[28] Olmi G. Investigation on the Influence of Temperature Variation on the Response of Miniaturised Piezoresistive Sensors. Strain 2009; 45: 63-76.

[29] Croccolo D, De Agostinis M, Fini S, Olmi G. Influence of the engagement ratio on the shear strength of an epoxy adhesive by push-out tests on pin-and-collar joints: Part I: Campaign at room temperature. Int J Adhes Adhes 2016; 67: 69-75.

[30] Croccolo D, De Agostinis M, Fini S, Olmi G. Influence of the engagement ratio on the shear strength of an epoxy adhesive by push-out tests on pin-and-collar joints: Part II: Campaign at different temperature levels. Int J Adhes Adhes 2016; 67: 76-85.

[31] Eliaz N, Gheorghiu G, Sheinkopf H, Levi O, Shemesh G, Ben-Mordechai A, Artzi H. Failures of bolts in helicopter main rotor drive plate assembly due to improper application of lubricant. Eng Fail Anal 2003; 10: 443-451.

[32] VDI-Richtlinie 2230: Systematische Berechnung hochbeanspruchter Schraubenverbindungen. Zylindrische Einschraubenverbindungen. Ausgabe Februar 2003, Berlin.

[33] Nassar , S. A.; Matin, P. H.; Barber, G. C.: Thread friction torque in bolted joints. Journal of Pressure Vessel Technology 2005 Vol. 127 pp. 387-393.

[34] Friedrich, C. Reliable light weight fastening of magnesium components in automotive applications. In: Proceedings of the 2004 SAE World Congress. Detroit (Michigan); March 8–11, 2004.

[35] Baragetti, S. Terranova, A.Vimercati, M. Friction behavior evaluation in beryllium-copper threaded connections. International Journal of Mechanical Sciences 51 (2009), 790–796.

[36] Bickford, J.: Introduction to the Design and Behavior of Bolted Joints. Fourth Edition, Taylor & Francis Group, New York 2008.

[37] Friedrich, C. Hubbertz, H. Dinger, G. Standardized calculation of bolted joints for future requirements, in Proceedings of the ASME 2011 International Mechanical Engineering Congress & Exposition IMECE2011, November 11-17, 2011, Denver, Colorado, USA.

[38] Friedrich, C., Designing Fastening Systems. In: Totten, G.E.; Xie, L.; Funatani, K. (editors): Modeling and Simulation for material selection and mechanical design. Dekker, New York 2004.

[39] Nassar, S. A. Zaki, A. M., Effect of coating thickness on the friction coefficients and torque-tension relationship in threaded fasteners. ASME Journal of Tribology 131 (2009), 1 – 11.

[40] Nassar, S. A. Ganeshmurthy, S. Ramanathan, M. R. Barber, G. C. Effect of tightening speed on the torque-tension and wear pattern in bolted connections. Journal of Pressure Vessel Technology 129 (2007), 426-440.

[41] Croccolo D., De Agostinis, M. Vincenzi, N. A contribution to the selection and calculation of screws in high duty bolted joints, International Journal of Pressure Vessels and Piping 96-97 (2012), 38 – 48.

[42] Toth G. R. Torque and Angle Controlled Tightening Over the Yield Point of a Screw—Based on Monte-Carlo Simulations, ASME Journal of Mechanical Design 126 (2004), 729 – 736.

[43] Heyman, J. S. Chern, E. J. Ultrasonic measurement of axial stress, Journal of Testing and Evaluation 10 (5) (1982), 202 – 211.

[44] G. Olmi, An experimental investigation on a crack propagating from a geartrain housing in an asphalt milling machine, Engineering Failure Analysis, 38 (2014) 38–48.

[45] EN 1563: 1997, Founding - Spheroidal graphite cast irons.

[46] ISO 898-1: 2009, Mechanical properties of fasteners made of carbon steel and alloy steel — Part 1: Bolts, screws and studs with specified property classes — Coarse thread and fine pitch thread.

[47] ISO 724: 1993, IS0 general-purpose metric screw threads - Basic dimensions.

[48] Niemann G., Winter H, Hohn BR. Maschinenelemente. Berlin: Springer-Verlag; 2005.

[49] Alkatan, F. Stephan, P. Daidie, A. Guillot, J. Equivalent axial stiffness of various components in bolted joints subjected to axial loading, Finite Elements in Analysis and Design 43 (2007), 589 – 598.

[50] Croccolo D, Cuppini R, Vincenzi N., Friction coefficient definition in compression–fit couplings applying the DOE method, Strain (2008), 44: 170-179.

[51] Olmi G, Freddi A, Croccolo D., In-Field Measurement of Forces and Deformations at the Rear end of a Motorcycle and Structural Optimisation: Experimental-Numerical Approach Aimed at Structural Optimisation, Strain (2008); 44: 453-461.

[52] Olmi G., Comandini M., Freddi A., Fatigue on Shot-Peened Gears: Experimentation, Simulation and Sensitivity Analyses, Strain (2010), 46: 382-395.

[53] Olmi G., Low Cycle Fatigue Experiments on Turbogenerator Steels and a New Method for Defining Confidence Bands, Journal of Testing and Evaluation (2012), 40(4): 539-552.

[54] Croccolo D., De Agostinis M., Mauri P., Olmi G., Influence of the engagement ratio on the joint strength of press fitted and adhesively bonded specimens, International Journal of Adhesion and Adhesives, 53 (2014) 80–88.

[55] Croccolo D., De Agostinis M., Vincenzi N., Experimental analysis on the tightening torque - Preloading force relationship in threaded fasteners, in Proceedings of ASME 2010 International Mechanical Engineering Congress & Exposition IMECE2010, November 12-18, 2010, Vancouver, BC, Canada. Vol. 3 (PARTS A AND B), pp. 525-533.

[56] Riahi A.R., Alpas A.T., Wear map for grey cast iron, Wear 255 (2003), 401–409.

4. Experimental investigation on the influence of the engagement ratio on the performance of a medium strength treadlocker

4.1 Introduction

Adhesively bonded joints are used in many mechanical applications, because they offer several advantages, such as the reduction of weight, the increasing of strength and the improvement of fatigue and fretting corrosion performances. These advantages have been demonstrated to be effective in the case of interference fitted and adhesively bonded joints [1], namely, hybrid joints, whatever is the production system. Many researches evaluated the strength of these joints in dependence of several variables, such as the assembly pressure level [2], the type of materials in contact [3-4], the curing methodology [5], the operating temperature [6-7], the loading type [8-9] and the type of joining technique [10-11]. In order to reduce the self-loosening phenomenon on bolted connections increasing the untightening torque, some anaerobic adhesives, named treadlockers, have been used since a long time. Threadlockers are divided, according to their static shear strength, between strong, medium and weak. In addition to their strength, these adhesives influence the tribological behavior of the threaded joint in different ways, due to their nature and especially the rate of polymerization. This type of adhesive begins to polymerize when confined in the airless pockets left by the roughness and the clearance between the mating surfaces. Generally, high strength threadlockers start to polymerize already during the tightening phase, causing an increase of the apparent friction coefficient of the joint, vice versa the medium and low strength types cause a decrease in the friction coefficient with respect to the dry state as reported in Loctite report. As seen in previous paragraphs, the adoption of a lubricant during tightening, leads to homogenizing the axial force generated by the screw, making the joint more accurate in terms of correlation between tightening torque and preload. Application of strong threadlockers is usually limited by adhesives manufacturers to joints which are not intended to be disassembled, such as head studs (these usually undergo angle controlled tightening). In order to obtain a lubricant effect united with an appreciable increase of the breakaway torque, a medium strength treadlocker could be chosen. However, in certain applications this kind of adhesive may not be adequate to achieve the desired breakaway torque. In order to increase such breakaway torque, one of the possible solutions is to increase the number of engaged threads, thus increasing the adhesion surface. In the literature [12] it has been proven that the performance of one of the most common medium strength threadlockers, (Loctite 243 by Henkel), is strongly influenced by the coupling pressure. In the previous sections, it has been shown that pressure on the thread contact surface varies between different threads of a same screw. Due to this, an increase in the untightening torque not proportional to the number of threads engaged may be expected. In order to evaluate the performance of a medium strength threadlocker for different engagement ratios (ER), defined as the ratio between the length of the screw engaged in the nut over the nominal diameter of the screw, an experimental campaign was carried out for three different levels of ER and three different screw nominal diameters. In

addition, for the different levels of ER it was decided to consider three different materials, due to their different characteristics of load distribution between the treads and their different affinity with the adhesive. (Tab 4.1)

4.2 Materials and methods

The research focuses on Loctite 243, due to its great diffusion which in turn leads to a large availability of information in the literature. The screws adopted were standard hexagonal head class 8.8, M6, M8 and M10, zinc coated, along with the respective zinc coated steel washers (according to ISO 898-1, ISO 7089). The experimental setup comprises: three machined plates Fig.4.1, manufactured with different materials, which allow to obtain different engaged lengths and a plane surface, perpendicular to the hole, some instrumented sleeves which allow to measure the preload force generated by the screw (Fig.4.2), an electronic torque wrench used to control the tightening and untightening torque and a cleaner, Loctite 7063, used to degrease the plate before tightening.

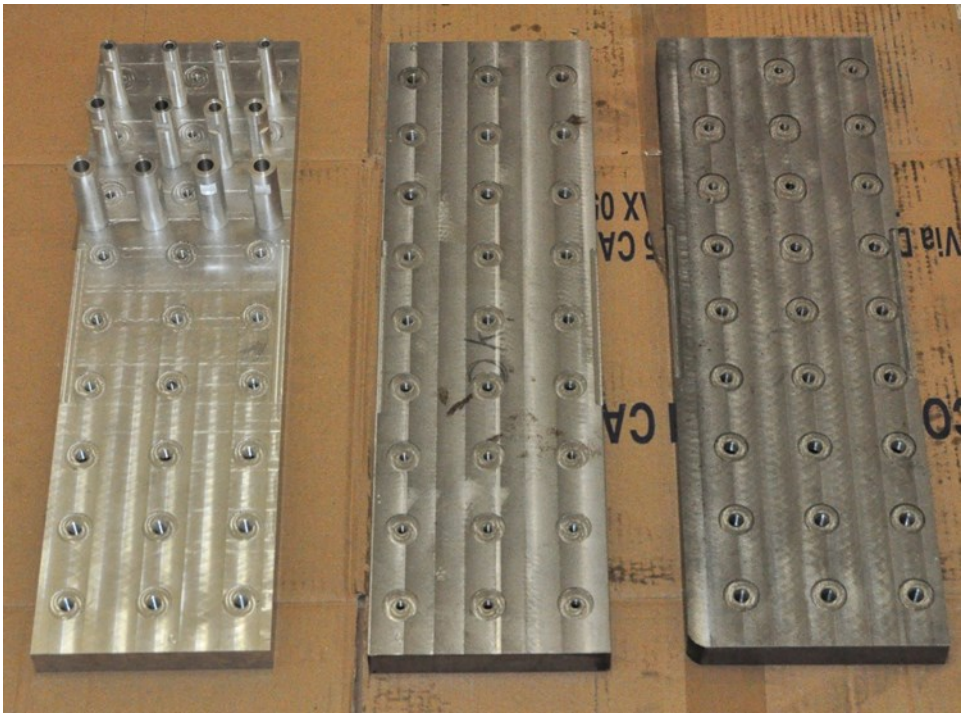

Fig. 4.1 Machined plates

Fig. 4.2 instrumented sleeves

The sleeve design adopted the same procedure described in paragraph 3.3.2, downstream the manufacturing phase they were instrumented with a quarter-bridge strain gauge, applied to the external cylindrical surface, with the main axis aligned with the screw axis. The threaded plates were made in three different materials: steel, cast iron and aluminum, whose details are given in Table 4.1. In fig. 4.3 it is shown the setting up of a generic specimen to be tested where it is possible to see the hole drilled part at the bottom of the plate (the nut of Figure 4.3) which controls the engagement length Lt. Each plate is provided with nine holes for each nominal dimension of the screws, equally divided between the three selected ER levels: 1, 1.5, 2. The expression of ER is given in Equation 4.1.

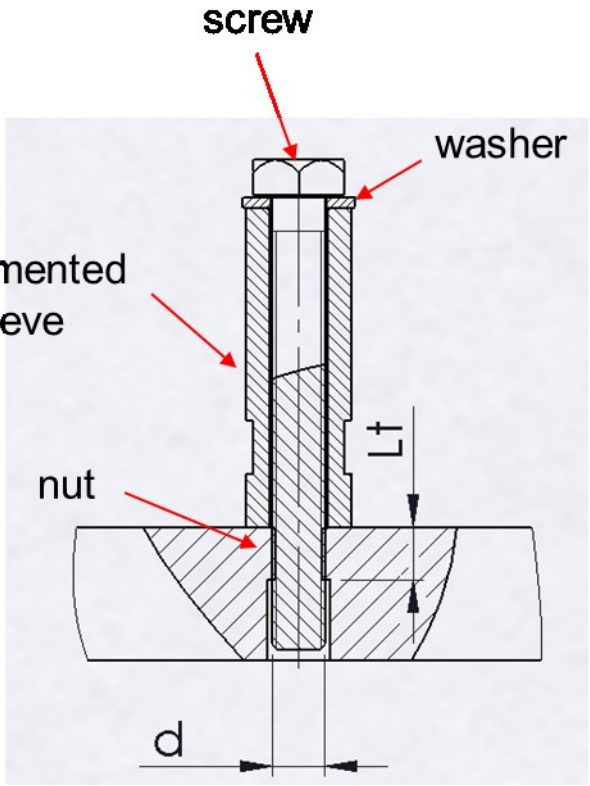

Fig. 4.3 Screw assembled with the sleeve, the plate and the washer

$$ER = \frac{Lt}{d} \tag{4.1}$$

Table 4.1

MATERIAL	UTS [Mpa]	Sy [Mpa]	A%	Elastic Modulus [Mpa]	Poisson's ratio v
EN AW 7075	540	485	7	72000	0,33
EN-GJS-500-7C	500	320	7	169000	0,275
S 275 JR	410	265	23	210000	0,30

4.3 Experimental test

For each material, ER and size of the screw three specimens were tightened sequentially by hand, recording the tightening torque and the axial preload generated. After curing for 48 hours at room temperature (as reported in the data sheet of the threadlocker to obtain a complete polymerization) the untightening of the screws was performed, recording the breakaway torque. For each repetition of the tightening operations and for each screw dimension the instrumented

sleeves were always the same, only the washer was changed at each tightening, in order to have the same friction condition in the underhead and, therefore, to isolate the effect of the threadlocker on the threads. The screws were tested as received, without degreasing them and the threadlocker was applied on the screw in the treads nearest to the tip, thus during the rotation the nut pushed the adhesive along the screw. This procedure is reported in the datasheet of the threadlocker for the application in through threaded holes (Fig 4.4).

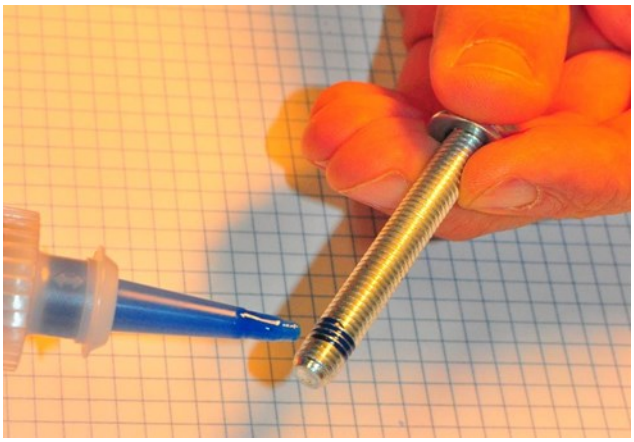

Figure 4.4 Threadlocker application

The adhesive remain entrapped in the volume between the threads (Fig 4.5) due to the tolerances adopted in the screw and in the nut, usually for commercial parts the tolerance is 6g for the screw and a 6H for the nut [ISO 965-1].

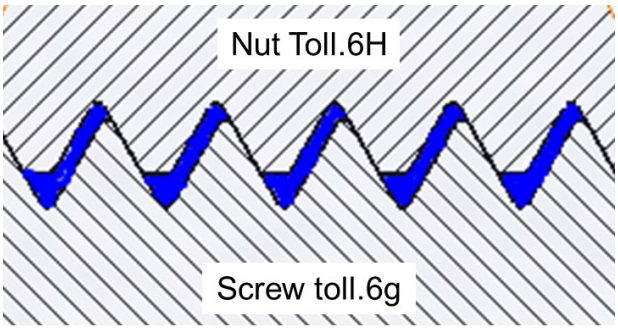

Figure 4.5 distribution of the adhesive

The screws were tightened following the prescription of the international standard ISO 261. The tightening operation was performed in torque control with a torque wrench: Torcotronic II 8455-120 produced by Gedore. The torque levels adopted are reported in Tab. 4.2.

Table 4.2

	steel T [N.m]	aluminum T [N.m]	castiron T [N.m]
M6	**11**	**10**	**11**
M8	**27**	**26**	**27**
M10	**54**	**52**	**54**

4.4 Results

All the materials have a mean friction coefficient (average of three measurements) which grows up increasing the number of engaged threads. Fig 4.6

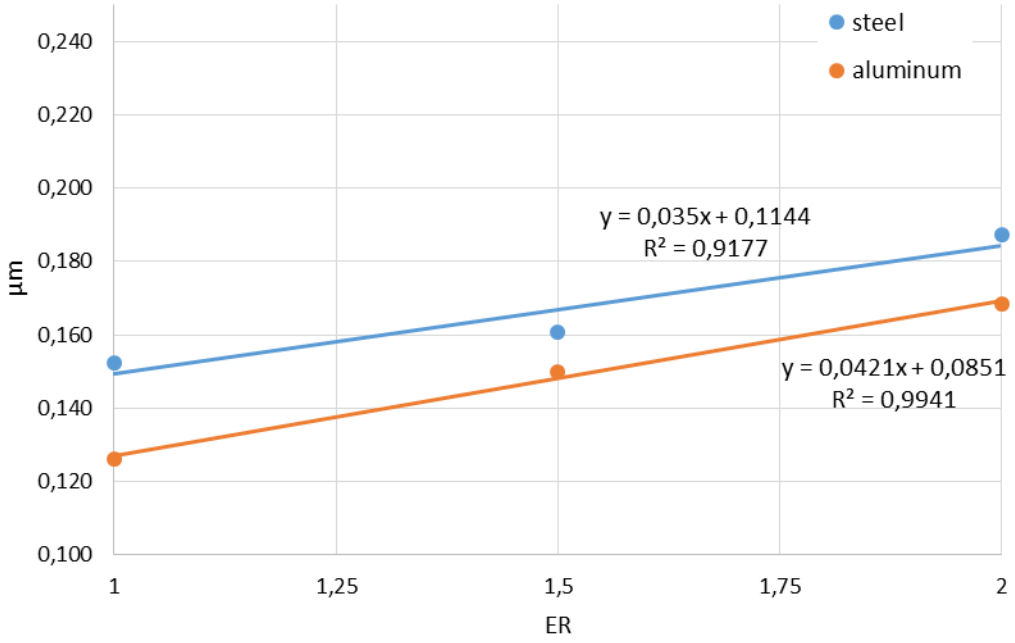

Figure 4.6 mean friction coefficient behavior for different materials in function of ER

The untightening torque T_u showed a linear behavior as well: T_u increases for increasing ER fig. 4.7 and fig. 4.8. For both friction coefficient and untightening torque, the behaviors were confirmed by the analysis of the variance of the results (ANOVA) [9,27–34] at a very high confidence level (around 90%) for steel and aluminium nut. The cast-iron specimens showed a greater scatter in the results, which does not allow to draw any conclusions about the effect of ER over the untightening torque.

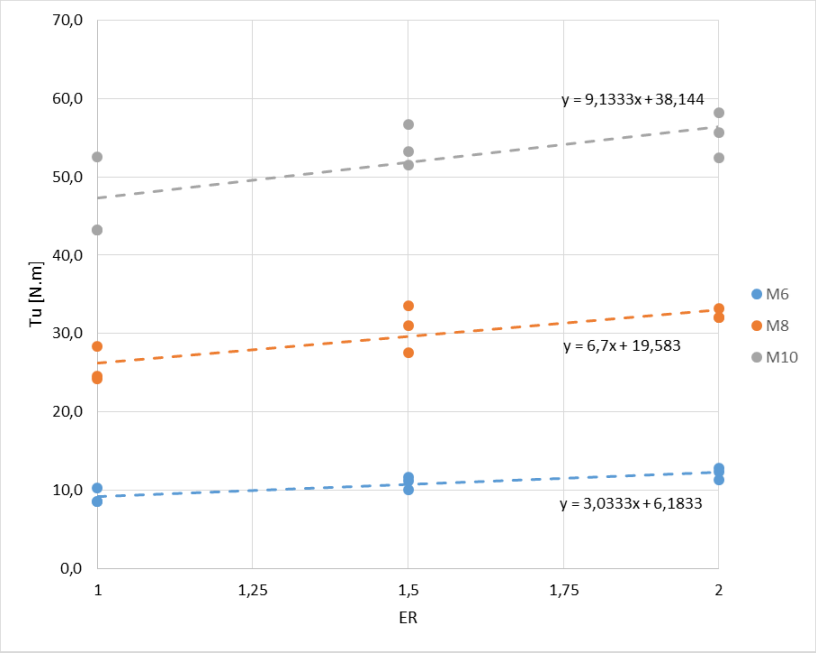

Figure 4.7 untightening torque for steel nut

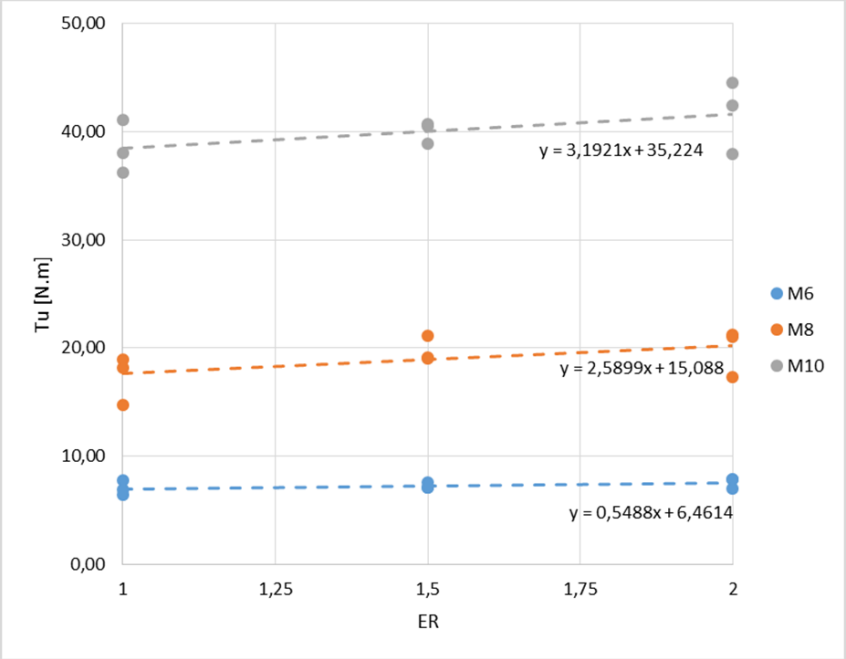

Figure 4.8 untightening torque for aluminium nut

For each combination between size of the screw and thread material the equation of the curve was calculated and reported in the plots of Figures. 4.7 and 4.8. Both steel and aluminum nuts showed an increasing slope of the curves when the nominal diameter of the screw was increased.

4.5 Discussion

The increasing effect of the ER on the friction coefficient can be considered localized in the thread, thanks to the adoption of a new washer in the underhead for each tightening. This finding makes the hypothesis of a lubrication effect of the threadlocker, at least in the case of aspect ratios ER greater than unity, less reliable. This behavior is due to a localized reduction of clearance between the threads, caused by an increase of the coupling length and probably to a beginning of polymerization due to a greater tightening time. In conclusion, the friction coefficient showed a dependence from ER. Increasing ER from 1 to 2 the friction coefficient grows up of 30% for the aluminum nut and 20% for the steel nut. Considering the results reported in section 3.2.1, where for a commercial nut (ER near to 1), the mean friction coefficient was measured and the mean friction coefficient measured for ER 1 with steel nut plus threadlocker the difference is negligible (μ_m=0.145 from section 3.2.1, μm=0.149 for the threadlocker). On the contrary, for the aluminum nut, it was observed a mean friction coefficient lower than that recorded for the steel nut, this result is quite unexpected for this material [13, 14]. This result can be explained by the lower wettability of the aluminum surface, which in turn leads to an overall lubricating effect of the adhesive during the tightening process.

Regarding the effect of ER on the untightening torque, it is possible to highlight that for a certain material the slope of the curves increases when the nominal diameter increases. This behavior depends on the relation between the untightening torque and ER that also depends on the pitch and on the screw diameter, as shown in Equation (4.2).

$$T_u \propto \tau \cdot A \cdot r_{mc} \cdot n \propto \tau \cdot d_2 \cdot p \cdot \frac{d_2}{2} \cdot \frac{d_2 \cdot ER}{p} \propto \tau \cdot d_2^3 \cdot ER \tag{4.2}$$

Equation 4.2 is a proportional analysis of the parameters which influence the relation between T_u and ER. In this equation, τ is the maximum shear stress of the adhesive, A is the adhesion area for one pitch, r_{mc} is the mean radius of the contact area and n is the number of engaged pitches. The contact area, the mean radius and the number of pitches can be expressed as a function of the pitch diameter d_2. All the constant values are omitted, τ is conserved due to its dependence on the clearance between the threads. This dependence is reported in the datasheet of the adhesive. Fig. 4.9

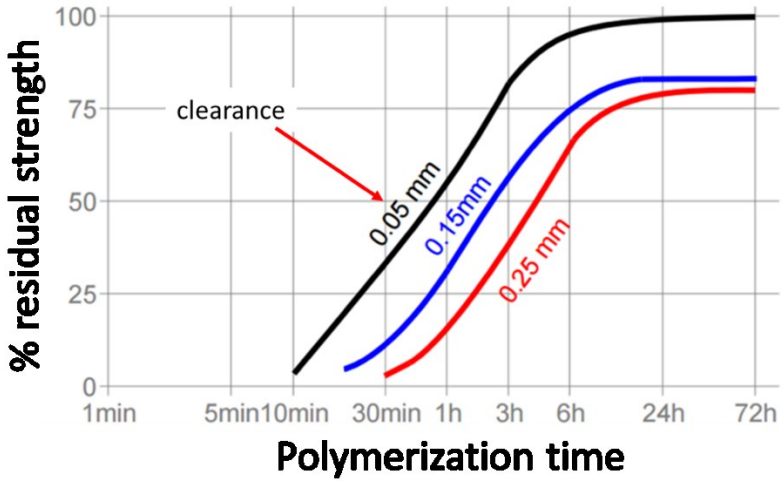

Figure 4.9 residual strength as a function of clearance between the joined parts for steel specimens [Loctite 243 data sheet]

The clearance between the threads for the whole screw dimensions can approximatively change from 0.03mm to 0.170mm considering a coupling tolerance 6H/6g (ISO 965-1) and, consequently, a difference of 20% can be found in the shear strength.(Fig.4.9). The curves referring to the aluminum nut exhibit a minor slope (Fig.4.8) if compared with those relevant for steel (Fig.4.7). This occurrence can be framed within the general lower wettability of aluminum surfaces with respect to steel ones [15, 16, 17]. Considering the macroscopic effect of ER on the untightening torque it can be concluded that the increasing ER produces a linear increasing of the breakaway torque. Increasing ER from 1 to 2, T_u increases its value of 25% for the steel nut and of 10% for the aluminum nut.

4.6 Reference of the chapter

[1] Croccolo D, De Agostinis M, and Vincenzi N. Design and optimization of shaft-hub hybrid joints for lightweight structures: Analytical definition of normalizing parameters. International Journal of Mechanical Sciences 2012; 56 (1): 77-85.

[2] Dragoni E and Mauri P. Intrinsic static strength of friction interfaces augmented with anaerobic adhesives. International Journal of Adhesion and Adhesives 2000; 20 (4): 315-321.

[3] Sekercioglu T. Shear strength estimation of adhesively bonded cylindrical components under static loading using the genetic algorithm approach. Intl J. Adhesion Adhesives 2005; 25: 352-357.

[4] Croccolo D, De Agostinis M, and Vincenzi N. Design of hybrid steel-composite interference fitted and adhesively bonded connections. International Journal of Adhesion and Adhesives 2012; 37:19-25. Special Issue on Joint Design 3.

[5] Mengel R, Haberle J, Schlimmer M. Mechanical properties of hub/shaft joints adhesively bonded and cured under hydrostatic pressure. Intl J. Adhesion Adhesives 2007; 27: 568-573.

[6] Da Silva LFM, Adams RD. Joint strength predictions for adhesive joints to be used over a wide temperature range. Intl J. Adhesion Adhesives 2007; 27: 362-379.

[7] Da Silva LFM, Adams RD. Adhesive joints at high and low temperatures using similar and dissimilar adherends and dual adhesives. International Journal of Adhesion and Adhesives 2007, 27 (3): 216-226.

[8] Adams J, Comyn R.D, Wake WC. Structural Adhesive Joints in Engineering. London: Chapman & Hall; 1997.

[9] Croccolo D, De Agostinis M, Vincenzi N. Static and dynamic strength evaluation of interference fit and adhesively bonded cylindrical joints. Intl J. Adhesion Adhesives 2010; 30: 359-366.

[10] Croccolo D, De Agostinis M, Mauri P. Influence of the assembly process on the shear strength of shaft-hub hybrid joints. Intl J. Adhesion Adhesives 2013; 44: 174-179.

[11] Castagnetti D, Dragoni E. Experimental Assessment of a Micro-Mechanical Model for the Static Strength of Hybrid Friction-Bonded Interfaces. The Journal of Adhesion 2013; 89 (8): 642-659.

[12] Dragoni, E., Mauri, P. Cumulative static strength of tightened joints bonded with anaerobic adhesives, 2002, Proceedings of the Institution of Mechanical Engineers Part L: Journal of Materials: Design and Applications, 216 (1), pp. 9-15

[13] Kopfer, H., Friedrich, C., De Agostinis, M., Croccolo, D. Friction characteristics in light weight design focusing bolted joints, 2012, ASME International Mechanical Engineering Congress and Exposition, Proceedings (IMECE) 3 (PARTS A, B, AND C), pp. 839-846

[14] Croccolo, D., De Agostinis, M., Vincenzi, N. Failure analysis of bolted joints: Effect of friction coefficients in torque-preloading relationship, 2011, Engineering Failure Analysis 18 (1), pp. 364-373

[15] C. Borsellino, G. Di Bella and V. F. Ruisi, Intl J. Adhesion Adhesives 29, 36–44 (2009).

[16] J. Comyn, Intl J. Adhesion Adhesives 12, 45–49 (1992).

[17] D. Croccolo, M. De Agostinis and N. Vincenzi, Experimental Analysis of Static and Fatigue Strength Properties in Press-Fitted and Adhesively Bonded Steel–Aluminium Components, Journal of Adhesion Science and Technology 25 (2011) 2521–2538

5. Conclusion

Starting from the general equations proposed by Motosh and Shygley to correlate the tightening torque with the axial force generated by the screw during the tightening, the effects of the different approximations introduced in these equations have been analyzed. One of the main cause of the error in the correlation between the tightening torque and the axial force, has been identified by Nassar's works in the assumption of a constant pressure distribution on the threads and on the underhead. However he has analyzed the effects of different pressure distribution without clarifying what the pressure distribution exactly is because strongly affected by the shape and the materials of the bodies involved in the screw connection. In order to assess the real pressure distribution, some FEA analyses were carried out considering the standard metric screws with hexagonal head. Despite their great diffusion and the large amount of information about the stress concentration factor in the threads or in the underhead, in literature it is not available an exhaustive quantity of data about pressure distribution, especially for different materials in contact and for this type of head. Thanks to these analyses it was possible to determine the correct contact radius to use in the equations. The analyses have highlighted slight differences in the effective radius compared to the mean radius for all the different materials analyzed. Starting from this clarification on the relation between the axial load and the tightening torque, a real case on selfloosening has been analysed. In this study it was highlighted that the adoption of inner sleeves to control the preload of the tapered roller bearing can transmit an undesired torque to the ring-nut and in addition that, if this ring-nut is not properly tightened – due to an uncontrolled friction torque – the pinion shaft could exhibit problems of selfloosening. However, the main reason for the adoption of the inner sleeve is the necessity to control the preload of the bearings with an imposed displacement instead of an accurate control of the tightening process, with an exact knowledge of the friction coefficient involved. This experience has highlighted the necessity of investigating the friction coefficients involved in the tightening process. Moreover, it is important to understand how we can control and regularize their behaviour, for a repeated tightening, perhaps with the adoption of a suitable lubrication.

In order to investigate the effect of different surface coatings and different lubrication conditions, an experimentation campaign has been carried out applying the tools of fractional factorial design, Magic square Taguchi method and orthogonal decomposition of variance. Based on the result of the screening, the attention was then focused on the effects of the screw pleating and of lubrication. The following investigation, which involved these two factors, indicated that Zinc coated screws exhibit a lower friction coefficient with respect to black oxidized ones. This is reduced by approximately 20% both in dry condition and under ceramic paste or oil lubrication. Ceramic paste by Interflon proved to be highly effective at decreasing friction. The related coefficient is reduced by 32% with respect to dry conditions and by 17% in comparison to Oil lubrication. A moderately significant interaction was detected between the studied factors.

A further campaign was, then, aimed at deepening the analysis of lubrication. The most interesting result, achieved by running a One-way Analysis of Variance, followed by pairwise tests and orthogonal decomposition, is that paste lubrication at the underhead has an essential role at enhancing the tribological behaviour of the joint. In particular, it dramatically reduces the amount of tightening torque that is lost by friction at the underhead, and which cannot be converted into axial preload. On the other hand, the lubrication in the threads retains a minor importance and appears to be even ineffective, when comparing the threads in dry condition. Variance decomposition indicates that a very large amount (84%) is due to the different tribological response in lubricated conditions (full or only underhead) with respect to other conditions, regardless of the screw being completely dry or lubricated in the threads only. Moreover, one of the main advantages of the screwed connections is the possibility to disassembly the parts connected. But what happens to the friction coefficient when the tightening operation is repeated? In order to address this issue, a second experimental campaign has been performed on a differential gear box, focusing on the effects of the ceramic past previously analysed. In this investigation the dry joint exhibited a remarkable increase of the friction coefficient, associated with a proportional decrease of the initial preload, due to a severe degradation of the mating surfaces. The addition of a ceramic paste proved to yield beneficial effects, since it leads to a significant decrease of the friction coefficient value, with consequent remarkably higher values of the preload. Moreover, the lubricated joint shows a constant friction coefficient over the entire set of repeated tightenings, with a much reduced scattering. This occurrence is due to the capability of the lubricant to preserve the iron surface from material removal, which in turn leads to severe wear. At the end of this experimentation it was clarified the effect of a solid lubricant, the ceramic paste, never investigated before. Another possibility to obtain a lubricant effect and in addiction an increase of the untightening torque is the adoption of a medium strength threadlocker. Different studies are available in literature, but nobody has investicated the effect of the number of threads engaged on the untightening torque. A new experimental campaign has been, therefore, carried out in order to highlight the influence of the engaged threads. The outcome of the tests indicates that the increase of ER produces a linear increase of the untightening torque for steel screws and nut made by steel or steel screws and aluminium nuts. For steel nuts and ER=1 it was detected a friction coefficient similar to the dry case, which significantly increases when ER increases. For the aluminium nuts it was observed the same trend with ER, but starting from a significantly lower value respect to the value retrieved by the literature. Therefore a relevant lubricant effect has been highlighted only for the aluminium nuts.